ISTANBUL TECHNICAL UNIVERSITY ★ GRADUATE SCHOOL OF SCIENCE ENGINEERING AND TECHNOLOGY

PREDICTION OF WAVE RESISTANCE BY EXPERIMENTAL AND COMPUTATIONAL METHODS

M.Sc. THESIS

Ömer Faruk SUKAS

Department of Naval Architecture and Ocean Engineering

Naval Architecture and Marine Engineering Programme

MAY 2014

ISTANBUL TECHNICAL UNIVERSITY ★ GRADUATE SCHOOL OF SCIENCE ENGINEERING AND TECHNOLOGY

PREDICTION OF WAVE RESISTANCE BY EXPERIMENTAL AND COMPUTATIONAL METHODS

M.Sc. THESIS

Ömer Faruk SUKAS
508121013

Department of Naval Architecture and Ocean Engineering

Naval Architecture and Marine Engineering Programme

Thesis Advisor: Prof. Dr. Şakir BAL

MAY 2014

İSTANBUL TEKNİK ÜNİVERSİTESİ ★ FEN BİLİMLERİ ENSTİTÜSÜ

DENEYSEL VE HESAPLAMALI YÖNTEMLER İLE DALGA DİRENCİ TAHMİNİ

YÜKSEK LİSANS TEZİ

Ömer Faruk SUKAS
508121013

Gemi İnşaatı ve Gemi Makineleri Mühendisliği Anabilim Dalı

Gemi İnşaatı ve Gemi Makineleri Mühendisliği Programı

Tez Danışmanı: Prof. Dr. Şakir BAL

MAYIS 2014

Ömer Faruk SUKAS, a **M.Sc.** student of ITU **Graduate School of Science Engineering and Technology** student ID **508121013**, successfully defended the **thesis** entitled "**Prediction of Wave Resistance by Experimental and Computational Methods**"which he prepared after fulfilling the requirements specified in the associated legislations, before the jury whose signatures are below.

Thesis Advisor :	**Prof. Şakir BAL** İstanbul Technical University	.....
Jury Members :	**Prof. Şakir BAL** Istanbul Technical University	.....
	Prof. Abdi KÜKNER Istanbul Technical University	.....
	Asst. Prof. Uğur Oral ÜNAL Istanbul Technical University	.....

Date of Submission : 05.05.2014
Date of Defense : 30.05.2014

To my nephew and cousin,

FOREWORD

I am very grateful to my advisor, Prof. Dr. Şakir BAL. His valuable insights and directions gave me a perfect guidance to complete this thesis. He provided motivation throughout all of my study at Istanbul Technical University.

I owe a huge debt of gratitude to Dr. Kemal KINACI for teaching me about free surface ship flows in CFD and giving me an opportunitiy to share his knowledge and available informations about CFD. This study would not have been possible without his support and encouragement. Also I would like to thank Prof.Dr. Hüseyin YILMAZ for the use of his workstation throughout CFD analyses.

Besides, I am very thankful to Research Assistants Ali DOGRUL, Cihad DELEN and technical staff from Ata Nutku Ship Model Laboratory. I would not have been able to complete this thesis without their help during towing tank experiments.

Finally, I would like to thank my parents and especially my uncle, who encouraged me and provided a great support during my studies, which made it possible for me to finish this thesis.

May 2014

Ömer Faruk SUKAS
Naval Arc.& Marine Eng.

TABLE OF CONTENTS

Page

FOREWORD ..... **ix**
TABLE OF CONTENTS ..... **xi**
ABBREVIATIONS ..... **xiii**
LIST OF TABLES ..... **xv**
LIST OF FIGURES ..... **xvii**
SUMMARY ..... **xix**
ÖZET ..... **xxi**
1. INTRODUCTION **1**
1.1 Motivation 1
1.2 Scope of the Thesis 2
1.3 Literature Review 3
1.4 Thesis Outline 6
2. COMPUTATIONAL METHOD **7**
2.1 A General Overview on RANSE 7
2.2 Computational Fluid Dynamics Methodology (CFD) 9
3. EXPERIMENTAL METHOD **13**
3.1 Experimental Fluid Dynamics Methodology (EFD) 13
3.2 Model Construction 15
3.3 Calibration 17
3.4 Experimental Setup 18
3.5 Data Recording 21
4. RESULTS **23**
4.1 Numerical Modeling of Fully Submerged Bodies 23
4.1.1 Ellipsoid 23
4.1.1.1 Geometry and Meshing Strategy 23
4.1.1.2 Numerical Settings 26
4.1.1.3 Validation and Results for a Fully Submerged Ellipsoid 29
4.1.2 Submarine 34
4.1.2.1 Geometry and Meshing Strategy 34
4.1.2.2 Numerical Settings 37
4.1.2.3 Results for a Fully Submerged Submarine 41
4.2 Numerical Modeling of Surface Piercing Bodies 43
4.2.1 Wigley Parabolic Hull 44
4.2.1.1 Geometry and Meshing Strategy 44
4.2.1.2 Numerical Settings 45
4.2.1.3 Validation and Results for a Wigley Parabolic Hull 48
4.2.2 A Modern Displacement Tanker 53
4.2.2.1 Geometry and Meshing Strategy 53
4.2.2.2 Numerical Settings 56

4.2.2.3 Validation and Results for a Modern Displacement Tanker 60
5. CONCLUSION AND DISCUSSION..... 67
REFERENCES 69
CURRICULUM VITAE 75

ABBREVIATIONS

CFD	**:** Computational Fluid Dynamics
EFD	**:** Experimental Fluid Dynamics
RANSE	**:** Reynolds Averaged Naiver Stokes Equations
SP	**:** Single Phase
MP	**:** Multi Phase
ITTC	**:** International Towing Tank Conference
AR	**:** Aspect Ratio
ITU	**:** Istanbul Technical University
VOF	**:** Volume of Fluid
SIMPLE	**:** Semi-Implicit Method for Pressure-Linked Equations
QUICK	**:** Quadratic Upstream Interpolation for Convective Kinematics
BEM	**:** Boundary Element Method
IBEM	**:** Iterative Boundary Element Method
SES	**:** Surface Effect Ship
R_T	**:** Total Resistance
R_F	**:** Frictional Resistance
R_V	**:** Viscous Resistance
R_{VP}	**:** Viscous Pressure Resistance
R_W	**:** Wave Resistance
C_T	**:** Total Resistance Coefficient
C_F	**:** Frictional Resistance Coefficient
C_V	**:** Viscous Resistance Coefficient
C_{VP}	**:** Viscous Pressure Resistance Coefficient
C_W	**:** Wave Resistance Coefficient
Fn	**:** Froude Number
Re	**:** Reynolds Number
k	**:** Form Factor
ρ	**:** Fluid Density
u	**:** Fluid Velocity in X – Direction
v	**:** Fluid Velocity in Y – Direction
w	**:** Fluid Velocity in Z – Direction
p	**:** Pressure
ε	**:** Rate of Dissipation of the Turbulent Kinetic Energy per Unit Mass
k	**:** Turbulent Kinetic Energy per Unit Mass
ϑ	**:** Kinematic Viscosity

LIST OF TABLES

Page

Table 4.1 : Comparison of two different meshing methods. 25
Table 4.2 : Default under relaxation factors. 26
Table 4.3 : Numerical Settings of the Ellipsoid for Single-Phase. 27
Table 4.4 : Numerical Settings of the Ellipsoid for Multi-Phase. 28
Table 4.5 : Dimensions of Topsail and Tailplanes. 36
Table 4.6 : Analysis parameters for the submarine. 38
Table 4.7 : Numerical Settings of the Submarine for Single-Phase Solution. 39
Table 4.8 : Numerical Settings of the Submarine for Multi-Phase Solution. 40
Table 4.9 : The effects of the appendages on the total resistance. 41
Table 4.10 : Numerical Settings of the Wigley Parabolic Hull for Single-Phase. 46
Table 4.11 : Numerical Settings of the Wigley Parabolic Hull for Multi-Phase. 47
Table 4.12 : Boundary conditions for the tanker. 55
Table 4.13 : Under relaxation factors for the displacement ship 57
Table 4.14 : Numerical Settings of the Displacement Hull for Single-Phase. 58
Table 4.15 : Numerical Settings of the Displacement Hull for Multi-Phase. 59
Table 4.16 : Hydrostatic properties of the tanker. 60

LIST OF FIGURES

Page

Figure 2.1 : Wave resistance calculation strategy with CFD. 11
Figure 3.1 : Elliposid model. 13
Figure 3.2 : Strut arrangement combined with ellipsoid model. 14
Figure 3.3 : CNC machine in Ata Nutku Ship Model Laboratory workshop. 15
Figure 3.4 : Cutting process on drawn lines of the ellipsoid model 15
Figure 3.5 : Prepared model for painting. 16
Figure 3.6 : Final model with strut. 16
Figure 3.7 : Measured force values corresponding to voltages. 17
Figure 3.8 : Calibration setup. 17
Figure 3.9 : Connection of the strut and dynamomter. 18
Figure 3.10 : One-component resistance dynamometer 19
Figure 3.11 : Amplifier. 19
Figure 3.12 : Connecting element. 20
Figure 3.13 : Experimental scheme for the ellipsoid. 20
Figure 3.14 : A capture of the measured force from CatmanEasy. 21
Figure 4.1 : Geometry of the ellipsoid model (profile view). 23
Figure 4.2 : Overall mesh configuration. 24
Figure 4.3 : Mesh configuration around free surface. 25
Figure 4.4 : A comparison of wave resistance coefficients (h/c=0.126). 29
Figure 4.5 : Wave pattern after using tetrahedral mesh for entire domain. 30
Figure 4.6 : A comparison of total resistance coefficients (h/c=0.3). 31
Figure 4.7 : A comparison of total resistance coefficients (h/c=0.5). 31
Figure 4.8 : A comparison of total resistance coefficients (h/c=0.75) 31
Figure 4.9 : A comparison of frictional resistance coefficient for the ellipsoid. 32
Figure 4.10 : Wave contour of submerged ellipsoid at Fn=0.7 for h/c=0.126. 33
Figure 4.11 : Wave-cuts of a submerged ellipsoid at Fn=0.7 for h/c=0.126 33
Figure 4.12 : Free surface effect on pressure coefficient distribution over the Farrell's ellipsoid 34
Figure 4.13 : Submarine model geometry (profile view). 35
Figure 4.14 : Submarine model geometry (front and rear view). 35
Figure 4.15 : Appendages of the submarine model (side and top views) 35
Figure 4.16 : Mesh configuration around free surface and appendages. 37
Figure 4.17 : Comparison of total resistance at h/c=0.5. 41
Figure 4.18 : Comparison of frictional resistance coefficients at h/c=0.5. 42
Figure 4.19 : Comparison of frictional resistance at h/c=0.5. 43
Figure 4.20 : Mesh configuration on the Wigley hull. 44
Figure 4.21 : Hexahedral elements around the Wigley hull. 44
Figure 4.22 : Boundary conditions of the Wigley hull. 45
Figure 4.23 : Wave profile along the Wigley hull for Fn=0.316 48

Figure 4.24 : Wave profile along the Wigley hull for Fn=0.350. 49
Figure 4.25 : Comparison of the wave resistance coefficients..... 50
Figure 4.26 : Free surface deformations for a Wigley hull at Fn=0.4..... 51
Figure 4.27 : Wave profile on the Wigley hull at Fn=0.4. 51
Figure 4.28 : Effect of the free surface and viscosity on the pressure coefficient distribution over the Wigley hull as compared to the inviscid work... 52
Figure 4.29 : A general view of the tanker..... 53
Figure 4.30 : Computational domain of the tanker. 53
Figure 4.31 : Hybrid meshing for the free surface wave flow of a ship. 54
Figure 4.32 : Cell size towards the boundaries of blocks. 55
Figure 4.33 : Wave resistance coefficient, numerical and experimental. 60
Figure 4.34 : Frictional resistance coefficient of the tanker..... 61
Figure 4.35 : A linear form factor analysis via single phase solutions by RANSE. . 62
Figure 4.36 : Free surface contours of the tanker at Fn=0.27. 63
Figure 4.37 : Free surface effect on the pressure coefficient distribution over the displacement tanker. 63
Figure 4.38 : A comparison of RANSE and experiment for generated waves at the bow of the tanker. 64
Figure 4.39 : Wave profile on the hull for Fn=0.27 65
Figure 4.40 : Streamlines at the aft region of the model tanker. 65
Figure 4.41 : Experimental and calculated nominal wakes at the propeller disc. 66

PREDICTION OF WAVE RESISTANCE BY EXPERIMENTAL AND COMPUTATIONAL METHODS

SUMMARY

The prediction of wave resistance in naval architecture is an important aspect especially at high Froude numbers where a great percentage of total resistance of ships and submerged bodies is caused by waves. In addition; during hull form optimization, especially wave resistance characteristics of a ship must closely be observed. There are potential, viscous and experimental methods to determine the resistance components of a ship.

RANSE based methods usually follow the experimental method that determines the form factor first. However, it is proven in recent studies that the form factor changes with the Reynolds number. As the Reynolds number increases; this change in the form factor is being neglected. In this study, a RANSE based prediction of wave resistance is presented that overcomes this flaw. The methodology is validated with the submerged and surface piercing bodies for the effectiveness of the proposed method. The results reveal the robustness of the present methodology.

Single-phase and multi-phase analyses have been done in this study by using the interface capturing approach that solves the RANS equations on a predetermined grid which covers the entire domain and Volume of Fluid (VOF) method to simulate the free surface flow for fully submerged and surface piercing bodies. An ellipsoid model and Wigley hull are used as benchmark problems to obtain the wave resistance and these benchmarks employed to validate the numerical resistance tests are presented. In addition to this, a total resistance estimation for an another ellipsoid which has a different aspect ratio is tried to be observed for different depths and Froude numbers by using CFD and experimental method. The comparison of these methods have been aimed to determine the accuracy of the conventional experimental method. On the other hand, a submarine model which is created by adding fins and a sail is alike with ellipsoid. The contribution of the appendages to total resistance is investigated. Only total resistance coefficients are taken into consideration for validations because the wave resistance caused by strut can not be negligible during experiments. Therefore, it is not appropriate to compare the wave resistance components. Finally, the proposed method for calculating the wave resistance was implemented on a modern displacement tanker and compared the CFD results with towing tank tests.

DENEYSEL VE HESAPLAMALI YÖNTEMLER İLE DALGA DİRENCİ TAHMİNİ

ÖZET

Su üstünde ve su altında giden üç boyutlu cisimler etrafındaki akımı çözebilmek oldukça karmaşık ve zor bir problemdir. Günümüzde potansiyel akım teorisinin kısıtlı kullanımı ve bazı durumlarda yetersiz kalmasından dolayı model deneyleri, su altı veya su üstünde belirli hızlarda ilerleyen cisimlerin direnç hesaplamalarında hala geçerliliğini korumakta olan bir yöntemdir. Ancak hem akademik çalışmalarda hem de sanayi uygulamalarında deney imkanlarının kısıtlı ve pahalı olması, cisimlerin etrafındaki akım problemlerinin incelenmesinde Hesaplamalı Akışkanlar Dinamiği (HAD) yazılımlarını popüler hale getirmiştir.

Bilgisayar kullanımının hızla gelişmesiyle beraber HAD tabanlı ticari programlar da gelişmiş ve bu yazılımlara ulaşmak daha kolay hale gelmiştir. Son yıllarda gemi etrafındaki akım problemlerinin incelenmesiyle ilgili literatürde yer alan makale ve tezlerde HAD yazılımlarının kullanımında ciddi bir artış olduğu gözlenmiştir. Bu tezde de cisimler etrafındaki akım problemlerinin incelenmesinde ticari bir HAD yazılımı kullanılmıştır.

Tezin konusu, serbest su yüzeyi altında giden (tamamen batmış) ve gemi gibi suyu yararak ilerleyen (yüzey yarıcı) cisimler için Reynolds Ortalamalı Navier – Stokes (RANS) denklemlerini çözen ticari bir yazılım yardımıyla direnç bileşenlerinin incelenmesidir. Özellikle dalga direnci için deneysel çalışmalarda uygulanan yöntemden farklı bir hesaplama yöntemi önerilmiştir. Bu önerilen yöntem, elipsoit gibi tamamen batmış bir cisim üzerinde uygulanmış olup yöntemin yüzey yarıcı cisimlerde de doğru sonuçlar verdiğini görebilmek amacıyla bir adet Wigley teknesi ile yumrubaşa sahip modern bir deplasman tanker üzerinde de doğrulaması olmuştur. Elde edilen dalga direnci değerleri literatürde yer alan bazı çalışmalarla karşılaştırılmıştır. Bu çalışmaya ilave olarak, yine su altında seyreden fakat farklı bir boy-genişlik oranına sahip ikinci bir elipsoit modeli için deneysel ve hesaplamalı olarak farklı hız ve derinliklerde toplam direnç hesabı yapılmış ve sonuçlar birbirleriyle kıyaslanmıştır. Deneyleri yapılan bu elipsoit modeline yelken ve finler eklenerek aynı boy ve genişliğe sahip bir denizaltı modeli oluşturulmuş ve eklenen bu takıntıların toplam dirence yüzdesel olarak ne kadar katkıda bulunduğu hesaplamalı analizler yardımıyla incelenmiştir. Yapılan çekme deneyinin deneysel kurulumu için elipsoit modeline bakır bir çubuk bağlanmış ve bu çubuğa da tek bileşenli dinamometre bağlanmıştır. Deney arabasının ilerlemesiyle beraber ilk önce elipsoit ve çubuğa eksenel yönde gelen toplam direnç okunmuş, daha sonra model çubuktan çıkarılarak yine aynı hız ve derinliklerde sadece çubuk üzerine gelen direnç değerleri kaydedilmiştir. Elde edilen ilk direnç değerlerinden sadece çubuğa etkiyen direnç

değerleri çıkartılıp sadece modele etkiyen toplam direnç değeri elde edilmeye çalışılmıştır. Deney sırasında model ile ekipmanların birbirleriyle olan etkileşimleri incelenmiş olup, bu tip yan faktörlerin sonuçlar üzerindeki etkisi tartışılmıştır.

Tez, altı ana bölümden oluşmakta olup bu bölümler kendi içlerinde alt başlıklara ayrılmıştır. Giriş bölümünde öncelikle tezin amacından bahsedilmiştir. Daha sonra literatürde konu ile ilgili olan çalışmalar ayrıntılı olarak incelenmiş ve sonrasında tezin genel içeriği bölümler halinde kısaca anlatılmıştır.

İlk olarak çalışmada kullanılan hesaplamalı ve deneysel yöntemler açıklanmış, yapılan bu analizlerin yakınsaması için dikkat edilmesi gereken hususlar bir liste halinde verilmiştir. Ayrıca kullanılan ticari yazılımın cisim etrafındaki direnç bileşenlerinin hesabını yaparken çözdüğü RANS denklemlerinin matematiksel olarak çıkarımı yapılmıştır. Dalga direnci hesabı için önerilen yöntem teorik ve şematik olarak verilmiştir. Bu yöntemde, tek ve çift fazlı iki adet analiz gerçekleştirilerek dalga direnci elde edilmekte olup, Prohaska yöntemi yardımıyla form faktörünün bulunmasına ihtiyaç duyulmamıştır. Batmış bir cisim için deneysel yöntem açıklanırken, cisim üzerine eksenel yönde gelen direncin hesaplanmasında izlenilen yoldan bahsedilmiştir.

Daha sonra direnç hesaplamaları yapılan elipsoit, denizaltı, Wigley ve modern bir deplasman tankeri için kullanılan HAD yöntemi anlatılmıştır. İlk olarak her bir cisime ait geometriler ve ana boyutları verilmiş, daha sonra oluşturulan ağ yapıları ve numerik ayarların kurulması ile ilgili açıklamalar yapılmış ve son olarak da sonuçlar verilmiştir. Piramit ve küp elemanlardan oluşturulan ağ yapılarındaki avantaj ve dezavantajlarından bahsedilmiştir. Hem zamanın kısıtlı olması hem de bilgisayar kapasitesi nedeniyle oluşturulan kontrol hacimleri "Karma" (hibrit) ağ yapısı kullanılarak modellenmiştir. Üçgen elemaların kompleks geometriler etrafında, kontrol hacminin geri kalan kısımlarında dörtgen elemanlar kullanılarak ağ yapısının oluşturulması konusu üzerinde durulmuştur. Ayrıca problemlerin çözüm şemalarının oluşturulması da tablolar halinde verilmiştir.

HAD yönteminin yanısıra kullanılan deneysel yöntem de başlı başına ayrı bir tez konusu olabilecek niteliktedir. Bu çalışmanın içeriği hesaplamalı ve deneysel yöntemlerle elde edilen direnç bileşenlerinin karşılaştırılması olduğu için belirsizlik analizi konusuna değinilmemiştir. Üçüncü bölüm kapsamında, batmış cisimler için İ.T.Ü Ata Nutku Gemi Model Deney laboratuvarında yapılan çekme tankı testlerinin deneysel kurulumu ve kalibrasyonu gibi işlemler sonucu alınan verilerin doğruluğu saptanmaya çalışılmıştır. Elde edilen deneysel sonuçlar bir elipsoit modeli için farklı hız ve derinliklerde HAD sonuçları ile karşılaştırılmıştır.

Önceki bölümlerde anlatılmış olan hesaplamalı ve deneysel yöntemler yardımıyla elde edilen sonuçlar her bir cisim için ayrı ayrı başlıklar altında verilmiştir. İlk kısımda batmış cisimler için örnek bir problem olan elipsoit modeli için literatürdeki diğer çalışmalarla yapılan karşılaştırmalı sonuçlar verilmiştir. Daha sonra yine farklı bir boy – genişlik oranına sahip elipsoit modeli için hem HAD hem de deneysel çalışma yapılmış ve elde edilen sonuçlar karşılaştırılmıştır. Sonuçların tutarlı olması ile beraber, çıplak elipsoit geometrisi üzerine yelken ve fin eklenerek yeni bir denizaltı modeli oluşturulmuştur. Eklenen bu takıntıların toplam dirençte ne kadarlık bir artışa sebep olduğu incelenmiştir. Ayrıca artan ıslak alana bağlı olarak sürtünme direncindeki değişim gözlenmiştir. Batmış cisimler için uygun sonuçlar elde ettikten sonra, önerilen yöntem serbest su yüzeyini yararak ilerleyen cisimler için literatürde deneme problemi olarak ele alınan Wigley teknesi üzerinde de uygulanmıştır. Wigley

teknesi için tekne gövdesi boyunca oluşan dalga profili, basınç dağılımları ve boyutsuz dalga direnci katsayıları literatürdeki yer alan deneysel ve hesaplamalı çalışmalarla karşılaştırılmış ve potansiyel teoriye göre gayet başarılı sonuçlar verdiği gözlenmiştir. Son olarak İ.T.Ü Ata Nutku Gemi Model Deney laboratuvarında deneyleri yapılmış olan tanker için direnç bileşenleri, dalga profili, tekne üzerindeki akım hatları, basınç dağılımları ve serbest su yüzeyi deformasyonları incelenmiş olup, deneysel ve hesaplamalı yöntemlerin karşılaştırılması yapılmıştır.

Son bölümde ise elde edilen tüm sonuçların değerlendirilmesi yapılmıştır. Her ne kadar bilgisayar teknolojisi yardımıyla yapılan analizler bize daha pratik ve hızlı bir çözümler sunsa da, yapılan bu numerik analizlerin belirli kabuller yaparak çözüm yaptığı unutulmamalıdır. Örneğin bu çalışmada bütün problemlerde aynı türbülans modeli kullanılmıştır. Fakat gerçekte, akışkanın Reynolds sayısına bağlı olarak türbülans şiddetinin sürekli değiştiği bilinmektedir. Bunun yanında yapılan tüm analizler zamandan bağımsız (daimi) olarak ele alınmıştır fakat gerçekte durum bundan farklıdır. Ancak bu tezde HAD ile yapılan çözümlerde elde edilen sonuçlar zamana bağlı analizler ile birbirine yakın sonuçlar verdiğinden dolayı zamandan da tasarruf edebilmek adına daimi analizler tercih edilmiştir. Sonuç olarak deneysel sonuçların doğrulanması için yapılan tüm HAD analizlerinde gerçekteki tüm fiziksel etkilerin hesaplara katılarak incelenmesi gerçek duruma bir adım daha yaklaşılmasını sağlayacaktır.

1. INTRODUCTION

1.1 Motivation

Model testing has been an indispensable part for the prediction of ship resistance due to the complexity nature of flow around an underwater hull. However; this dependency to model tests is decreasing slowly as new calculation methods are developed by researchers and designers. As widely known, total resistance of a ship could be broken down into sub parts such as; frictional resistance, viscous pressure resistance and wave resistance. Frictional resistance of a ship can be calculated by ITTC formulation but it is still a problem today to compute the viscous pressure resistance and wave resistance empirically for ship like bodies as similar to the frictional resistance.

In model testing, the viscous pressure resistance is calculated by towing the model at very low speed generally at the towing tank and implementing the method of Prohaska or other approaches recommended in ITTC procedures [1]. It is possible to follow the same procedure using the RANSE based CFD software to obtain the viscous pressure resistance numerically instead of model tests. The wave resistance can be generally calculated by implementing the potential flow based boundary element methods [2]. The viscous resistance can be come from RANSE based CFD method and all these resistance components may be added to obtain the total resistance; however, the solutions found are still dependent on whether the assumptions made or the mesh structure etc.

Today, several CFD methods were developed for free surface wave flows to simulate it according to potential flow or turbulent viscous flow theory. As generally known, free surface flows are not easy to simulate because of their moving boundaries. Therefore, two boundary conditions must be dictated on the free surface [3] :

i. Kinematic condition which requires that the free surface assumed to be a sharp boundary splitting the two fluids that allows no flux transition between them.

ii. Dynamic condition which requires that the forces acting on the fluid at the free surface are in equilibrium, which is momentum conservation.

Using RANSE based CFD, it is possible to calculate the resistance components by implementing the same boundary conditions mentioned above but RANSE does not directly calculate the wave resistance of a ship. Instead, it calculates pressure resistance (which is the addition of viscous pressure resistance component and wave resistance component) and frictional resistance to obtain total resistance. If a naval architect wants to solely observe the wave resistance characteristics of a ship, s/he generally consults to potential flow based solutions which ignore the viscosity of the fluid and linearize the free surface deformations.

Results of RANSE, linearized and the experimental methods were generally in accordance with each other and CFD is often correctly predicting the free surface elevation and the total resistance. However, there was no comparison made in terms of wave resistance because RANSE solving CFD programs can only predict pressure and frictional resistance. A gap in the literature exists for a wave resistance predicting methodology for RANSE. Based on the author's knowledge, the only method to calculate the wave resistance is to calculate the form factor first to determine the viscous resistance with the help of ITTC correlation line; and deduce this value from the total resistance. Experimental determination of wave resistance assumes the form factor to be constant for all Froude and Reynolds numbers. However; a study on this topic made by Garcia Gomez , revealed that the effect of the Reynolds number on the form factor cannot be neglected [4]. This study proposes a method that automatically eliminates the flaws that may arise from form factor – Reynolds number dependency.

1.2 Scope of the Thesis

CFD has proved itself to be a great tool to assess a ship's hydrodynamics in the pre-design stage. Before making any experiments in the towing tank, it is possible today to investigate a ship's performance with CAD and using RANSE. However, a complete analysis must involve single phase and multiphase setup of the physics of ship flow.

The initial goal was only the calculation of total resistance for an ellipsoid model experimentally for infinite depth and validate it with computational fluid dynamics single phase (SP) results. However; while performing experiments it is nearly

impossible to avoid from free surface effects due to the limited sizes of the towing tank. If the ellipsoid model is tried to be scaled smaller to ignore free surface effects and provided deep water condition, this time Reynolds similarity cannot be provided. Thus, it was clearly understood that free surface effect should be included in CFD analysis for proper comparison with experimental results.

First scope of the thesis is total resistance prediction of an ellipsoid for different depths and Froude numbers by using CFD and experimental method. The methods are compared that shows the accuracy of the conventional experimental method especially in high Froude numbers. Also the efficiency of towing tests of submerged bodies is tried to be determined with conventional method using a strut in I.T.U Ata Nutku Ship Model laboratory. Only total resistance coefficients are taken into consideration for validations with CFD. The waves caused by strut can not be negligible during experiments, therefore it is not appropriate to compare the wave resistance coefficients. Then by using the ellipsoid geometry, a strategy is developed to optimize the numerical settings within the FLUENT results were validated with towing tank tests before analyzing the submarine model geometry for better convergence and accurate solution. Bare geometry of the submarine which has only tailplane and topsail is alike with ellipsoid. Also it was investigated the contribution of the appendages (topsail, fin) to the total resistance.

Second part is about a new method for calculating the wave resistance based on Reynolds Averaged Navier-Stokes Equations (RANSE) by using CFD. An ellipsoid and Wigley hull were selected as a benchmark problems to demonstrate the accuracy of the method applied and the results were compared with the studies in literature. As with the get reasonable results from the benchmark analyses then the proposed method was implemented to a tanker and compared the resistance components with its experimental results.

1.3 Literature Review

There are lots of potential flow theory based papers in the literature to calculate the wave drag of a body inside the fluid, however generally wave resistance is determined by linearized potential flow theory and most of them rely on Havelock's theory [5]. The first known wave resistance calculation starts with the linear theory of wave resistance developed by John Henry Mitchell in 1898. His works are noticed a quarter

century after by other scientists. Meanwhile in the early 1900's, Havelock developed a potential flow theory for calculating the wave resistance around a hull [6]. Another significant study is the work of Farrell who has solved the flow around a spheroid at different aspect ratios. He has solved the problem in the form of a distribution of sources on the surface of the spheroid and compared his results with Havelock's approximation and experimental results [7].

In the work of Rigby et al., wave resistance is calculated by potential theory using Rankine sources [8]. The method was first evaluated on a sphere with infinite depth that the analytical solution has been known. Then the effects of the free surface to the potential method were introduced and the wave resistance of Wigley hull was computed and compared with the experimental data.

Uslu and Bal have made a numerical prediction of wave drag for fully submerged and surface piercing bodies [9]. They have used an iterative boundary element method (IBEM) in their study for the case of a 2-D hydrofoil with an angle of attack. Also, the effect of Froude number and distance to the free surface of a submerged body on pressure distribution and wave drag values were investigated. Furthermore, they have applied Dawson's method to predict the wave drag of an ellipsoid and a surface piercing body. The wave pattern and wave resistance of surface piercing bodies were also predicted by Bal with an iterative boundary element method. The free surface and surface of piercing body were treated separately to unite for a solution. The convergence was achieved after several iterations. The effects of cavitation were also included in the study. [10]

A modified Rankine source panel was used to investigate the flows around Wigley and Series 60 hulls by Tarafder and Suzuki [11]. In the modified method, Rankine sources are distributed along the surface of the geometry as well as its image and on the free surface. They have compared their results with the experiments and found good accordance in predicting the wave pattern and wave resistance.

Wave drag component of a body is higher than viscous drag in surface piercing problems at high Froude numbers. Related studies in such cases for surface piercing bodies also exist in literature. For instance, Pranzitelli A. has performed a study about resistance predictions for a ship hull with steady-state calculations [3]. He has implemented Volume of Fluid (VOF) method in Reynolds Averaged Navier-Stokes (RANS) equations and employed a panel method with free surface effect. Both of these methods were assessed on Wigley parabolic hull and Series 60.

A prolate spheroid was used for submerged body and Wigley Hull was used to demonstrate the power of the method. Belibassakis et al. have investigated the two phase flow around a prolate spheroid, Wigley Hull and Series 60 ship with an iso-geometric analysis applied into Boundary Element Method (BEM) [13]. The wave resistances, pressure distributions and wave profiles are investigated inside their study and comparisons made with experiments and other numerical results from the literature. On the other hand, a broad history of the developments in understanding the waves generated by ships can be found in the works by Wehausen [14], Newman [15] and Tulin [16].

Other than linearized potential flow methods, fully nonlinear RANSE based solutions were also studied broadly in the literature. Repetto R.A. has a PhD thesis which is relevant to free surface flow around ships [17]. He has investigated the accuracy of free surface RANSE computations to predict frictional and total resistance of a ship at a constant speed and examined the effects of mesh quality, mesh resolution and turbulence modelling in CFD analysis.

In 2000, a CFD workshop held in Gothenburg (Sweden) was a stimulating conference to present the developments in house CFD codes. Three different benchmark vessels were investigated by different institutions and universities with different codes implementing RANSE and their results were evaluated in that workshop. A brief comparison of all the results for these three ships generated with different CFD codes are made in the study of Larsson et al [18]. In a report published by Bartesaghi and Viola [19], the total resistance and wave pattern of a Wigley hull is investigated using RANSE. The pressure, viscous and total resistances along with wave pattern along the hull is evaluated in the report. . On the other hand, wave resistance values of the Wigley hull are not given. A multiphase analysis of a surface effect ship with RANSE is made by Maki et al. investigating the effect of the air cushion between the hulls of the SES (Surface Effect Ship) [20]. The results of RANSE and the linearized method were in accordance with each other, correctly predicting the free surface elevation and the total resistance.

1.4 Thesis Outline

In Chapter 2, the first section outlines a general overview on the RANS equations and turbulence model used. Second section describes the computational methods and introduces an overview of the proposed CFD strategy that calculates the wave resistance in two steps.

Chapter 3 is compromising the experimental methodology of the ellipsoid model. The steps of model construction, calibration, setup and data recording are explained clearly. Figures of arrangements used and a setup scheme are also given in this chapter. The efficiency of towing tests for submerged bodies is tried to be determined with conventional method using a strut in I.T.U Ata Nutku Ship Model Laboratory.

Chapter 4, Results, exhibits the results obtained through numerical simulations individually for each geometry. Meshing strategies and general numerical settings are also explained in this chapter. Hybrid meshing method on complex geometries and blocking the whole domain is illustrated briefly. The benchmarks employed to validate the resistance tests are presented. The results for two type of ellipsoid with different aspect ratios are compared with experimental data and potential based studies. Second benchmark geometry is Wigley hull that is validated with the other works in literature. Wave profile on the hull and wave resistance coefficient are compared in the second part. The other parts of this chapter is concerning with the resistance results of a submarine model and a tanker whose tests are performed in Ata Nutku Ship Model Laboratory. Bare geometry of the submarine which has only tailplane and topsail is alike with ellipsoid. Also it was investigated the contribution of the appendages (topsail, fin) to the total resistance. The aim of the displacement tanker application is to show the flexibility and accuracy the proposed method that determines the wave resistance by using single phase and multiphase analyses in ANSYS Fluent 14.0.

The last chapter provides a summary of the entire study and highlights of some of the important conclusions.

2. COMPUTATIONAL METHOD

2.1 A General Overview on RANSE

As widely known, there are three conservation laws of physics which are used to solve the fluid dynamics problems in the nature. These laws are:

- Conservation of fluid mass
- Conservation of momentum
- Conservation of energy

The conservation equations of fluid mass (2.1) and momentum (2.2) for a steady, incompressible and viscous flow are:

- Continuity equation becomes:

$$\nabla . U = 0 \tag{2.1}$$

- Momentum equations become:

x component:

$$\rho \frac{Du}{Dt} = -\frac{\partial p}{\partial x} + \mu \nabla^2 u + \rho . f_x \tag{2.2}$$

y component:

$$\rho \frac{Dv}{Dt} = -\frac{\partial p}{\partial y} + \mu \nabla^2 v + \rho . f_y$$

z component:

$$\rho \frac{Dw}{Dt} = -\frac{\partial p}{\partial z} + \mu \nabla^2 w + \rho . f_z$$

where ρ is the fluid density, U=(u,v,w) the fluid velocity, p is the pressure, f=(f_x, f_y, f_z) is body force and D/Dt denotes the material derivative that is given below (2.3) :

$$\frac{D}{Dt} = \frac{\partial}{\partial t} + u \frac{\partial}{\partial x} + v \frac{\partial}{\partial y} + w \frac{\partial}{\partial z} \tag{2.3}$$

Here, the energy equation is disregarded since the continuity and momentum equations are necessary to solve flow field in an incompressible flow.

The velocity components in RANSE is represented by (2.4) :

$$U = U(x) + U'(x,t) \tag{2.4}$$

where $U(x)$ is the mean and $U'(x,t)$ is the unsteady disturbance values, such that $\overline{U'} = 0$. Then, the equation 2.2 becomes on time averaging (2.5):

$$\rho\left[\frac{\partial(u^2)}{\partial x} + \frac{\partial(uv)}{\partial y} + \frac{\partial(uw)}{\partial z}\right] = -\frac{dP}{dx} + \frac{\partial}{\partial x}\left[\mu\frac{\partial u}{\partial x} - \rho\overline{u'^2}\right] + \frac{\partial}{\partial y}\left[\mu\frac{\partial u}{\partial y} - \rho\overline{u'v'}\right] + \frac{\partial}{\partial z}\left[\mu\frac{\partial u}{\partial z} - \rho\overline{u'w'}\right] \tag{2.5}$$

y and z components are similar with the equation above and the terms of $\rho\overline{u'^2}$, $\rho\overline{u'v'}$, $\rho\overline{u'w'}$ are acting as extra stress that depends on the turbulent flow.

The best way to understand the turbulence effect is to assume that the extra stresses mentioned above as an additional viscosity that called as "eddy viscosity" and it also products the local velocity.

k-ϵ model is a two equation turbulence model that is used extensively in industrial applications due to its stability and easiness in implementation. The general references and the model's mathematical background are given in the study of Launder and Sharma [21] and called in the literature as standard k-ϵ model [22]. The ellipsoid is a streamlined body with low pressure gradients and k-ϵ turbulence model is known to return good results for these cases [22]. Realizable k-ϵ model is an improved version of the standard model and returns enhanced results [23]. Due to the relatively low number of mesh that this method requires (y+ is expected to lie in the range between 30 and 300 as dictated in the ANSYS Fluent User Manual), the applicability of k-ϵ model is suitable [24].

Eddy viscosity is shown as below (2.6):

$$\vartheta_{e=} \frac{C_\mu k^2}{\varepsilon} \tag{2.6}$$

Where C_μ is a constant value of 0.09, k is the turbulent kinetic energy per unit mass and ε is the rate of dissipation of the turbulent kinetic energy per unit mass. It should be noted that the crucial point is the $k - \varepsilon$ turbulence model is mostly implementable

at high Reynolds number and production and dissipation of turbulence should be in balance [25].

2.2 Computational Fluid Dynamics Methodology (CFD)

RANSE solving softwares need experienced users. Especially for ship flow problems, experience may be more important than other fields of engineering due to the complex geometry and high number of elements to represent the geometry and the domain. Other than strong fundamentals of fluid mechanics, users also need time to be able to converge such analyses. The most known and widely used approach to predict the resistance for 2-D or 3-D bodies using CFD is solving the Reynolds Averaged Navier-Stokes (RANS) equations.

A traditional RANSE solving software divides total resistance into two parts which is formulated as:

$$C_T = C_P + C_F$$

Here, C_T denotes total resistance coefficient while C_P is pressure resistance coefficient and C_F is frictional resistance coefficient. The pressure resistance coefficent can also be broken down into:

$$C_P = C_W + C_{VP}$$

C_W is wave resistance and C_{VP} is viscous pressure resistance. Keeping in mind that a fully submerged body inside a fluid with infinite depth has zero wave resistance; pressure resistance in this case becomes equal to the viscous pressure resistance.

$$C_P = C_{VP} \rightarrow at\ infinite\ depth$$

Within this context, the viscous pressure resistance of a body inside water may be derived from single phase analysis; which totally ignores the resistance caused by the free water surface.

The methodology proposed in this study starts with the calculation of viscous pressure resistance of the body inside water with a single phase (SP) analysis. After determining C_{VP} this way, a multiphase analysis (MP) for the same geometry including the free surface effects is made. The viscous pressure resistance from the single phase analysis is subtracted from the pressure resistance determined from the multiphase analysis.

$$C_{W\ of\ the\ body} = C_{P(mp)} - C_{VP(sp)}$$

Here, mp and sp inside the brackets refer to multiphase and single phase respectively.

Multiphase analyses may be time consuming because the acquisition of a meaningful free surface contour is more "painful" in greater depths. One may easily get wrong results if s/he only watches residuals to be stabilized. Residuals usually perfectly get stabilized although wave contours and resistance values are not acceptable, misguiding the user that a correct physical incident is modeled by CFD. There are some parameters other than residuals that should be watched closely before deciding that the analysis is finalized.

If any one of these parameters do not seem to be converged or are still oscillating, it would not be a good decision to stop the analysis because the final condition of the flow is not yet reached. The list below suggests a check list to be followed if a healthy case is to be found.

Checklist:

1. Watch all the residuals to get stabilized reasonably.
2. Determine if the total resistance is converged.
3. Check whether the total flux is close to zero, implying the conservation of mass.
4. Observe if there is a Kelvin wake pattern on the free surface.
5. Pay attention to the pressure resistance obtained from the multiphase analysis. This value must be greater than the pressure resistance obtained from the single phase analysis. Wave resistance cannot be less than zero.
6. Check out whether frictional resistance from the multiphase analysis is compatible with the frictional resistance obtained from the single phase analysis.

The flow chart of the CFD solution methodology is given in the Figure 2.1.

Multiphase analyses usually require finer mesh due to the complexity of tracking the surface correctly and obtaining brighter results. A denser mesh around the hull and the free surface will respond with decreased errors in calculation and stable residuals. Hexahedral elements are recommended especially for multiphase solutions of ship flows. On the other hand, tetrahedral elements are easier to use and manage to return good results for single phase analyses; however, they suffer to capture the free surface correctly in multiphase analyses.

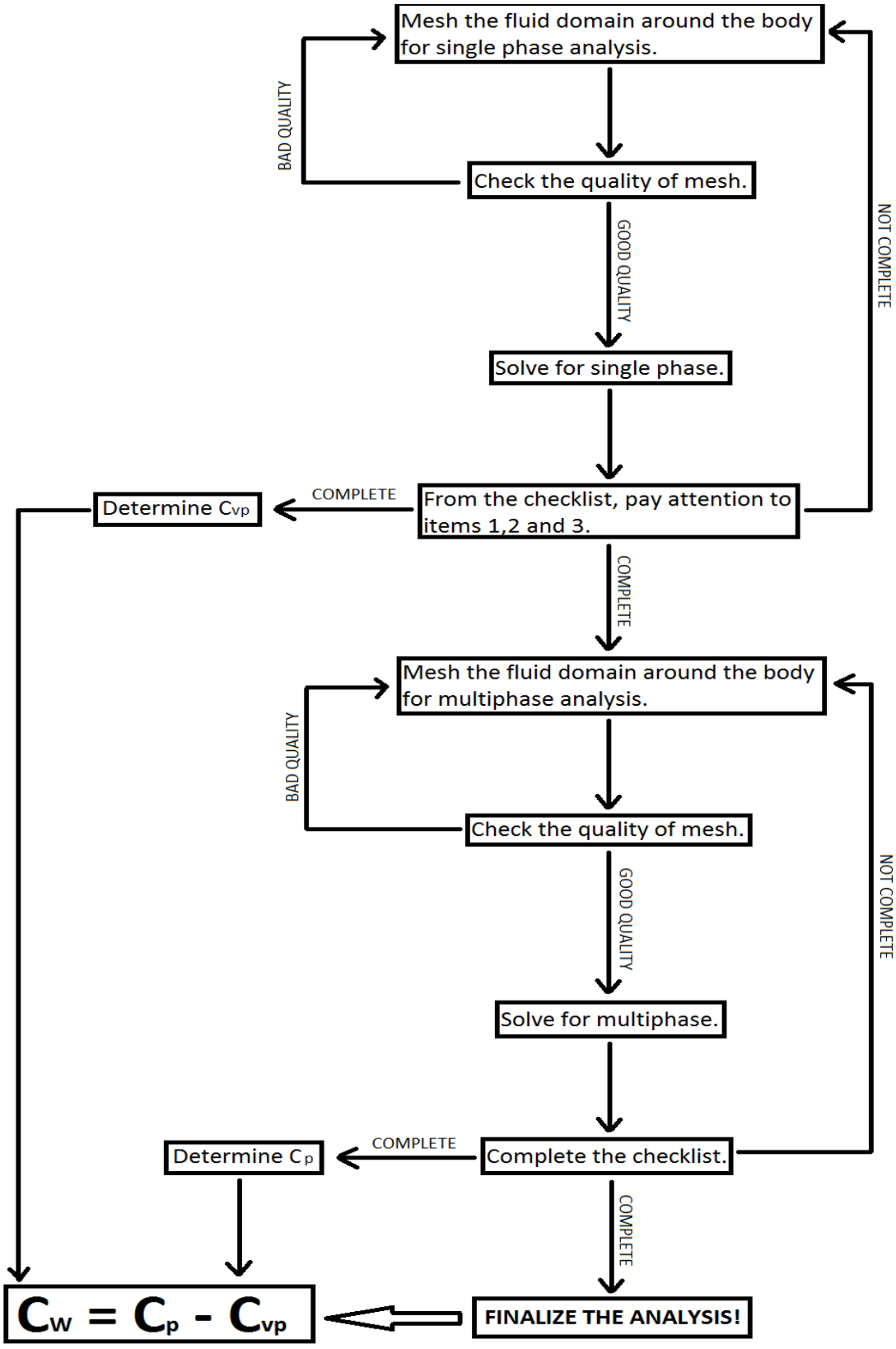

Figure 2.1 : Wave resistance computation methodology with CFD.

3. EXPERIMENTAL METHOD

3.1 Experimental Fluid Dynamics Methodology (EFD)

Experimental testings was performed in the towing tank at Istanbul Technical University, Ata Nutku ship model basin which has 6 meters breadth, 3.4 meters depth and 160 meters length, is equipped with a numerically controlled carriage that runs on two rails on each side. The towing carriage speed is maximum 6 m/s and has a capability to tow the naked model or follow the self-propelled model, and is equipped with devices to control. The length of the ship models manufactured in the laboratory workshop can be up to 5 m. The resistance, self-propulsion, open-water propeller tests and wake field measurements can be carried out. The wave generator can be used to measure the motions of ship models in regular and irregular waves.

In this thesis, the towing tank serves to measure the total resistance for an ellipsoid model for different depths and Froude numbers. Because of the several experimental studies of Wigley hull exist in literature, only ellipsoid model's tests were needed to be performed to validate the CFD results. The ellipsoid model and its dimensions are shown in Figure 3.1.

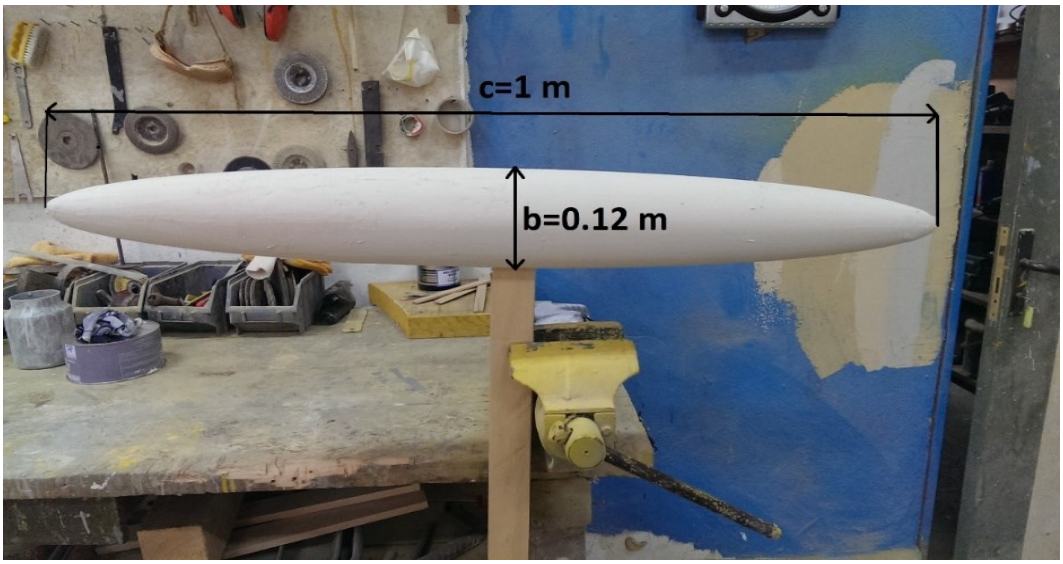

Figure 3.1: Ellipsoid model.

The towing tank testing of fully submerged ellipsoid is carried out by using a strut arrangement which is between the towing tank carriage and the model. Additionally, a single component resistance-gauge is integrated to the combined strut. Strut arrangement is shown in Figure 3.2. It is fixed to the ellipsoid model at its longitudinal midst.

Figure 3.2: Strut arrangement combined with ellipsoid model.

Using a single strut is enough to test the model due to the size of the model. As the size of the model increases, only one strut may not be adequate to get accurate results due to the vibration problem and yaw-pitch motions begin to trouble the experiment as the speed of the towing carriage increases.

Only one strut is used to hold the model at the desired depth and run to determine total resistance at increasing Froude numbers. After each test, the strut is run independently at the same Froude numbers and depths to determine its contribution to the total resistance. Finally, the resistance of the model is found by subtracting the strut resistance from the total combined (ellipsoid + strut) resistance.

3.2 Model Construction

The ellipsoid model manufactured in the Ata Nutku laboratory workshop. Initially, boundary lines had drawn on the woods before cutting process. Then the dimensions of the model was entered as inputs into the CNC machine which cuts the model automatically. The CNC machine and the cutting process are seen in Figure 3.3 and 3.4 respectively.

Figure 3.3 : CNC machine in Ata Nutku Ship Laboratory workshop.

Figure 3.4 : Cutting process on drawn lines of the ellipsoid model.

After cutting, the model was finished by hand. A hole was opened at the longitudinal midst of the model to attach the strut. The surface should be smoothed with dry paper, as seen in Figure 3.5 and therefore it would have been prepared for painting process.

Figure 3.5 : Prepared model for painting.

The final model that is joined with strut can be seen in Figure 3.6. After the drying process, estimated errors due to the construction that may caused by long drying times or some shrinkages can be negligible.

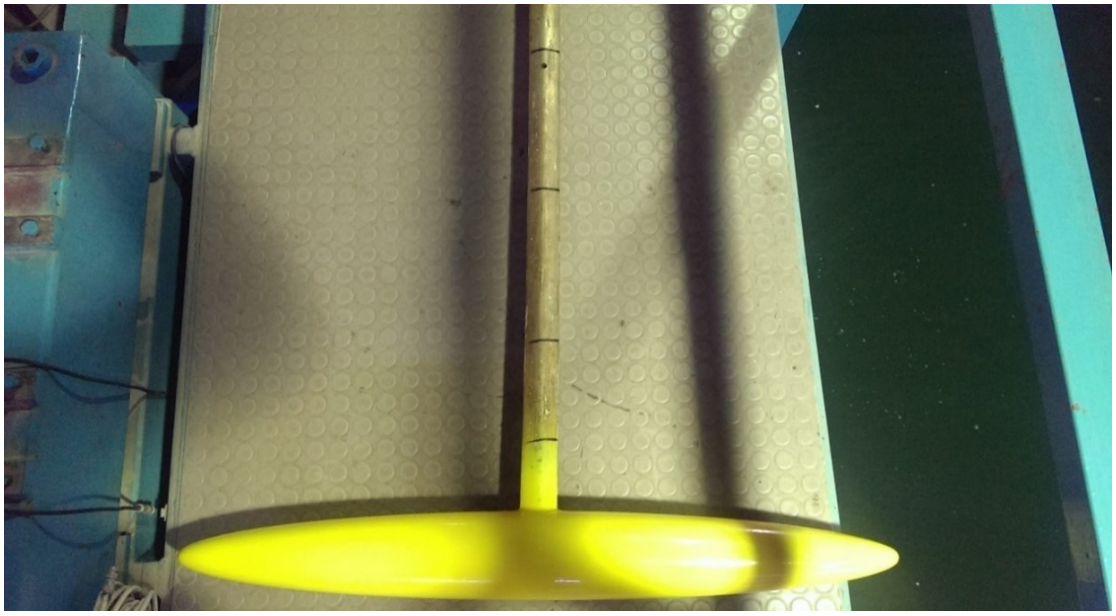

Figure 3.6 : Final model with strut.

3.3 Calibration

In order to calculate only x-axis force throughout experiments, calibration of one-component force measurement device was carried out before testing. A wire was attached to measurement device and a pan also attached to the end of wire. Then putting weights on into the pan one by one, force values corresponding to the weights was read from computer. CatmanEasy software was used for calibration and data recording while performing the experimental testings. Figure 3.7 and Figure 3.8 illustrate a plot generated by CatmanEasy and the calibration setup, respectively.

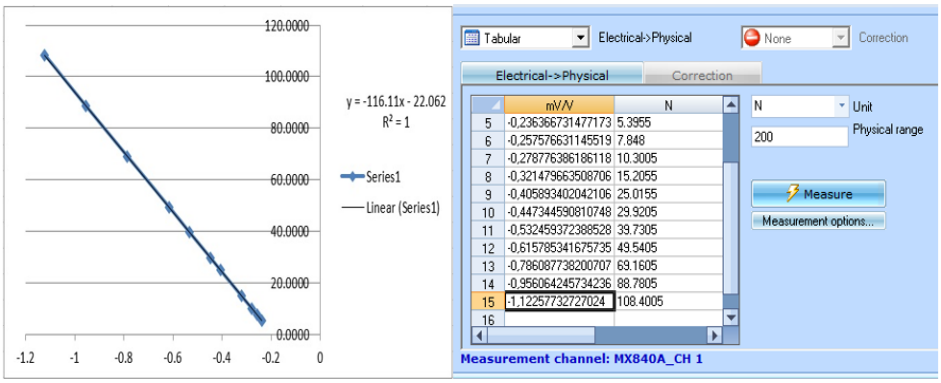

Figure 3.7 : Measured force values corresponding to voltage values.

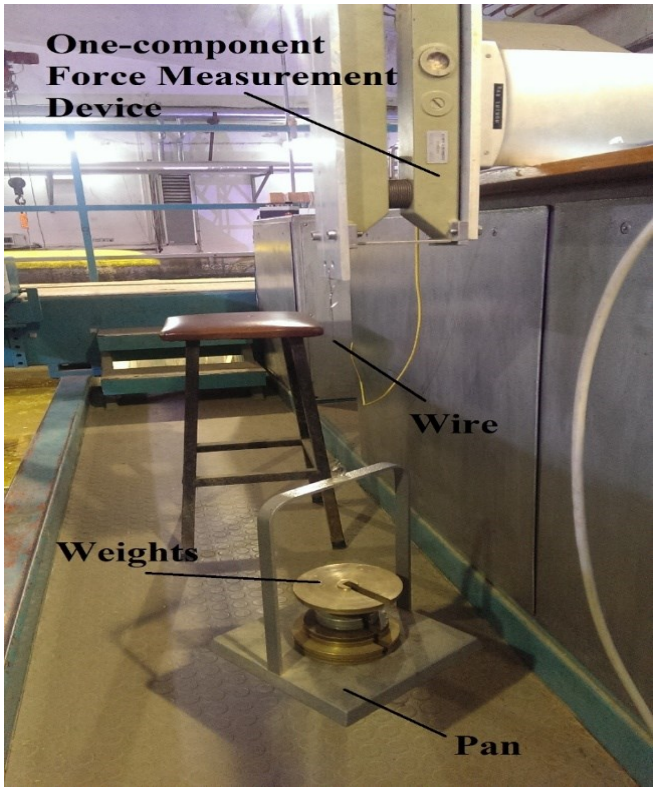

Figure 3.8 : Calibration setup.

3.4 Experimental Setup

The towing tank testing of fully submerged ellipsoid is carried out by using a strut arrangement which is between the towing tank carriage and the model. After each test, the strut is run independently at the same Froude numbers and depths to determine its contribution to the total resistance. Total resistance of the model is found by subtracting the strut resistance from the total combined (ellipsoid + strut) resistance. Please refer to Figure 3.9.

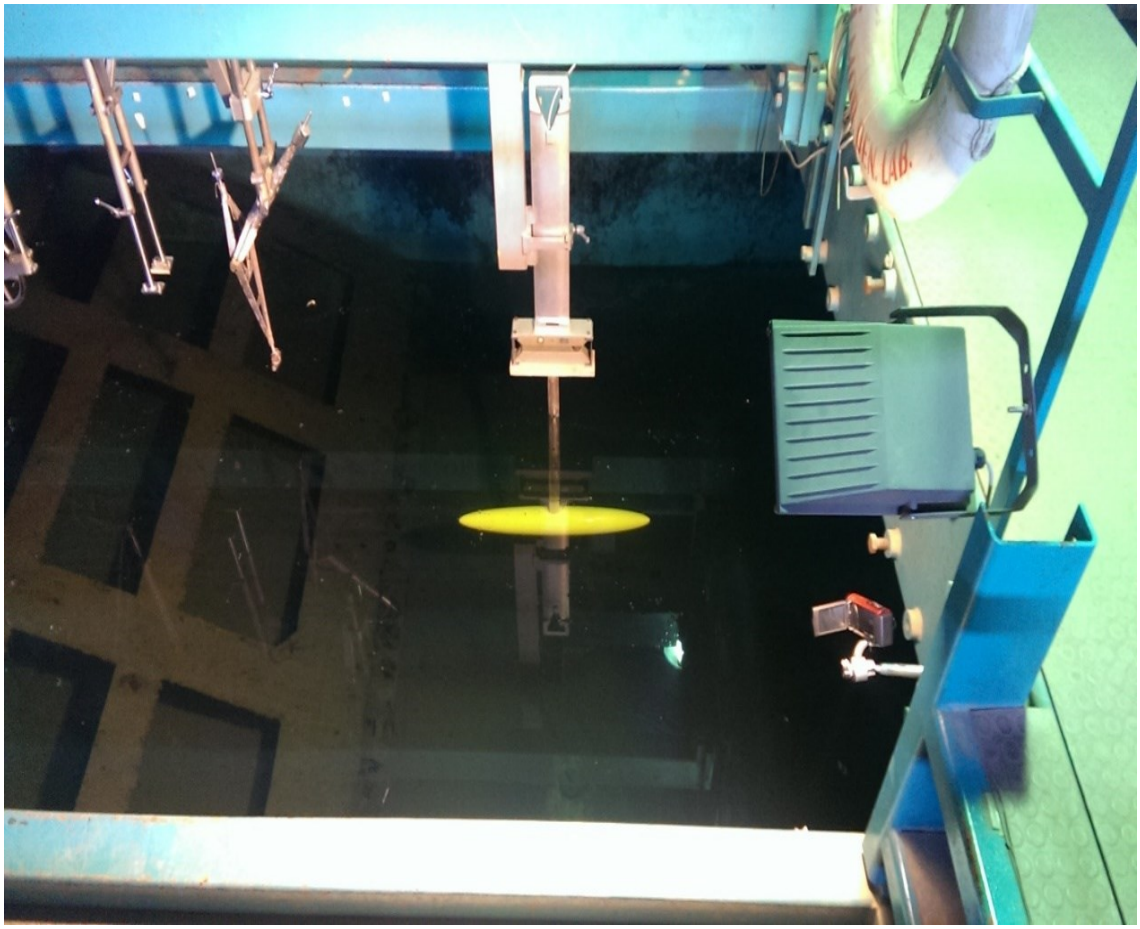

Figure 3.9 : Connection of the strut and dynamometer.

One component resistance dynamometer which can be seen in Figure 3.10 measures the force on the strut and ellipsoid only in x-axis direction.

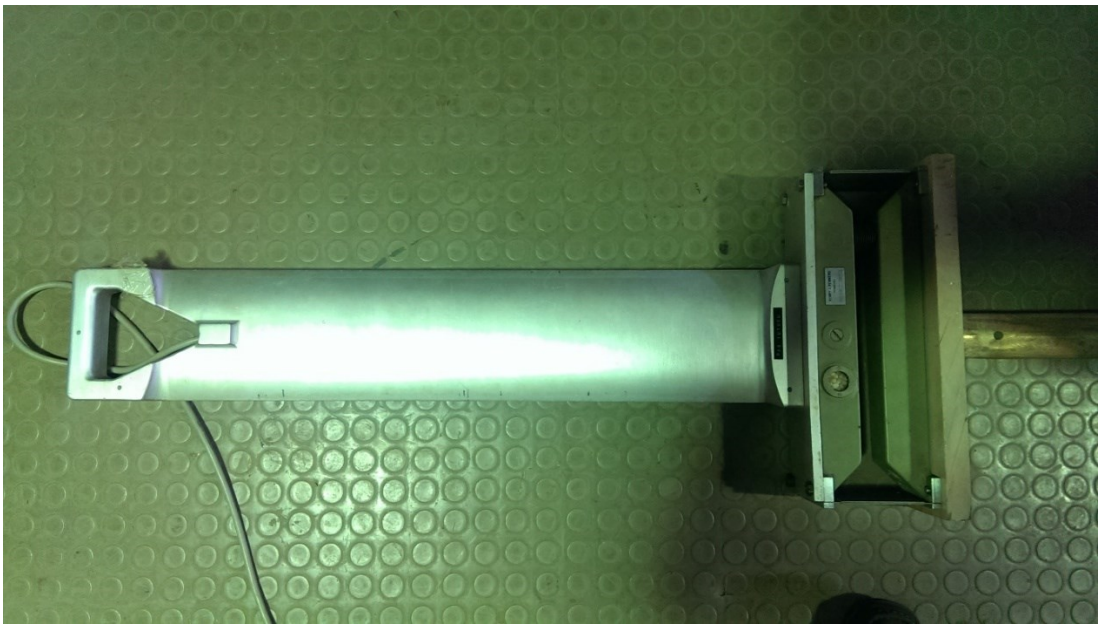

Figure 3.10 : One-component resistance dynamometer.

Dynamometer is connected to amplifier which is an electronic device that increases the power of a signal with the help of wire, as seen in Figure 3.11.

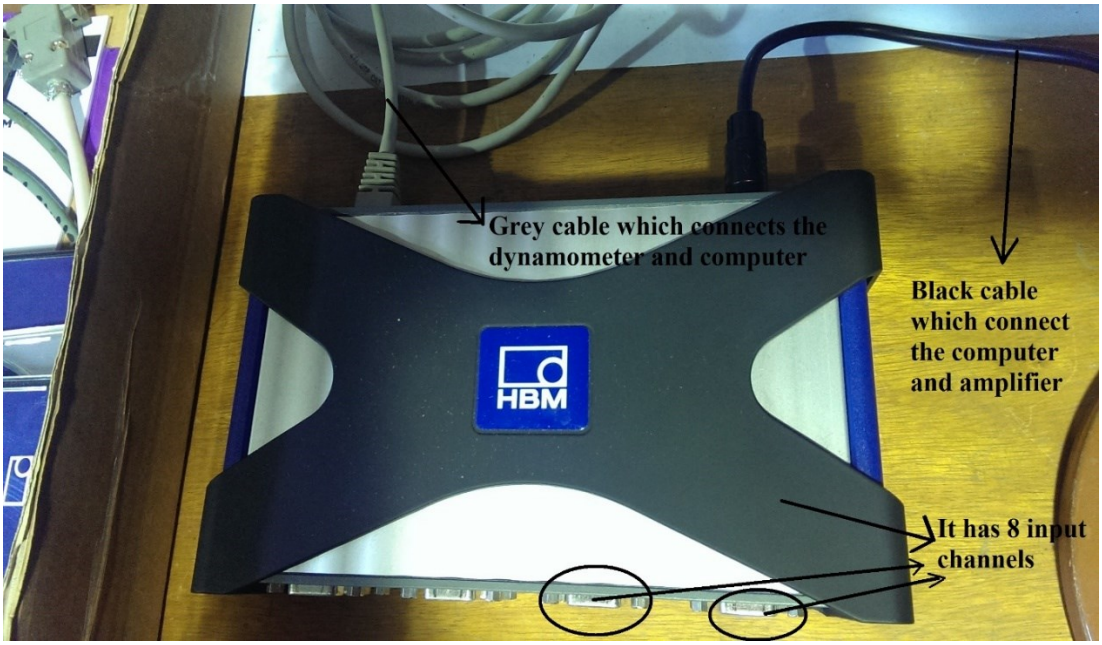

Figure 3.11 : Amplifier.

After the calibrations of the dynamometer have been done out of the water, then a connecting element which is made from rigid plank was manufactured in Ata Nutku Laboratory workshop. Since the strut is heavy, the plank provides a rigid connection between the strut and dynamometer to decrease the vibration and increasing the

rigidity while performing the experiments. Figure 3.12 illustrates the connection between strut and dynamometer.

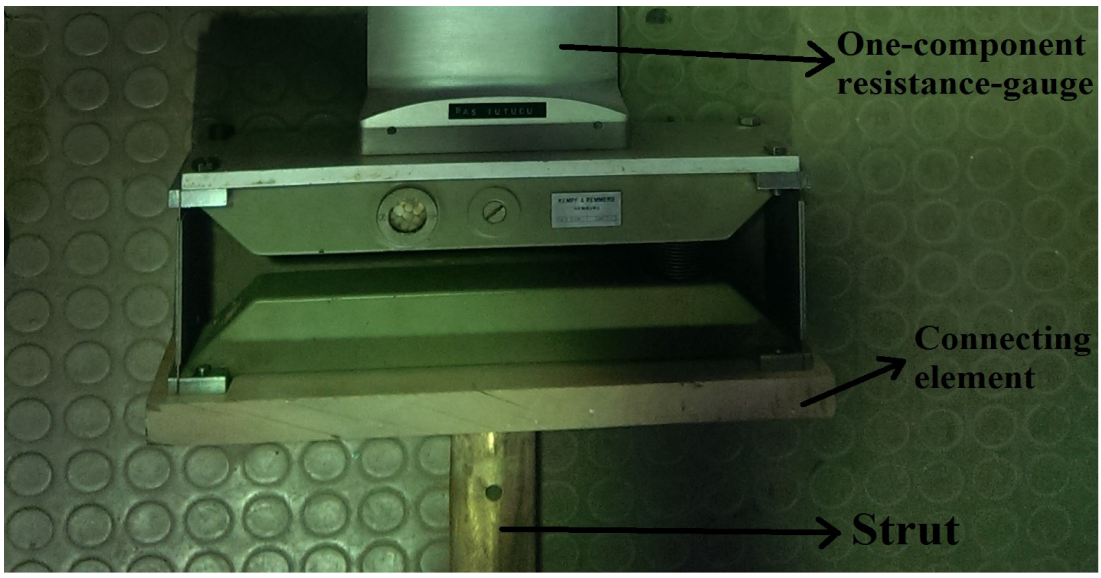

Figure 3.12 : Connecting element.

Consequently, the final experimental setup scheme is basically shown in Figure 3.13. The model was towed for two times in all Froude numbers and depths to determine the experimental errors and uncertainties.

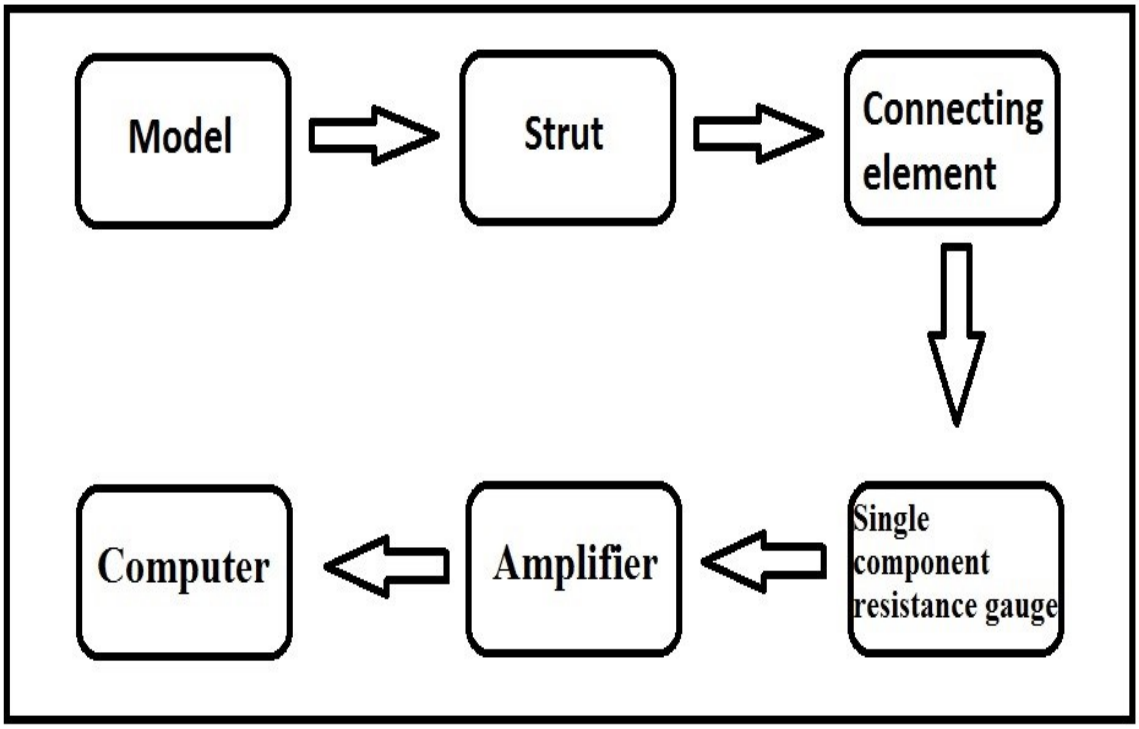

Figure 3.13: Experimental scheme for the ellipsoid.

3.5 Data Recording

Recording of the experimental data was done by using CatmanEasy software package. Before beginning to each run, zero reading of the force was taken. After this step, forces were recorded for approximately 10-15 seconds when the carriage velocity had stabilized. A plot of the measured force (N) as a function of time was created by the help of a computer. A capture, as seen in Figure 3.14, was taken during the experiments. Waiting period is at least ten minutes to ensure that the water in the towing tank is settled adequately so as not to effect the results.

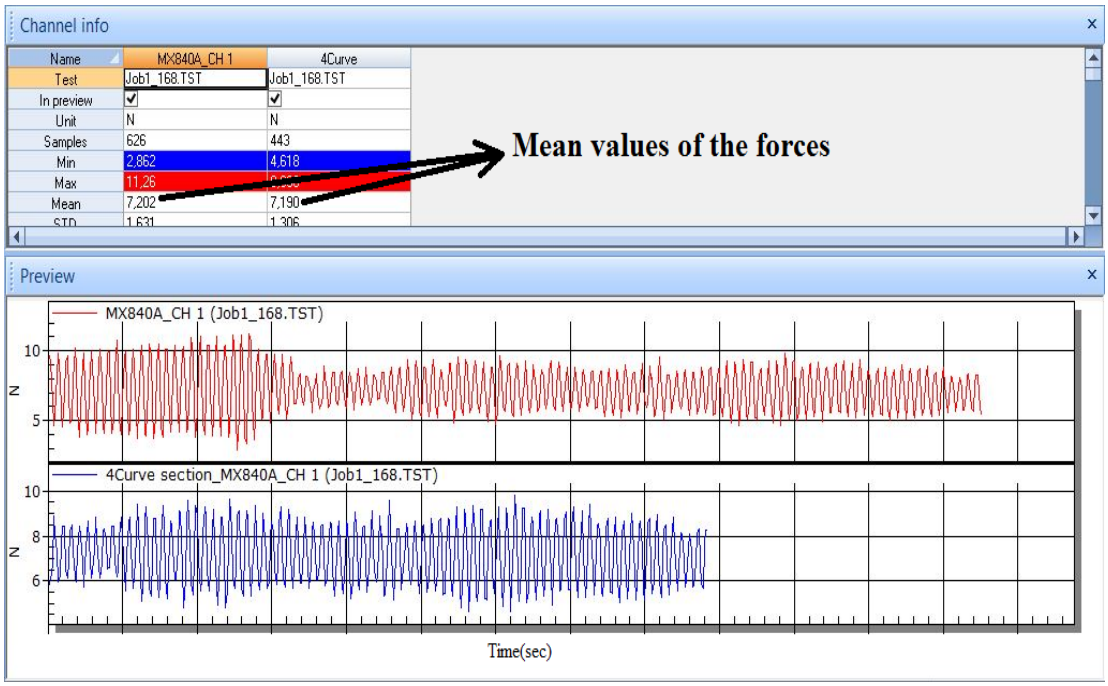

Figure 3.14: A capture of the measured force from CatmanEasy.

It should be noted that the red lined analysis illustrates the record from beginning to end. However, the blue line shows the record where the vibration is not occurred and the velocity of the carriage is stabilized. Hence the final resistance values were taken from these kind of intervals to get the accurate results.

4. RESULTS

4.1 Numerical Modeling of Fully Submerged Bodies

Hydrodynamic forces change as a submerged body gets closer to boundaries such as free surface or sea bottom. Otherwise, there is no interaction between free surface and submerged body in infinite depth. The most important difference between deeply submerged and near-free surface conditions is wave resistance factor. Deeply submerged conditions have only viscous pressure resistance and frictional resistance. As it gets closer to the boundary defined by the free surface; wave resistance is added and becomes a major part of total resistance.

4.1.1 Ellipsoid

4.1.1.1 Geometry and Meshing Strategy

An ellipsoid is selected as a benchmark problem due to its simple geometry. Since several works with different AR (aspect ratio) exist in literature, the proposed method can solely compared with other experimental and computational results. Aspect ratio of the ellipsoid model used in this study is selected as approximately 8 which is suitable for the Farrell's work to compare the results. Geometry is shown in Figure 4.1 and where b denotes the diameter and c is the chord length.

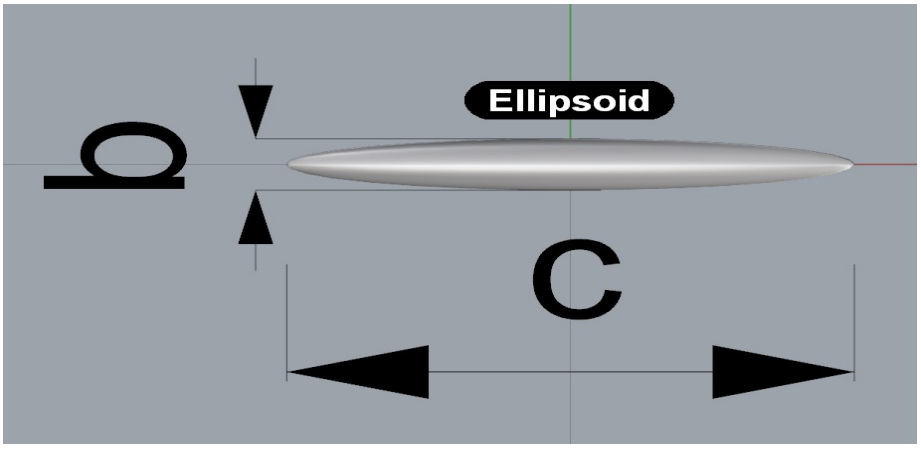

Figure 4.1 : Geometry of the ellipsoid model (profile view).

As widely known, wave elevations for fully submerged bodies in finite depth are generally smaller than surface piercing bodies due to the depth and Froude number.

The grid quality is directly relevant with grid type and mesh configuration. In certain cases, using tetrahedral cell is adequate to obtain accurate results. Also using tetrahedral/prism type grids shorten the solution time considerably in comparison with constructing with hexahedral mesh. Especially at high Froude numbers either in fully submerged and surface piercing conditions, wave pattern and resistance values are generally satisfactory due to the increasing wave elevations and converges to steady condition physically. However, it is nearly impossible to get not only proper Kelvin wave pattern but also sensible resistance values at lower Froude numbers for deeper conditions or surface piercing cases in steady solutions.

The strategy that is used for the meshing process is generate unstructured tetrahedral mesh around the ellipsoid and hexahedral mesh on free surface and air. An overall mesh configuration around the ellipsoid is given in Figure 4.2. As explained in the previous section, hexahedral cells were used around the free surface is convenient for this case (fully submerged condition) because of the smaller wave elevations on the free surface.

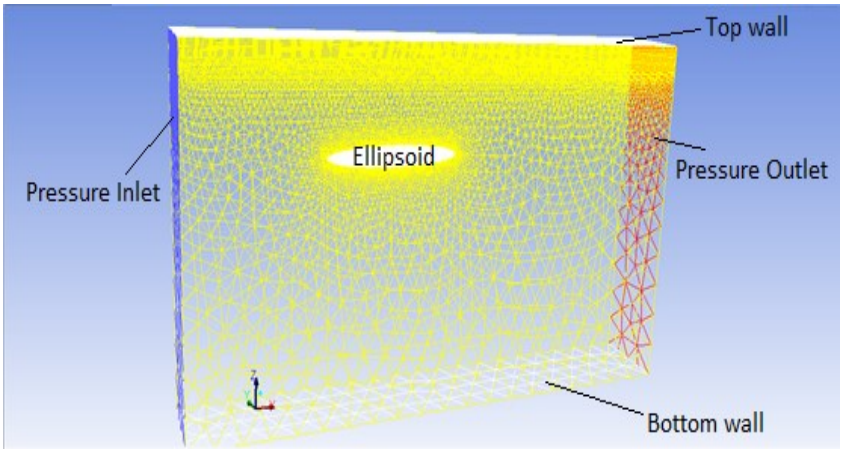

Figure 4.2: Overall mesh configuration.

The meshing process is completed by checking on the mesh to find any errors that may cause problems during the analysis. Resulting mesh has 1.2 million cells for all depths. Hexahedral mesh around free surface is shown in Figure 4.3. For this study the shape of the domain (fluid volume) is the box shape, since it is convenient for generating the mesh around the solid body. The domain extents are 4c in the flow direction (1L for upstream, 1L for the ellipsoid and 2L for downstream), 2L of in the depth direction and 1.25L in the direction of breadth is found to be appropriate for this study. In

addition to creating the fluid volume, naming the surfaces that represent the boundary conditions will help later with FLUENT setup. Also y^+ values are closely observed to remain between 30 and 300 during calculations.

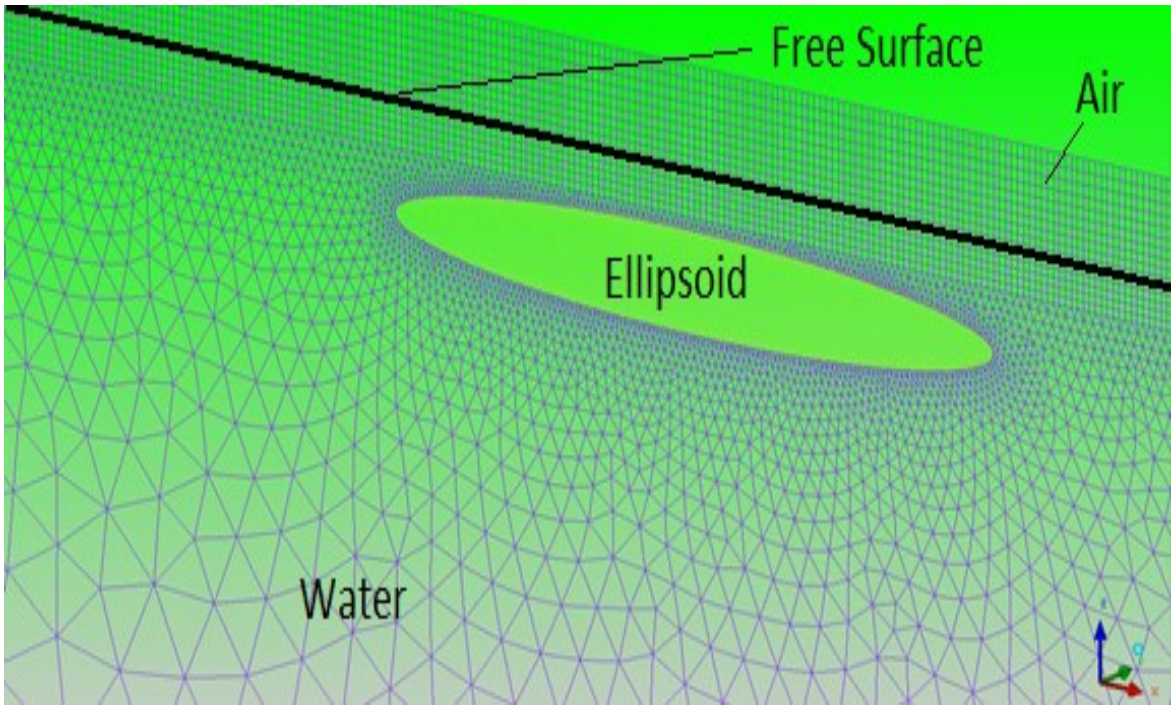

Figure 4.3: Mesh configuration around free surface.

The comparison of two different meshing methods are given in Table 4.1.

Table 4.1: Comparison of two different meshing methods.

Comparison of mesh types	
Tetrahedral Grids	**Hexahedral Grids**
• Less time consuming	• Better convergence characteristics
• Easier meshing for beginners	• Uses fewer elements
• Less effective at lower Froude numbers	• Accurate results at both low and high Froude numbers
• Mesh smoothing is automatic to increase mesh quality	• Ability to control manual meshing at all stages
• Compatible with all geometries	• Problematic for complex geometries

4.1.1.2 Numerical Settings

The CFD setup for single and multiphase analyses are all pressure based steady solutions. Steady-state solutions in all cases were performed to reduce the solution time. Wall functions may be used in places where adverse pressure gradients are not high. Flows around bluff bodies will generally have boundary layer separations of which the boundary layer should be very finely meshed all the way through the wall. Bodies inside water are generally well streamlined which allows wall functions to be used. In this study, standard wall function of realizable k-ϵ turbulence model is used. The SIMPLE algorithm is selected for pressure-velocity coupling and in spatial discretization pressure is set to be "Body force weighted". All the other parameters under spatial discretization and under-relaxation factors are at default that can be seen in Table 4.2.

Table 4.2: Default Under Relaxation Factors.

Under Relaxation Factors	
Pressure	0.3
Density	1
Body Forces	1
Momentum	0.7
Volume Fraction	0.5
Turbulent Kinetic Energy	0.8
Turbulent Dissipation Rate	0.8
Turbulent Viscosity	1

Besides that, volume fraction in spatial discretization is set to QUICK which was used for discretizing either the convection and diffusion terms [3]. One difference between these analyses of an ellipsoid is, inlet is "velocity inlet" in single phase and "pressure inlet" in multiphase analysis. Open channel flow of multiphase analysis only works with boundary conditions of "mass flow inlet" and "pressure inlet" and out of the two, pressure inlet is selected. Flow specification method at the inlet is "free surface level and velocity" where the user must specify the vertical coordinates of free surface level and the bottom of the domain. The velocity magnitude specified in pressure inlet of open channel in multiphase flow is also used as an input for the "velocity inlet" in single phase flow. All of these settings are shown in Table 4.3 and Table 4.4, respectively.

Table 4.3: Numerical Settings of the Ellipsoid for Single-Phase.

Numerical Set-up		
		Single-phase
General	**Type**	Pressure Based
	Time	Steady
	Velocity Formulation	Absolute
Models	**Turbulance model**	k-ε, Realizable
	Near Wall Treatment	Standard Wall Func.
Boundary Conditions	**Inlet**	Velocity Inlet
	Outlet	Pressure Outlet
	Turbulent Intensity(%)	1
	Turbulent Viscosity Ratio	1
Solution Methods	**Pressure-Velocity Coupling**	SIMPLE
	Gradient	Least Squares Cell Based
	Pressure	Second Order Upwind
	Momentum	Second Order Upwind
	Turbulent Kinetic Energy	Second Order Upwind
	Turbulent Dissipation Rate	Second Order Upwind
Solution Controls	**Under - Relaxation Factors**	Default
Solution Initialization	**Initialization Method**	Standard Initialization
	Reference Frame	Relative to Cell Zone

Table 4.4: Numerical Settings of the Ellipsoid for Multi-Phase.

Numerical Set-up		
		Multi-phase
General	**Type**	Pressure Based
	Time	Steady
	Velocity Formulation	Absolute
Models	**Multiphase model**	Volume of Fluid
	Scheme	Implicit
	Body Force Formulation	Implicit Body Force
	Number of Eularian Phases	2
	Options	Open Channel Flow
	Turbulance Model	k-ε, Realizable
	Near Wall Treatment	Standard Wall Func.
Boundary Conditions	**Inlet**	Pressure Inlet
	Outlet	Pressure Outlet
	Operating Density(kg/m3)	1.225
	Gravity (m/s2)	-9.81
	Turbulent Intensity(%)	1
	Turbulent Viscosity Ratio	1
Solution Methods	**Pressure-Velocity Coupling**	SIMPLE
	Gradient	Least Squares Cell Based
	Pressure	Body Force Weighted
	Momentum	Second Order Upwind
	Volume Fraction	QUICK
	Turbulent Kinetic Energy	Second Order Upwind
	Turbulent Dissipation Rate	Second Order Upwind
Solution Controls	**Under - Relaxation Factors**	Default
Solution Initialization	**Initialization Method**	Standard Initialization
	Open Channel Initialization Method	Flat
	Reference Frame	Relative to Cell Zone

4.1.1.3 Validation and Results for a Fully Submerged Ellipsoid

The first validation of the proposed method was first made for a fully submerged body under free surface. Comparison of the wave resistance coefficient was made with Farrell's study. The length of this ellipsoid is same as the previous model whose CFD results are compared with experiment, however this model has an aspect ratio of 6.

The results of the first ellipsoid which has an aspect ratio of 6 are compared with the results of Farrell who has solved the flow around an ellipsoid at different aspect ratios [7]. He has used potential flow theory to generate his results and the comparison is made for an aspect ratio of 6. The distance of the free surface to the ellipsoid is 0.126c. The wave resistance is calculated with the method explained in the "CFD Methodology" section above and it is non-dimensionalized by the formulation given in Farrell's study:

$$C_W = \frac{R_W}{\pi \rho g c^3}$$

The results of the wave resistance coefficient in comparison with Farrell's work are shown in Figure 4.4. The wave resistance coefficients in both studies seem in accordance with each other.

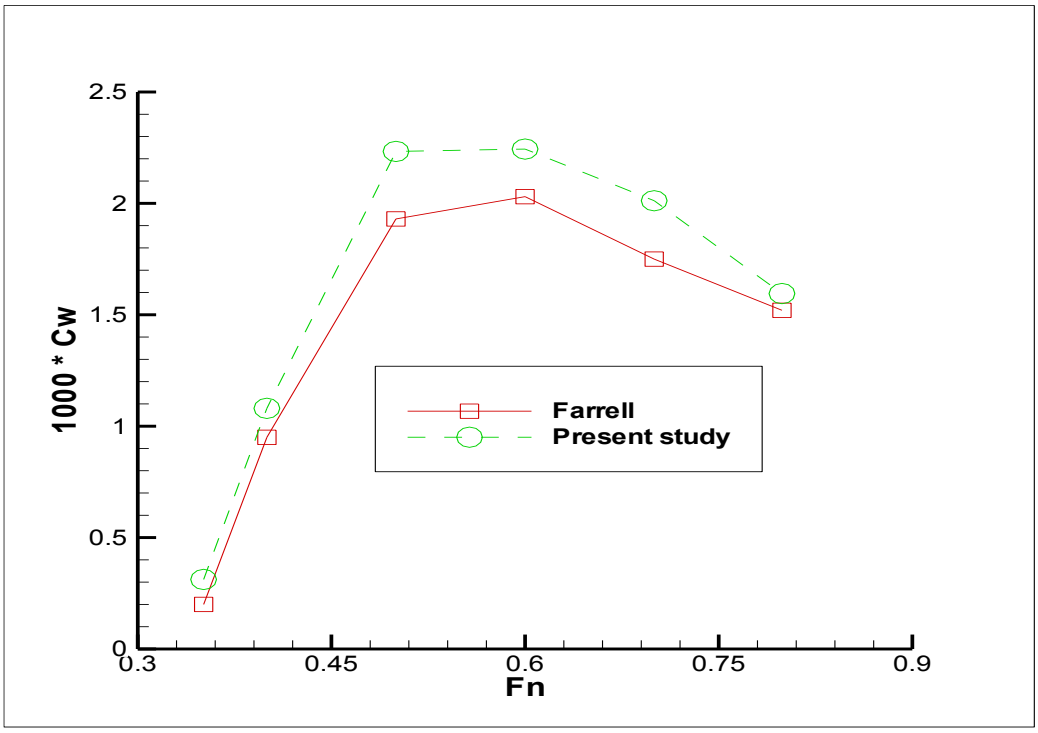

Figure 4.4: A comparison of wave resistance coefficients. (h/c= 0.126).

As it mentioned before, meshing strategy plays a crucial role in this section for the accuracy of viscous solutions. If the grid resolution and grid quality are not sufficiently good, wave contours are not accurate at low Froude numbers. Please see the Figure 4.5.

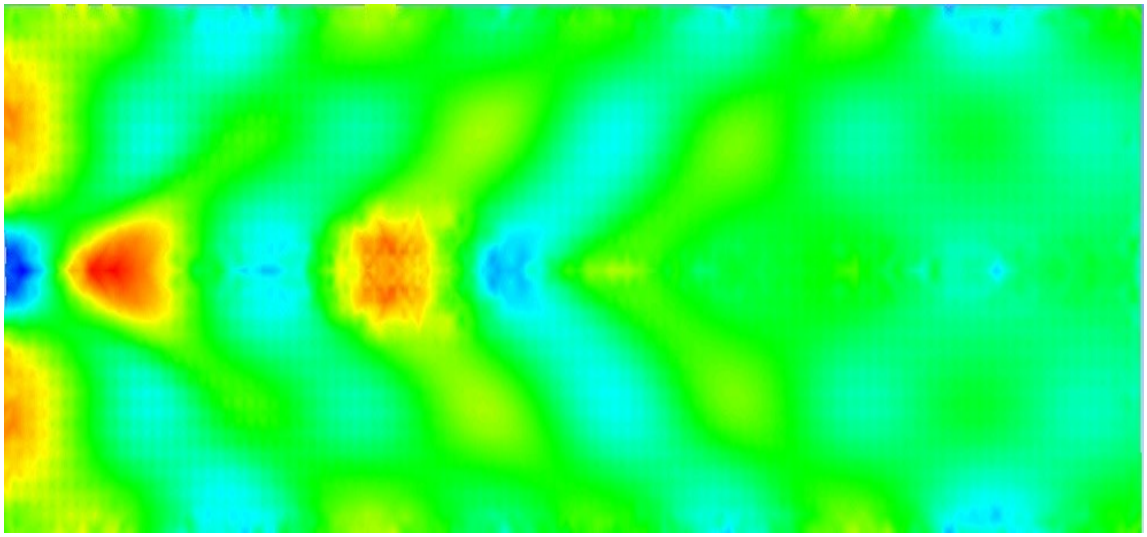

Figure 4.5 : Wave pattern obtained after using tetrahedral mesh for entire domain.

The compatibility of the results seem better for lower Froude numbers and the discrepancy between both studies seem to get greater as the Froude number increases. There seems to be only one point where both results overlap at around Fn=0.78; but then the results seem to go in different paths. This difference at high Froude numbers may be due to more violent wave patterns that may be observed at higher speeds where the linearized potential flow theory fails to grab the correct wave contours. RANSE is fully non-linear and is more pertinent to catch wave patterns at higher speeds. In addition, the submergence depth ratio (h/c=0.126) for this case is so small that the nonlinearities on the free surface become dominant.

A second validation was made again for an ellipsoid which has an aspect ratio of 8. This time comparison was made with experimental results for Froude numbers of 0.16 to 0.48 and different h/c ratios of 0.3, 0.5 and 0.75 where the h is distance from the free surface and c is the length of the model.

The experimental results of the total resistance and also frictional resistance coefficients were compared with CFD results for varying depths are shown below:

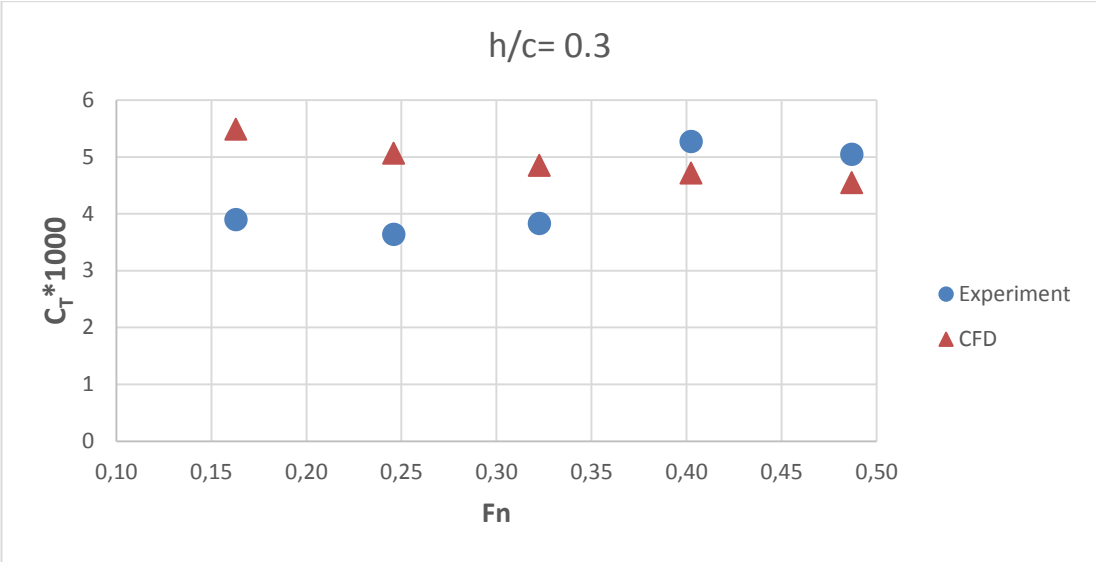

Figure 4.6 : A comparison of total resistance coefficients (h/c= 0.3).

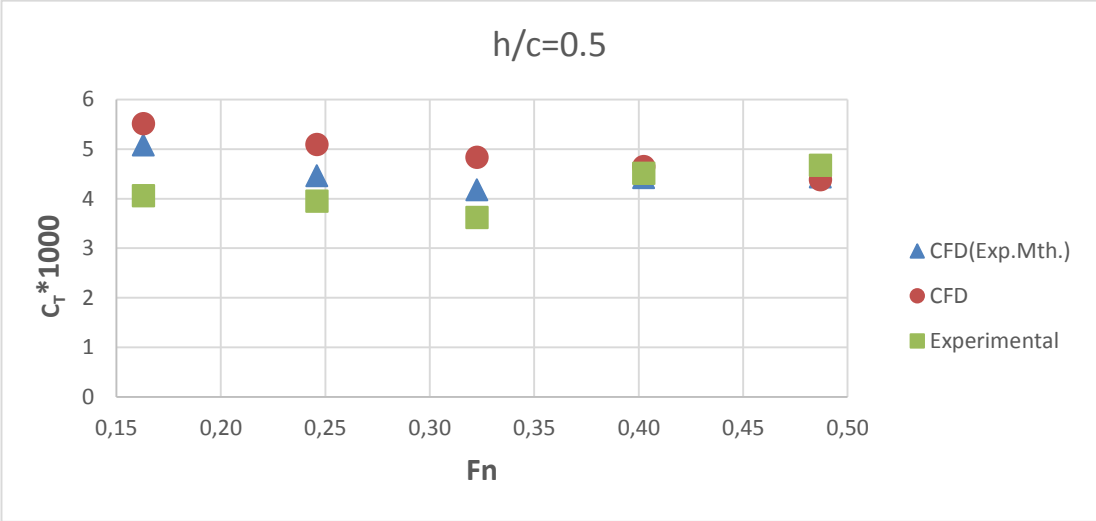

Figure 4.7 : A comparison of total resistance coefficients (h/c= 0.5).

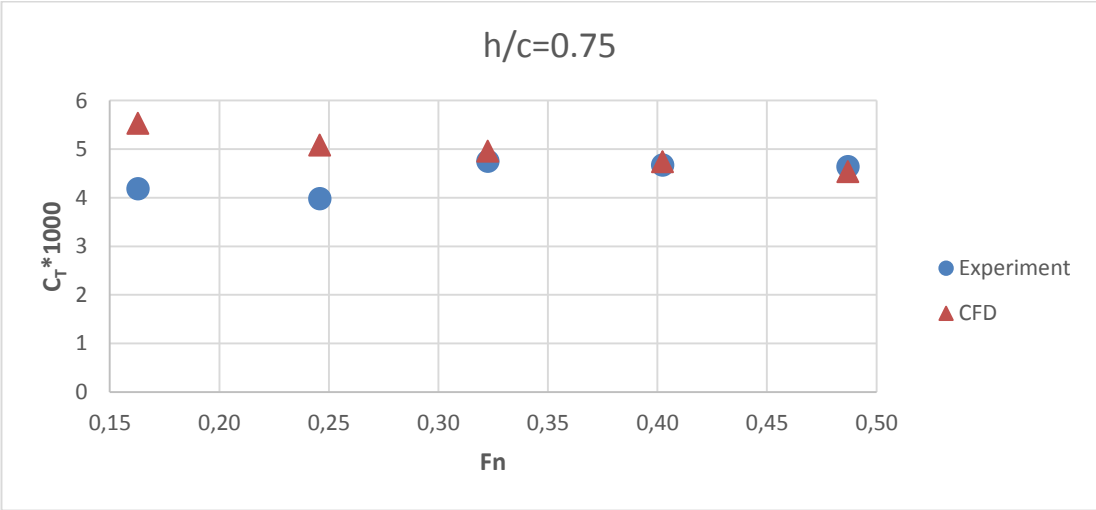

Figure 4.8 : A comparison of total resistance coefficients (h/c= 0.75).

Towing tests were performed two times to see that the results are consistent and then the obtained results were averaged. An uncertainty analysis which is completed using the methods of ITTC is implemented to those of the experimental results [26]. It was calculated from two repeated runs under the same condition. It would be possible to repeat more runs to obtain efficient results, however there is no time to repeat much more towings due to its time consuming process. For the best determination of uncertainities ITTC recommends the use of up to 15 repeats in experiments. The average uncertainty of total resistance was calculated at 20% for the condition of h/c=0.3.

In Figure 4.7, experimental method is implemented in CFD to show the accuracy of the method that the model is towed with the help of a strut. A satisfactory agreement is obtained with the results. On the other hand, the maximum variation of CFD results with respect to experimental results is about 20 percent at low Froude numbers whilst the average variation at high Froude numbers is about %4-5.

ITTC 57' formulation is normally implementable for surface piercing bodies which has a length to beam ratio with the range of 5 to 7. However, the comparison of frictional resistance coefficients which can be seen in Figure 4.9 seem in accordance with each other for a totally submerged body.

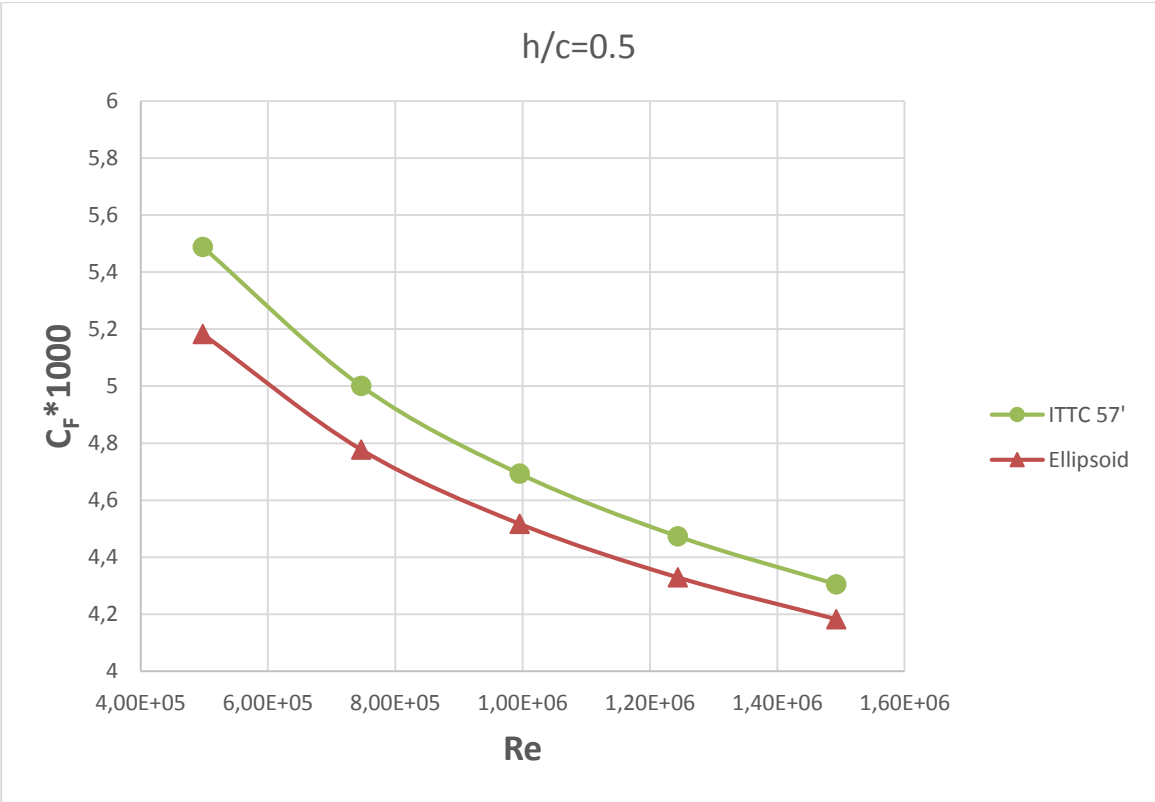

Figure 4.9 : A comparison of frictional resistance coefficients for the ellipsoid.

The wave pattern for another fully submerged ellipsoid at different submergence depths for an aspect ratio of 6 are obtained by RANSE for the whole domain. The results of the wave patterns at Fn=0.7 are given in Figure 4.10. Also, the wave contour of first ellipsoid which was compared with Farrell's study at Fn=0.7 for h/c=0.126 is given with longitudinal wave cut shown at Figure 4.11.

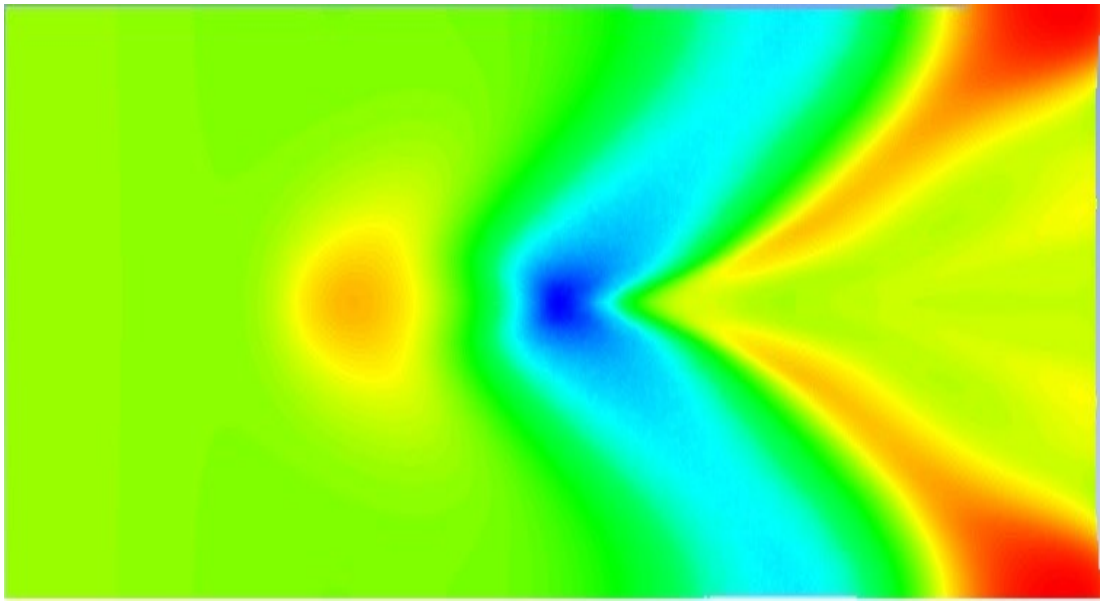

Figure 4.10 : Wave contour of a submerged ellipsoid at Fn=0.7 for h/c=0.126.

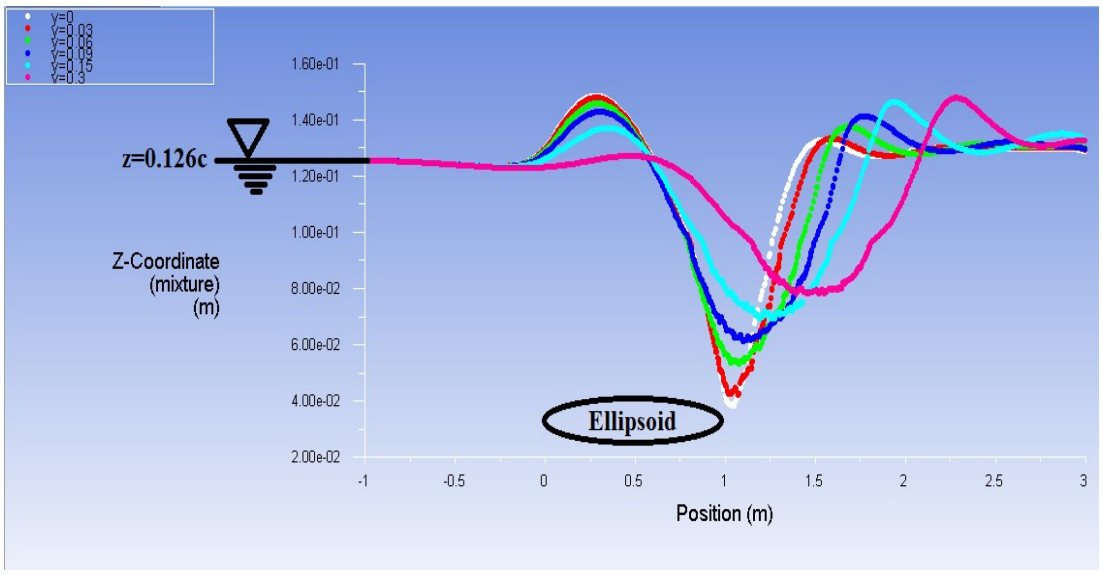

Figure 4.11 : Wave-cuts of a submerged ellipsoid at Fn=0.7 for h/c=0.126. (Ellipsoid is not scaled in z direction)

Due to the limited fluid domain at the computations the radiation condition cannot be seen from Figure 4.11. However, it is possible to visualize the radiation of the waves at both ends of the domain but this is a matter of time and capability as greater domains require more time and memory.

Respectively, Figure 4.12 exhibits the free surface effect depending on the depth and pressure coefficient distribution over the ellipsoid at Fn=0.5 for finite and infinite depths.

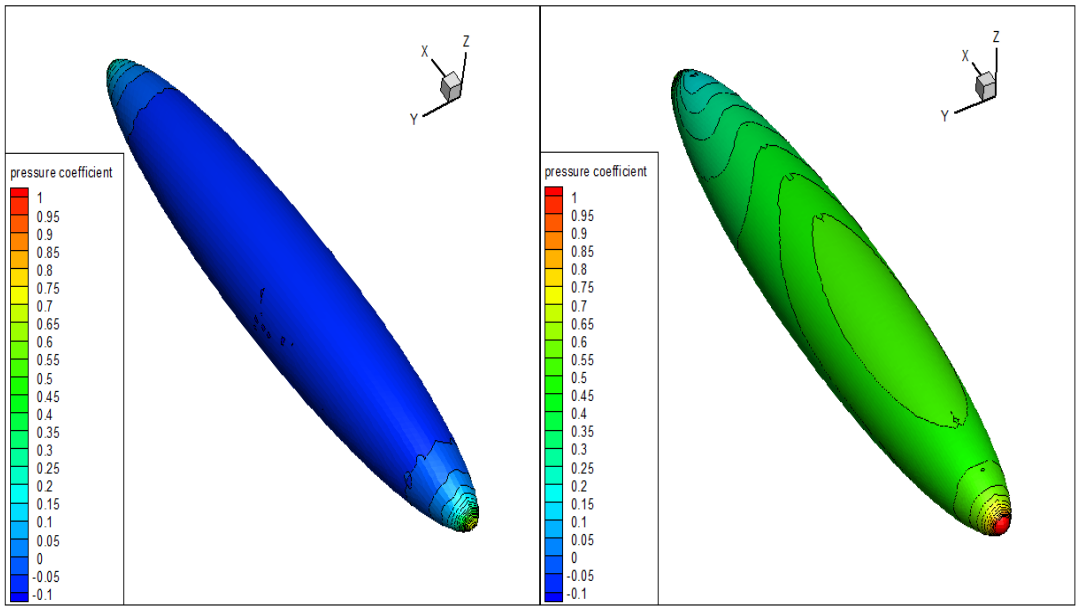

Figure 4.12 : Free surface effect on pressure coefficient distribution over the Farrell's ellipsoid. The figure on the left is at infinite depth while the one on the right has submergence depth (h=0.126c) from the free surface and Fn=0.5.

4.1.2 Submarine

4.1.2.1 Geometry and Meshing Strategy

After getting the resistance results with the experiment are found compatible with CFD for the ellipsoid, the next step is to create a new submarine model. The model is tried to be kept simple with the addition of appendages such as the topsail and the fins to the ellipsoid. Please refer to Figures 4.13, 4.14 and 4.15 to see the locations of these appendages. Main dimensions are kept the same with the ellipsoid and the size of appendages is set arbitrarily. Figure 4.13 and 4.14 shows the submarine geometry and the appendages are shown in Figure 4.15. As it is mentioned in the previous chapter; c represents the length and b is diameter.

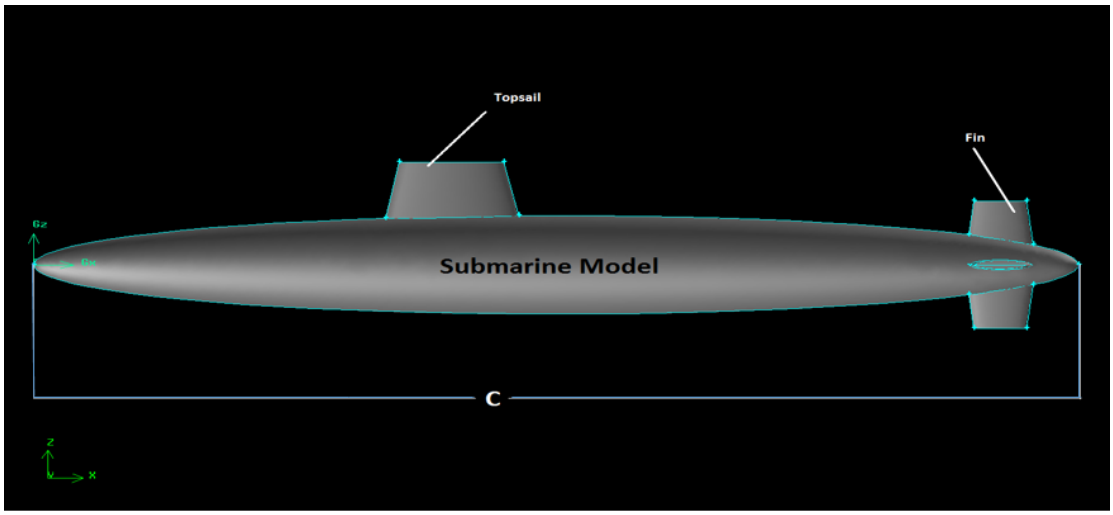

Figure 4.13 : Submarine model geometry (profile view).

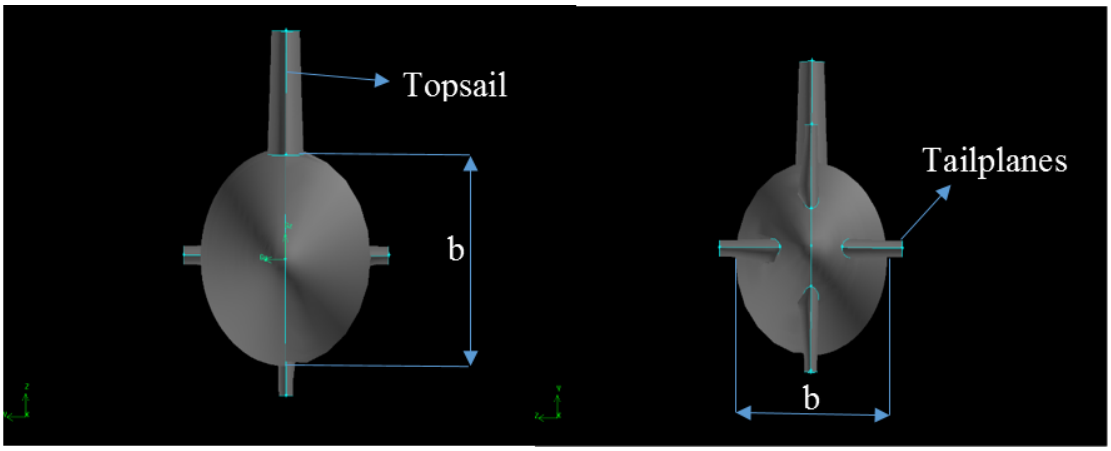

Figure 4.14 : Submarine model geometry (front and rear view).

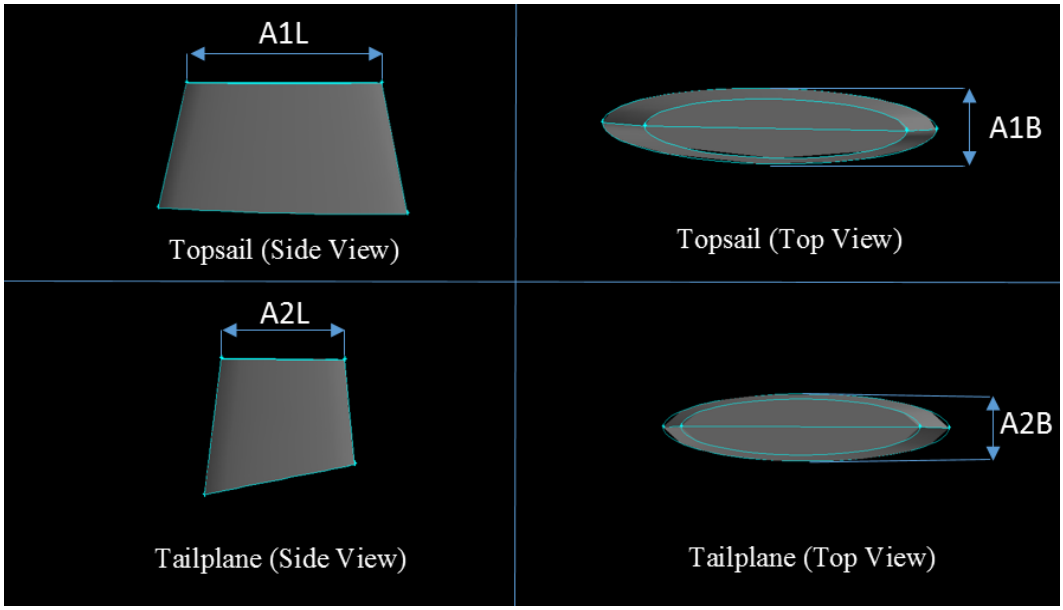

Figure 4.15 : Appendages of submarine model (side and top views).

A1L denotes the length of the topsail and A1B shows the maximum breadth. Similarly, A2L refers to the length of the tailplane and A2B describes its maximum breadth. There are four fins on the aft side of the submarine model and each have the same dimensions. Figure 4.15 may be referred to see the geometry of all these fins. Dimensions of these parts are given below, please see Table 4.5.

Table 4.5: Dimensions of Topsail and Tailplanes.

	A1L(m)	A1B(m)	A2L(m)	A2B(m)
Topsail	0.1	0.01	N/A	N/A
Tailplanes	N/A	N/A	0.05	0.035

Mesh processing of the submarine for single phase analyses was carried out by using ICEM CFD that has a good capability with the ease of quick and good quality meshing for tetrahedral elements. Maximum element size in the entire domain was defined in 'Global Mesh Setup'. Increasing mesh size with certain growth rate from the body to the domain boundaries was determined by using 'Part Mesh Setup' option. In addition to these settings, a denser mesh box was created to represent the turbulence region around topsail and tailplane zones due to expected flow separation over these chaotic zones. Since wave deformation is not a case in single-phase analyses, using tetrahedral elements for meshing is convenient. It is enough to quickly converge single phase analyses and provide a significant advantage to the user to obtain desired frictional resistance results quickly. The major difference between the single phase and the multi-phase analyses is the contribution of free surface effect which needs better meshing inside the domain.

In multi-phase analyses, a new volume is created for free surface additively and it was meshed with fine hexahedral grids by using Gambit in order to represent the wave elevations accurately especially in low Froude numbers. Figure 4.16 illustrates regions of denser mesh around the appendages and shows the hexahedral meshes on free surface.

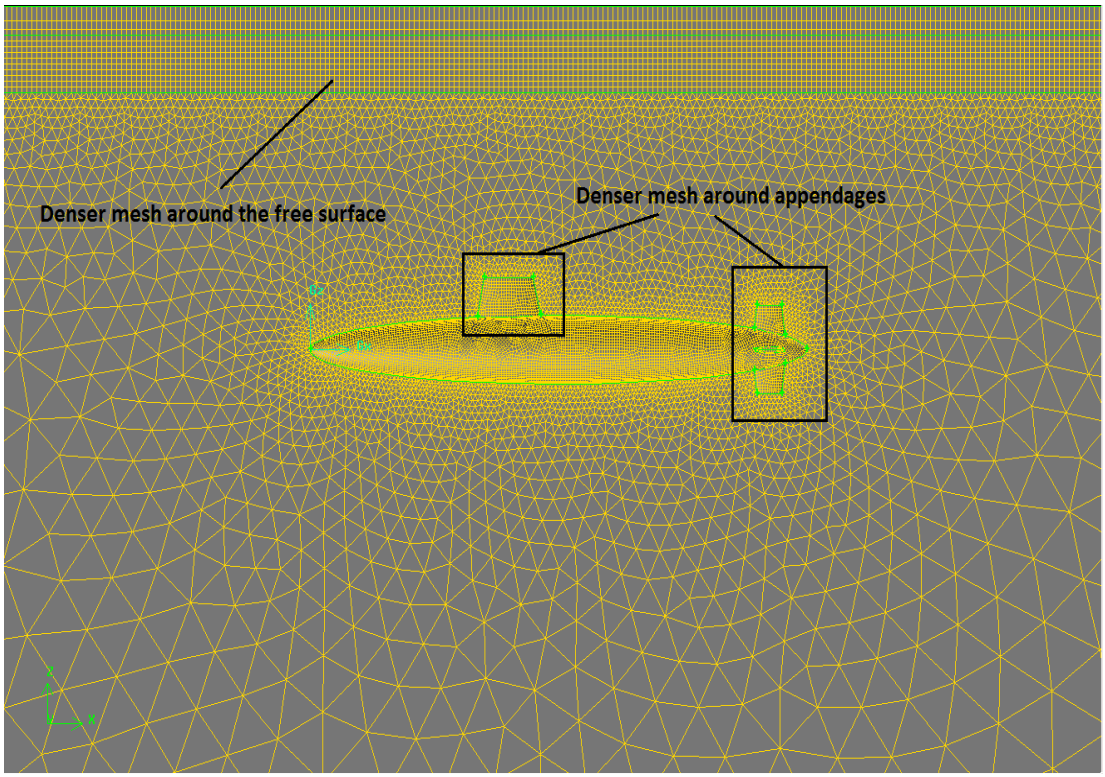

Figure 4.16 : Mesh configuration around free surface and appendages.

Boundary conditions are easily defined in ICEM CFD or Gambit before exporting the mesh file to the FLUENT solver. Special attention must be paid while determining the boundary conditions for single phase analyses; the top side of the domain must be defined as 'Symmetry' in order to create double body solution and to get the accurate viscous pressure value. Also mesh smoothing may be necessary to improve the mesh quality. The mesh quality is increasing from 0 to 1 in ICEM CFD while it is vice versa in Gambit.

The user can smooth the meshes automatically in ICEM CFD by entering the input values which are 'Smoothing Iterations and 'Up to value'. The process is completed by performing a check on the mesh to find any errors which may cause a problem during the analyses in FLUENT. Gambit is an older technology and does not support mesh smoothing.

4.1.2.2 Numerical Settings

Simulation of the submarine is nearly the same with previous benchmark problem. The effect of the appendages to the total resistance of the body may also be observed in comparison to the ellipsoid. As it may be detected by just looking at the body forms of the ellipsoid and the submarine; ellipsoid is a streamlined body and the submarine

is a more complex body in contrast to the ellipsoid. Therefore, flow separation from the body is an incident which may occur; and this will also be examined for the submarine model.

Flow model which is selected from the model setup is set to viscous and the selected turbulence model for the simulations is the realizable k – ε turbulence model. Standard wall functions is chosen as it also was in the previous application. Multiphase flow model is selected to characterize the free surface deformations and its effect on the submarine. VOF model is used for multiphase analysis and implicit scheme is defined as volume fraction parameter. For all the applications involving multi-phase analyses found in this thesis, open channel flow option is selected. Also body force formulation is set to implicit body force. Especially in low Froude numbers, if the residuals continued to increase after a number of iterations, the under relaxation factors were then reduced.

Analyses were performed for the submarine and compare the results with the ellipsoid. Please refer to Table 4.6. This way, the effect of the appendages on the resistance can be detected.

Table 4.6: Analysis parameters for the submarine.

Analysis	h/c	Fn_c	Fn_d
1	0.5	0.1596	0.2258
2	0.5	0.2395	0.3386
3	0.5	0.3193	0.4515
4	0.5	0.3991	0.5644
5	0.5	0.4789	0.6773

A summary for single and multi-phase analysis setups are shown in Tables 4.7 and 4.8, respectively.

Table 4.7: Numerical Settings of the Submarine for Single-Phase.

Numerical Set-up		
		Single-phase
General	**Type**	Pressure Based
	Time	Steady
	Velocity Formulation	Absolute
Models	**Turbulance model**	k-ε, Realizable
	Near Wall Treatment	Standard Wall Function
Boundary Conditions	**Inlet**	Velocity Inlet
	Outlet	Pressure Outlet
	Turbulent Intensity(%)	1
	Turbulent Viscosity Ratio	1
Solution Methods	**Pressure-Velocity Coupling**	SIMPLE
	Gradient	Least Squares Cell Based
	Pressure	Second Order Upwind
	Momentum	Second Order Upwind
	Turbulent Kinetic Energy	Second Order Upwind
	Turbulent Dissipation Rate	Second Order Upwind
Solution Controls	**Under - Relaxation Factors**	Depending on the behavior of residuals
Solution Initialization	**Initialization Method**	Standard Initialization
	Reference Frame	Relative to Cell Zone

Table 4.8: Numerical Settings of the Submarine for Multi-Phase.

Numerical Set-up		
		Multi-phase
General	**Type**	Pressure Based
	Time	Steady
	Velocity Formulation	Absolute
Models	**Multiphase model**	Volume of Fluid
	Scheme	Implicit
	Body Force Formulation	Implicit Body Force
	Number of Eularian Phases	2
	Options	Open Channel Flow
	Turbulance Model	k-ε, Realizable
	Near Wall Treatment	Standard Wall Function
Boundary Conditions	**Inlet**	Pressure Inlet
	Outlet	Pressure Outlet
	Operating Density(kg/m3)	1.225
	Gravity (m/s2)	-9.81
	Turbulent Intensity(%)	1
	Turbulent Viscosity Ratio	1
Solution Methods	**Pressure-Velocity Coupling**	SIMPLE
	Gradient	Least Squares Cell Based
	Pressure	Body Force Weighted
	Momentum	Second Order Upwind
	Volume Fraction	QUICK
	Turbulent Kinetic Energy	Second Order Upwind
	Turbulent Dissipation Rate	Second Order Upwind
Solution Controls	**Under - Relaxation Factors**	Depending on the behavior of residuals
Solution Initialization	**Initialization Method**	Standard Initialization
	Open Channel Initialization Method	Flat
	Reference Frame	Relative to Cell Zone

4.1.2.3 Results for a Fully Submerged Submarine

The effects of the appendages of the submarine on the total resistance is investigated and observed at different Froude numbers for only one depth. Please see the Table 4.9 and Figure 4.17. As it is mentioned before, the submarine model is tried to be kept simple with the addition of appendages such as the topsail and the fins to the ellipsoid.

Table 4.9 : The effects of the appendages on the total resistance.

Fn	Total Resistance (N) Ellipsoid	Total Resistance (N) Submarine	Variations in total resistance respect to the ellipsoid (%)
0.2258	0.2089	0.2813	25.7
0.3387	0.4335	0.5909	26.6
0.4516	0.7296	1.0092	27.7
0.5645	1.0958	1.5339	28.6
0.6774	1.4864	2.2078	32.7

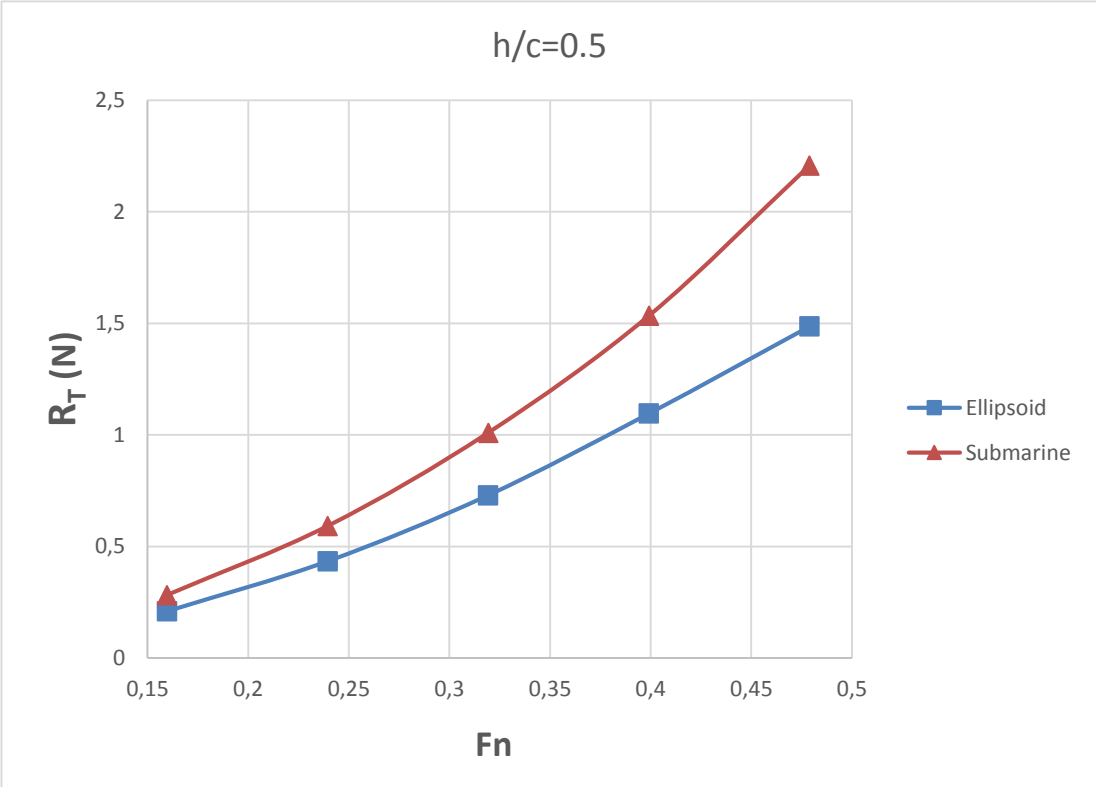

Figure 4.17 : Comparison of total resistance at h/c= 0.5.

According to Table 4.9, contribution of the topsail and fins on the total resistance approximately thirty percent. It can also be seen that depending on the increase in Froude number, variations in total resistance slightly grows up. The reason is that the formation of eddy viscosity depending on the velocity where the flow seperation occurs. The dimensions and locations of the fins and topsails are determined arbitrarily, however by making the appendages more streamlined, then the total resistance can be reduced.

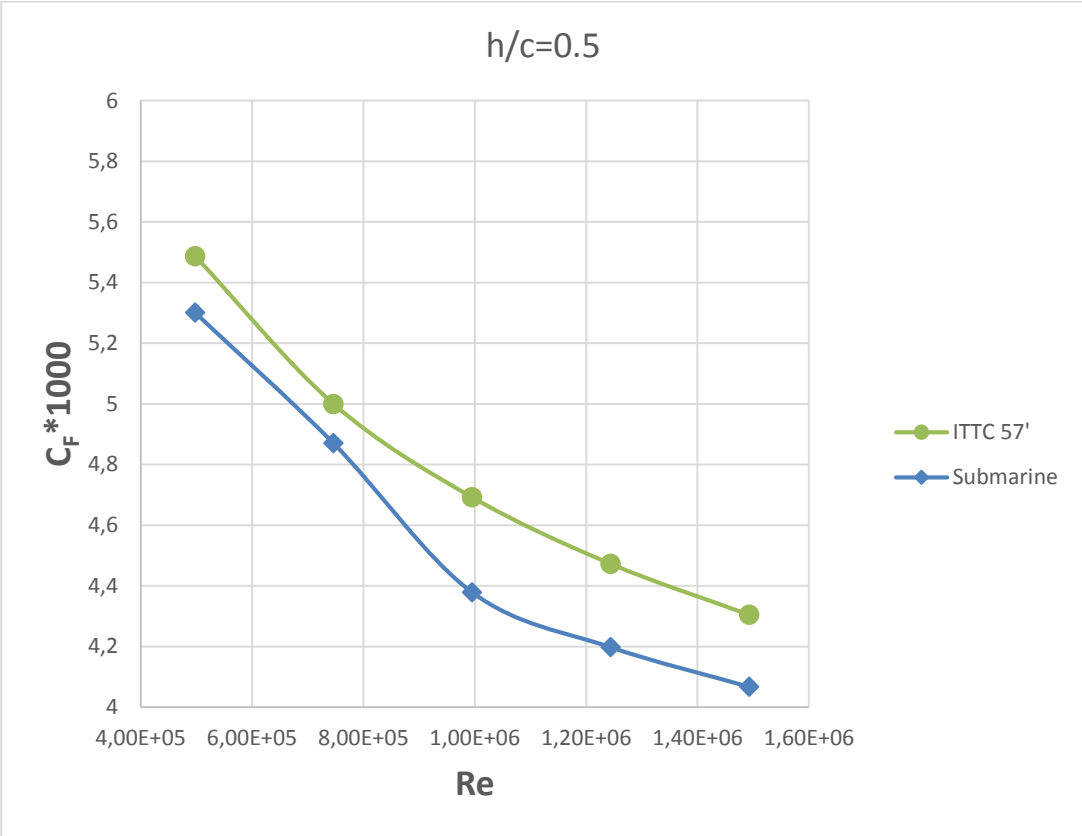

Figure 4.18 : Comparison of frictional resistance coefficients at h/c = 0.5.

Addition of the fins and top sails to the elipsoid changes the frictional resistance due to the increase in the wetted area. Total surface area of appendages is %10 of ellipsoid. A plot of the frictional resistance coefficient as a function of Froude number for ITTC and submarine is given in Figure 4.18. Also the comparison of frictional resistance for ellipsoid and submarine can be seen in Figure 4.19.

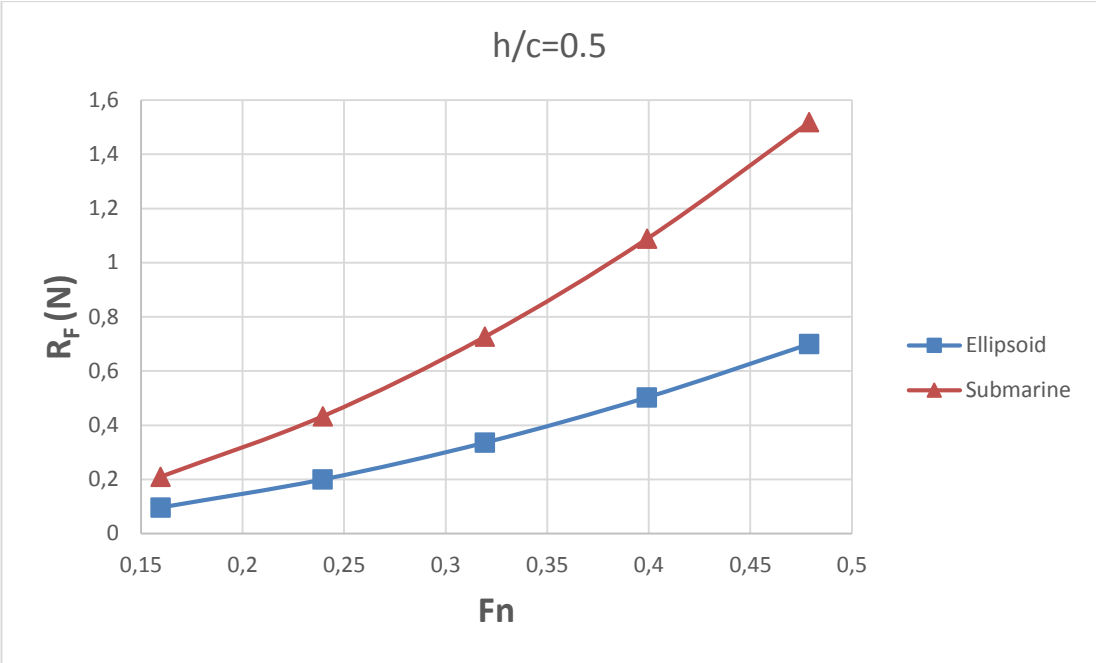

Figure 4.19 : Comparison of frictional resistance at h/c = 0.5.

4.2 Numerical Modeling of Surface Piercing Bodies

A RANSE based CFD method associated with the Volume of Fluid (VOF) method is employed to get the free surface wave flow around ship and multiphase flow has been carried out to compute the resistance forces of surface piercing bodies. Single phase analyses was performed and double body solution method was used at the same Froude numbers to get the viscous pressure force for obtaining the wave resistance accurately. Wave resistance is more dominant in this condition with compared to fully submerged bodies except the range of Prohaska (Fn =0.12-0.20). Since meshing the free surface zone with hexahedral elements is not easy as submerged bodies, hybrid mesh method was used to get accurate results. Entire domain was divided into 12 blocks and 11 blocks was meshed with fully hexahedral elements. Only one block where the ship is in was meshed with denser tetrahedral elements. Other numerical settings are explained in later chapters.

4.2.1 Wigley Parabolic Hull

4.2.1.1 Geometry and Meshing Strategy

Wigley parabolic hull is widely used test case for surface piercing problems since it has a simple geometry and there is a large amount of experimental and CFD data in the literature. In these analysis, a fully hexahedral mesh containing approximately 2.1 million cells was created for all Froude numbers by using Gambit. First, hull surface was meshed with quadrilateral elements. Please see Figure 4.20. Then, hexahedral mesh was used around free surface and entire domain. It is also shown in Figure 4.21. Domain extents are 1L upstream, 1L the Wigley hull itself and 2L downstream, L of depth and 0.5L of breadth; which seems sufficient.

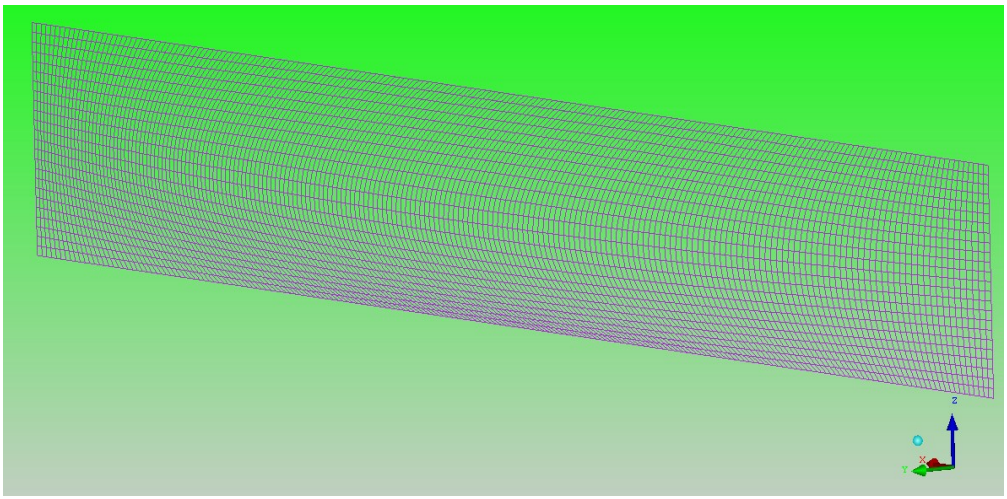

Figure 4.20: Mesh configuration on Wigley hull.

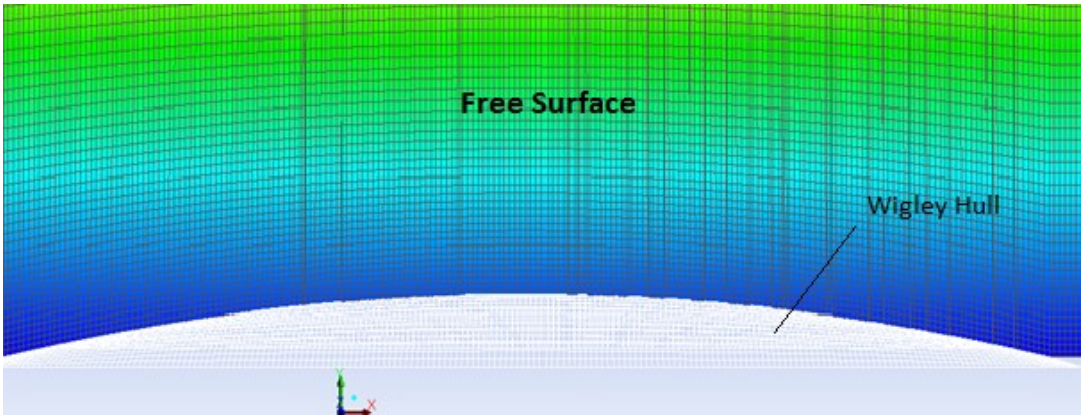

Figure 4.21: Hexahedral elements around Wigley hull (top view).

4.2.1.2 Numerical Settings

CFD setup strategy of the Wigley hull is similar to that of the ellipsoid. The purpose of this simulation is to obtain the wave resistance coefficient accurately in surface piercing condition. The settings for single and multiphase analyses are pressure based steady solutions. The turbulence model was selected as realizable k-ε with standard wall function. The SIMPLE algorithm is selected for pressure-velocity coupling and in spatial discretization, pressure is set to be "Body Force Weighted". Two phases were used in multiphase solutions and air was determined as primary phase while water was assigned as the secondary phase, as it is dictated for multiphase flows in ANSYS Fluent User Guide [24]. In addition to this, open channel flow mode was selected. Analyses are carried out using this option that is implemented inside ANSYS Fluent. Open channel mode allows simulations to be made that are similar to the experiments being made at the towing tanks. The free surface is still at the beginning; both experimentally and numerically. To dictate this condition numerically to the solver, open channel initialization method is selected as *flat*.

Because of the symmetrical characteristics of the flow, half of the domain was modelled and symmetrical boundary condition was used to reduce the mesh size and solution time. The final version of the boundary conditions adopted are shown in Figure 4.22.

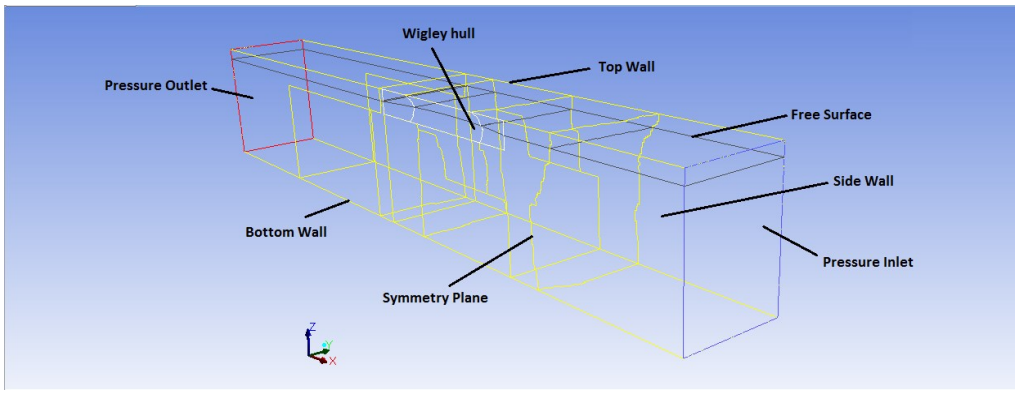

Figure 4.22: Boundary conditions of the Wigley hull.

It was mentioned that under-relaxation factors were set as default in the previous ellipsoid simulation due to its simple geometrical form and lack of turbulence at the stern side, whereas during the simulation of the Wigley hull, momentum and turbulence factors may partially be reduced to stabilize the governing equations and numerical instabilities at higher Froude numbers. All details to summarize the settings for single and multiphase were given in Table 4.10 and Table 4.11 respectively.

Table 4.10: Numerical Settings of the Wigley Parabolic Hull for Single-Phase.

Numerical Set-up		
		Single-phase
General	**Type**	Pressure Based
	Time	Steady
	Velocity Formulation	Absolute
Models	**Turbulance model**	k-ε, Realizable
	Near Wall Treatment	Standard Wall Func.
Boundary Conditions	**Inlet**	Velocity Inlet
	Outlet	Pressure Outlet
	Turbulent Intensity(%)	1
	Turbulent Viscosity Ratio	1
Solution Methods	**Pressure-Velocity Coupling**	SIMPLE
	Gradient	Least Squares Cell Based
	Pressure	Second Order Upwind
	Momentum	Second Order Upwind
	Turbulent Kinetic Energy	Second Order Upwind
	Turbulent Dissipation Rate	Second Order Upwind
Solution Controls	**Under - Relaxation Factors**	Reduced at higher Froude numbers manually
Solution Initialization	**Initialization Method**	Standard Initialization
	Reference Frame	Relative to Cell Zone

Table 4.11: Numerical Settings of the Wigley Parabolic Hull for Multi-Phase.

Numerical Set-up		
		Multi-phase
General	**Type**	Pressure Based
	Time	Steady
	Velocity Formulation	Absolute
Models	**Multiphase model**	Volume of Fluid
	Scheme	Implicit
	Body Force Formulation	Implicit Body Force
	Number of Eularian Phases	2
	Options	Open Channel Flow
	Turbulance Model	k-ε, Realizable
	Near Wall Treatment	Standard Wall Func.
Boundary Conditions	**Inlet**	Pressure Inlet
	Outlet	Pressure Outlet
	Operating Density(kg/m3)	1.225
	Gravity (m/s2)	-9.81
	Turbulent Intensity(%)	1
	Turbulent Viscosity Ratio	1
Solution Methods	**Pressure-Velocity Coupling**	SIMPLE
	Gradient	Least Squares Cell Based
	Pressure	Body Force Weighted
	Momentum	Second Order Upwind
	Volume Fraction	QUICK
	Turbulent Kinetic Energy	Second Order Upwind
	Turbulent Dissipation Rate	Second Order Upwind
Solution Controls	**Under - Relaxation Factors**	Reduced at higher Froude numbers manually
Solution Initialization	**Initialization Method**	Standard Initialization
	Open Channel Initialization Method	Flat
	Reference Frame	Relative to Cell Zone

4.2.1.3 Validation and Results for a Wigley Parabolic Hull

This validation is made for a Wigley hull of which many studies in the literature exist. In order to obtain a satisfactory result for wave resistance, the wave profiles of the wake and along the hull must be correctly predicted. There are various studies (most of them relying on potential theory) made to predict the wave profiles along the Wigley hull and all these results are tried to be validated with experiments. One of these studies is the work of Tarafder and Suzuki [11]. They have used modified Rankine source panel method to obtain the wave profile along the hull and compared their results with an experiment made for Fn=0.316. The comparison of computed wave profile with that of RANSE is given in Figure 4.23.

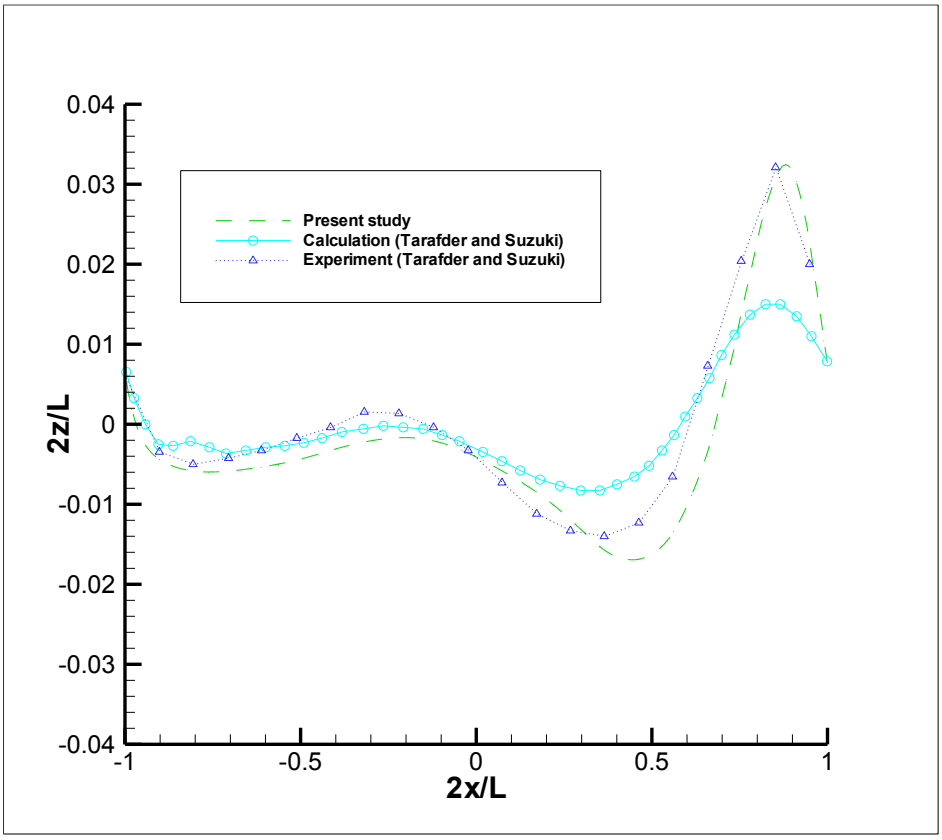

Figure 4.23 : Wave profile along the Wigley hull for Fn=0.316.

The wave pattern acquired with RANSE is more compatible with the experiments especially at the bow region where there is a high free surface elevation.

Another experiment is performed by He at Fn=0.350 to validate the newly developed based on an iterative Boundary Element Method [27]. The RANSE result produced in this study is compared with his calculation and experiment for the wave pattern along the Wigley hull as shown in Figure 4.24.

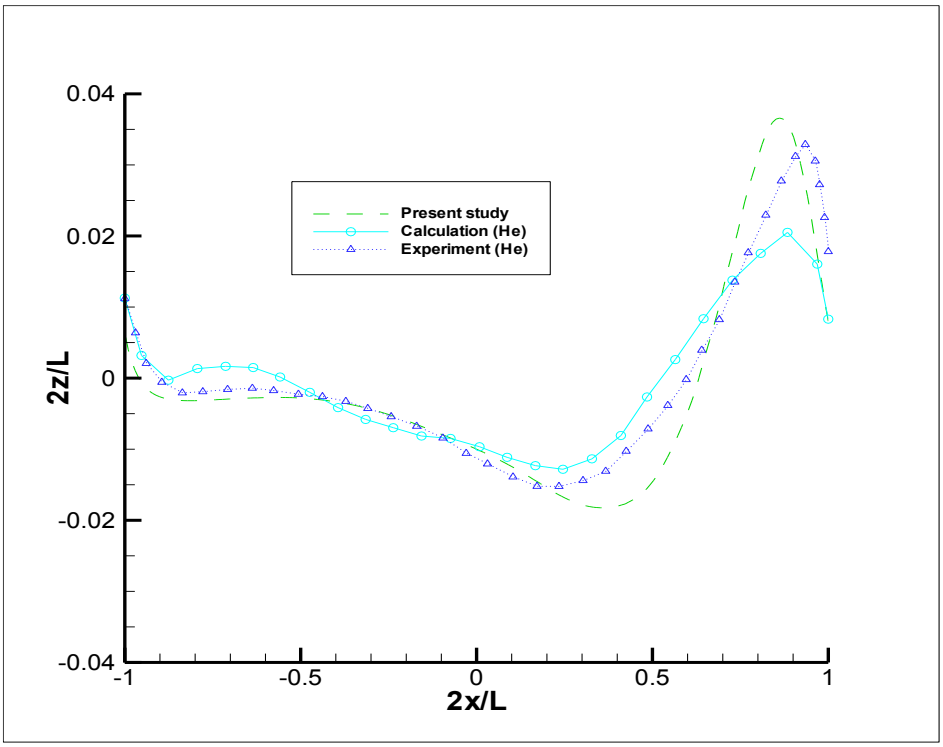

Figure 4.24 : Wave profile along the Wigley hull for Fn=0.350.

The wave pattern obtained by RANSE seems in better accordance with the experiments. The same case applies here as well; potential theory predicts lesser wave elevations especially in places where the perturbation of the free surface is greater as in the previous case.

The wave resistance values of the Wigley hull is not published in He's article. Tarafder and Suzuki have shared their results up to Fn=0.6. As mentioned before, RANSE is fully nonlinear and can grab satisfactory wave profiles and wave resistance values even in higher Froude numbers. For wave resistance coefficient values computed with the proposed method, comparisons are made with the calculations made by Moraes et al. who computed the wave resistance up to Fn=0.9 [28]. However, experimental results are not included in their study. Therefore, experiments made at different Froude numbers are taken from the work of Millward and Bevan [29]. The compared results are given in Figure 4.25. The wave resistance coefficient here is calculated as:

$$C_W = \frac{2R_W}{\rho S V^2}$$

The wave resistance computation seems to be compatible both with the calculations of Moraes et al. and the experiments of Millward and Bevan. It could also be said that proposed methodology gives better results.

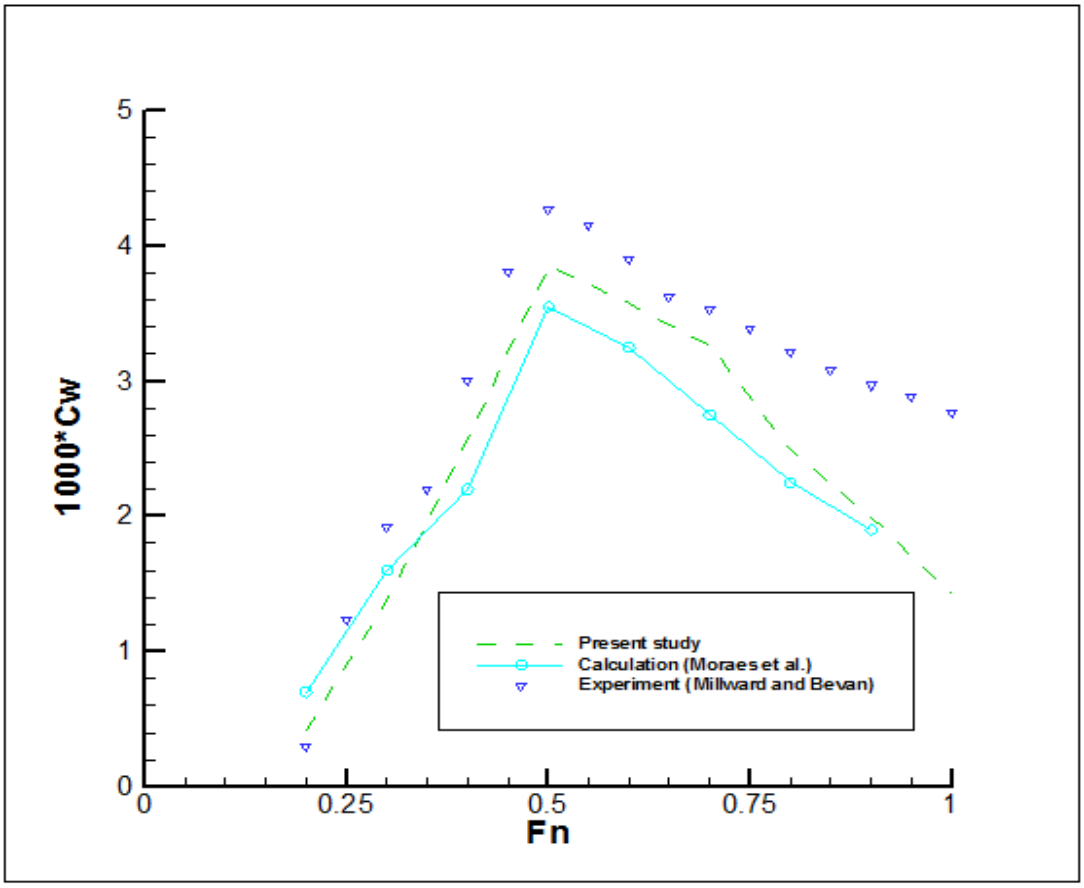

Figure 4.25: Comparison of wave resistance coefficients.

The discrepancy between present methodology and the experiments are in an increasing trend at higher Froude numbers. The same thing applies for Moraes et al. as well. The reason for this may be due to the calculation of residual resistance at experiments. The resistance of the static wetted area is subtracted from the residual resistance to obtain wave resistance in a towing tank. The wetted area of the hull does not deviate much due to smaller free surface elevations at lower Froude numbers; however, this is not the case at higher Froude numbers. The deviation of the wetted area of the hull is greater at higher speeds but during calculation of wave resistance at the towing tank, only the static wetted area is calculated and subtracted. Rigby et al. have suffered from the same problem and they have also mentioned such a statement in their study [8]. This point must be kept in mind while comparing the calculated and experimented results at high Froude numbers. In other terms, although during the experiments, the model is free to sinkage and trim, in CFD computations, it is fixed to trim and sinkage.

The free surface deformation for Fn=0.4 is given in Figure 4.26. The wave profile over the Wigley hull at the same Fn is given in Figure 4.27.

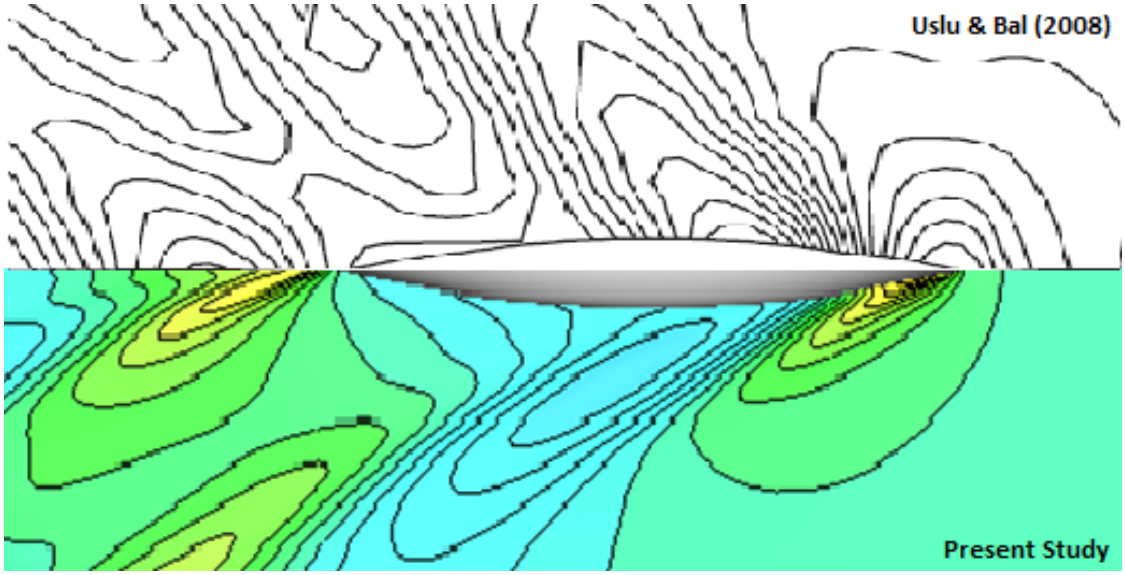

Figure 4.26 : Free surface deformations for a Wigley hull at Fn=0.4 compared with the results of Uslu and Bal [9].

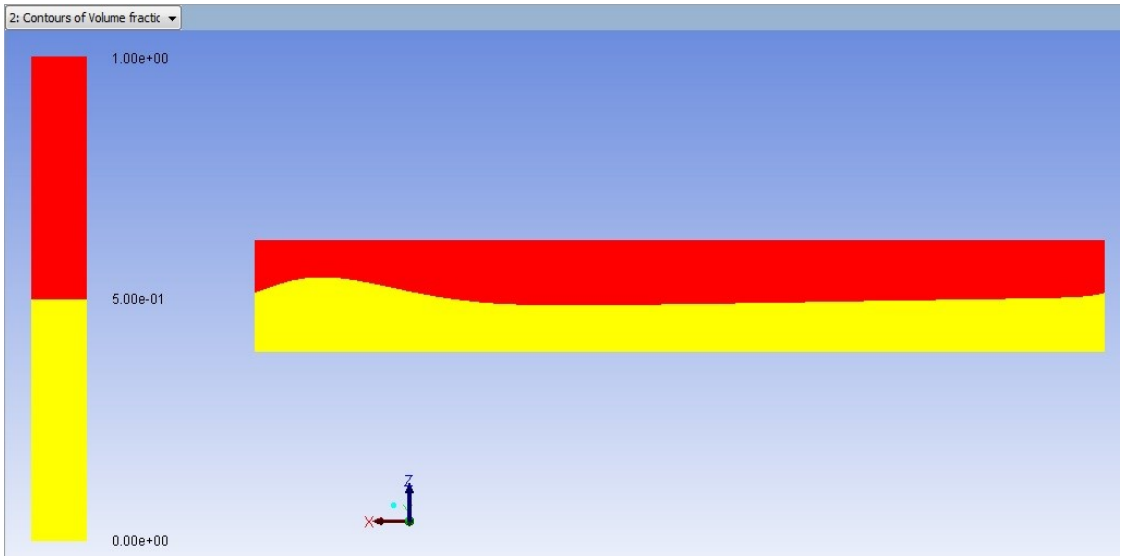

Figure 4.27 : Wave profile on the Wigley hull at Fn=0.4.

In Figure 4.27, volume fraction is used as a discretization between air and water; where 0 refers to water and 1 refers to air. The yellow part of the hull shows the wetted surface area of the Wigley hull. The effect of free surface and viscosity on pressure distribution on the Wigley hull is given in Figure 4.28. There seems a good compatibility for cases of unbounded flow domain (which is a single phase solution) and free surface effect included domain (which is a multiphase solution).

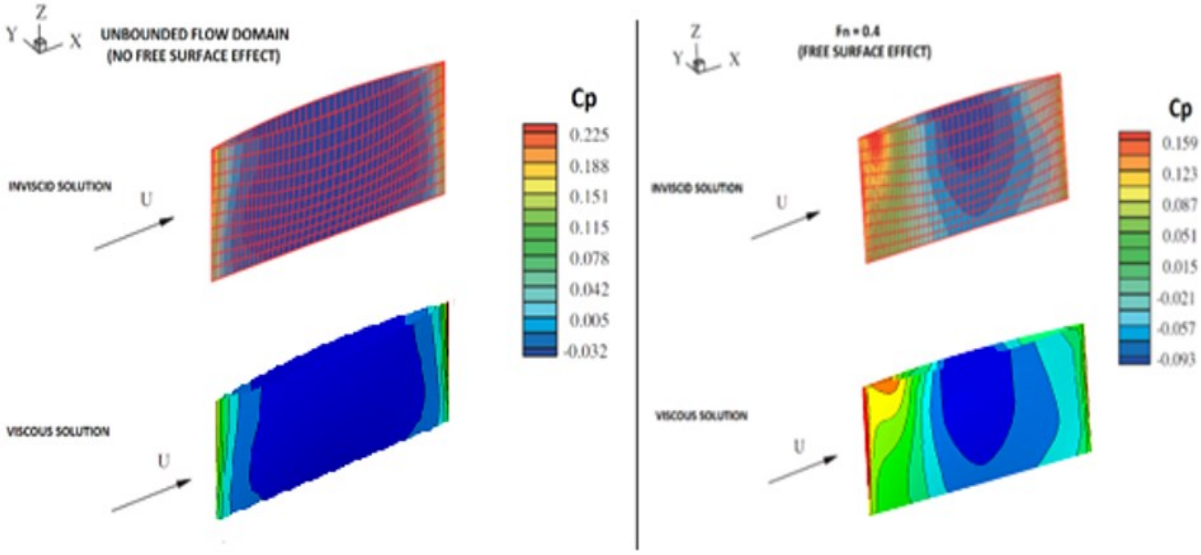

Figure 4.28 : Effect of free surface and viscosity on pressure coefficient distribution over the Wigley hull as compared to the inviscid work of Uslu and Bal [9].

The free surface elevations change the pressure distribution along the hull, as can be seen from Figure 4.28. The pressure decreases at points where wave troughs are found while it increases in places of wave crests. From the same figure, the places of wave crests over the hull can be determined.

In Figure 4.28, there is some difference at the bow in RANSE calculations and that is due to RANSE being a fully nonlinear method. Keeping in mind the better results obtained by RANSE given in Figures 4.23 and 4.24, it may be said that the pressure distribution obtained is better than the potential methods. Wigley hull has a slender body and the stern part of the hull is not complex. This is the place where the effects of viscosity must show up the most but due to the thin geometry of the hull, the results are nearly the same.

4.2.2 A Modern Displacement Tanker

4.2.2.1 Geometry and Meshing Strategy

A modern displacement tanker was used in the analyses and same approach used for this ship to prove the robustness of the proposed method that is successfully implemented on Wigley parabolic hull to obtain the wave resistance. The geometry is quite different from Wigley parabolic hull due to the presence of bow-bulb and two skegs at stern side. Also towing tank test results are available for this ship and tests were carried out in Ata Nutku Ship Model Testing Laboratory at Faculty of Naval Architecture and Ocean Engineering of Istanbul Technical University.

Since the ship geometry is symmetrical, only half of the domain was considered for simulations. Position of inlet and outlet surfaces at 1L and 2L from the model, respectively. Bottom at 1L below the baseline and the distance between side surface and symmetry plane is 1.5L. Here, L denotes the overall length of the hull. The zero point is located at the intersection of design waterline and aft perpendicular. Figure 4.29 and Figure 4.30 show the hull geometry and computational domain with its dimensions.

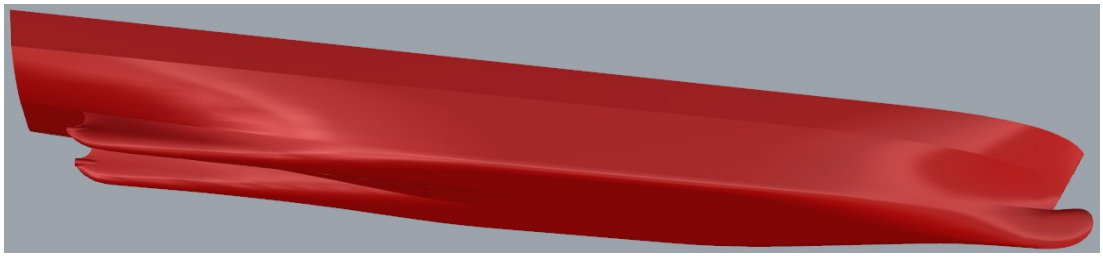

Figure 4.29 : A general view of the tanker.

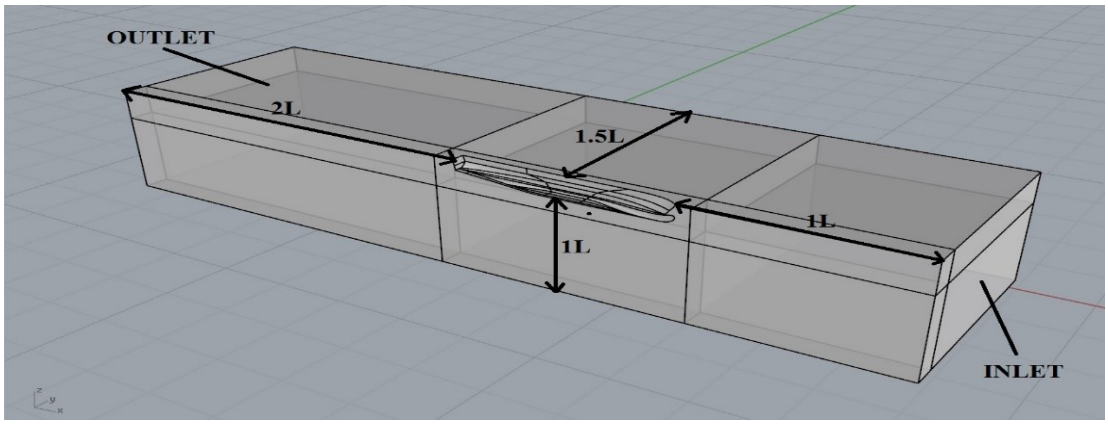

Figure 4.30 : Computational domain for the tanker.

Since free surface flows in CFD analyses strictly rely on the mesh quality, meshing process is vital step of the numerical solutions and generally it requires a lot of hours of work. Actually how much time is spent depends on the type of mesh element. Tetrahedral elements are easy to construct and less time consuming so it is highly preferred in ship building industry. However hexahedral elements requires more ability, experience and time for meshing.

Tetrahedral elements are good to evaluate forces along the ship hull but fail to smoothly capture the interface in multiphase ship flows. Hexahedral elements are both good in evaluating resistance and capturing the free surface; however, they are hard to implement to complex geometries such as ship hulls. Therefore; hybrid mesh system, which is a mix of both type of elements, offers a good way to go around this problem and practically solve multiphase ship flows. A hybrid meshing approach using tetrahedral elements around complex geometries and hexahedral meshing in the rest of the domain, especially in the vicinity of free surface, was suggested [30]. From this point of view, in this part of the thesis, hybrid mesh method was preferred to get accurate results and capturing the free surface elevations adequately.

As it mentioned before, whole domain was divided into 12 blocks and 11 blocks was meshed with fully hexahedral elements by using Gambit, while unstructured tetrahedral meshing was used at only one block where the ship is in. Hybrid mesh generation for the free surface wave flow of a ship (MP analysis) can be seen in Figure 4.31.

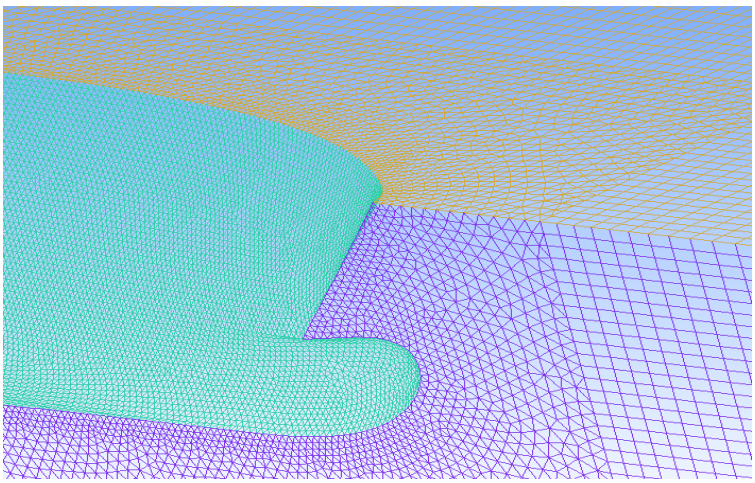

Figure 4.31 : Hybrid meshing for the free surface wave flow of a ship.

Tetrahedral-shaped elements are not adequate to capture the free surface elevations, especially far away from the ship where the wave height is low. Actually the grid types

should be flat enough to catch the small wave elevations and sufficiently wide to avoid an excessive number of elements. On the other hand hexahedral cells are more appropriate to capture the small variations of wave elevations without sacrificing the accuracy of the solution [3]. Either size of the hexahedral and tetrahedral elements have a growth ratio in their own blocks to prevent an excessive number of cells. Please see Figure 4.32.

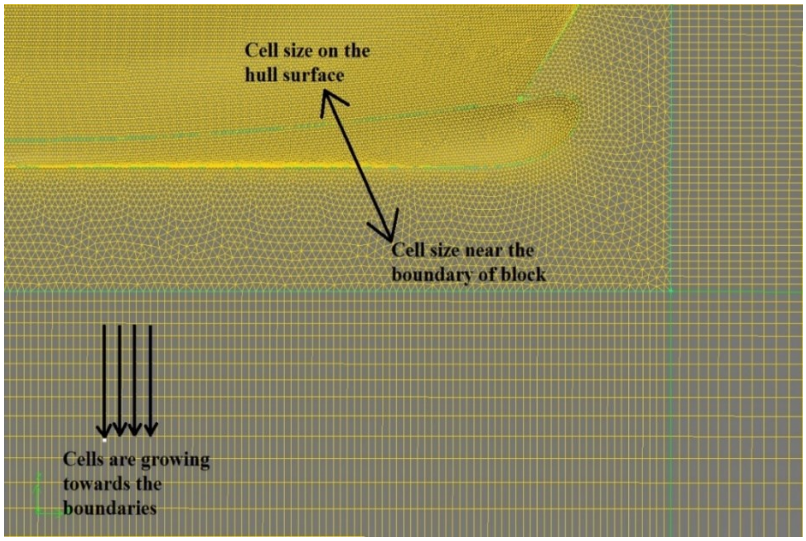

Figure 4.32 : Cell size towards the boundaries of blocks.

To prevent the reflection of the waves due to advance of the ship, the domain was kept widely enough. For obtaining a good calculation, approximately %90 of the domain was meshed with hexahedral type of grids and final mesh containing 4.5 million cells.

Finally, boundary conditions were determined. For single phase flows, inflow surface was assumed as velocity inlet and outflow surface is pressure inlet. Symmetry plane was defined as symmetry because computations had been done for half domain. Top, bottom and side wall were set as wall. In multi-phase analyses, only difference is pressure inlet for inflow surface. Please refer to Table 4.12.

Table 4.12 : Boundary conditions for the tanker.

	Boundary Conditions	
	Single Phase Analysis	***Multi Phase Analysis***
Inlet	Velocity Inlet	Pressure Inlet
Outlet	Pressure Outlet	Pressure Outlet
Wall	Symmetry	Symmetry
Top	No slip / Stationary wall	No slip / Stationary wall
Bottom	No slip / Stationary wall	No slip / Stationary wall
Symmetry	Symmetry	Symmetry

4.2.2.2 Numerical Settings

Many multiphase ship flow problems are solved for only the service speed of the hull in the industry; however, analyses at low speed may also be needed for academic purposes. If a low Froude number analysis is to be made for a ship flow problem, two options exist:

- Decrease the size of the mesh elements which will increase the time to complete one iteration.
- Decrease under-relaxation factors to obtain a solution with more iterations.

A good compromise between these two options must be made to obtain quicker and compatible results. Many multiphase ship flow problems suffer from momentum under-relaxation factor; this value should be decreased with great care. The continuity residual gives a notion of how much to decrease momentum under-relaxation factor and should be watched closely.

Due to the chaotic flow for ships, turbulent kinetic energy and turbulent dissipation rate may also pose a problem. Residuals such as k, ϵ, ω etc. (depends on which turbulence model is selected) should be followed to change under-relaxation factors dealing with turbulence.

RANSE simulations for this model were carried out at velocities 0.829 m/s to 1.658 m/s which is equal to Froude number of 0.134 to 0.268. The Froude of 0.268 is equal to service speed of ship. The model was fixed at design draft and there is no trim angle for the simulations. The volume of fluid method was used to achieve the free surface flow around the ship. Volume of fluid method (VOF in short notation) is used to track complicated free surface deformations. Waves generated due to the existence of a hull with a submerged transom or bulb may be complex and VOF is a widely used method for even spilling breaking waves and bubbly free surface [31]. Several numerical schemes that are tested involving the multiphase flow problem of a surface piercing hydrofoil can be referred from [31]. Simulations were performed by using implicit scheme and body force formulation was selected as implicit body force. The SIMPLE algorithm was used for the pressure-velocity coupling, “Body Force Weighted” scheme for the pressure interpolation. SIMPLE is the most straightforward CFD algorithm for predicting pressure and velocities in a fluid domain iteratively. Owing to its simplicity, computational efforts are relatively less compared to its peers. It has been reported in the book by Versteeg and Malalasekera [32] that although SIMPLEC

is a more stable algorithm, calculations involved are %30 greater. Its disadvantage is that the algorithm needs good initial and under-relaxation values or the analysis may diverge.

Open channel mode was selected as in the previous simulations. Second order upwind was selected for momentum equations. Also QUICK scheme was set as the solution of the volume fraction equations.

The primary phase must be the lower density fluid, so air was selected as primary phase for this simulation and reference pressure location should be set as a region which always contains the air [33]. There are several RANSE turbulence models in Fluent. Since simulations in this thesis involve only fixed-body solutions and therefore the flow is largely attached to the hull, the k- ε turbulence model with a standard wall function was selected as turbulence model.

Under-relaxation factors were changed with the behavior of the residuals, but generally it reduces with the increasing of Froude numbers. Under relaxation factors between Froude 0.13-0.27 are shown in Table 4.13 for this displacement ship. There is no criteria for the residuals to confirm the convergence. For more information about convergence criteria, please refer to "Checklist" in CFD Methodology in Chapter 2. All details of the numerical settings for single and multiphase were given as a table format in Table 4.14 and Table 4.15 respectively.

Table 4.13 : Under Relaxation Factors for the displacement ship for Fn=0.13-0.27.

Under Relaxation Factors	
Pressure	0.3
Density	1
Body Forces	1
Momentum	0.3
Volume Fraction	0.5
Turbulent Kinetic Energy	0.5
Turbulent Dissipation Rate	0.5
Turbulent Viscosity	1

Table 4.14 : Numerical Settings of the Displacement Hull for Single-Phase Solution.

Numerical Set-up		
		Single-phase
General	**Type**	Pressure Based
	Time	Steady
	Velocity Formulation	Absolute
Models	**Turbulance model**	k-ε, Realizable
	Near Wall Treatment	Standard Wall Func.
Boundary Conditions	**Inlet**	Velocity Inlet
	Outlet	Pressure Outlet
	Turbulent Intensity(%)	1
	Turbulent Viscosity Ratio	1
Solution Methods	**Pressure-Velocity Coupling**	SIMPLE
	Gradient	Least Squares Cell Based
	Pressure	Second Order Upwind
	Momentum	Second Order Upwind
	Turbulent Kinetic Energy	Second Order Upwind
	Turbulent Dissipation Rate	Second Order Upwind
Solution Controls	**Under - Relaxation Factors**	Shown in Table 3.5
Solution Initialization	**Initialization Method**	Standard Initialization
	Reference Frame	Relative to Cell Zone

Table 4.15: Numerical Settings of the Displacement Hull for Multi-Phase Solution.

Numerical Set-up		
		Multi-phase
General	**Type**	Pressure Based
	Time	Steady
	Velocity Formulation	Absolute
Models	**Multiphase model**	Volume of Fluid
	Scheme	Implicit
	Body Force Formulation	Implicit Body Force
	Number of Eularian Phases	2
	Options	Open Channel Flow
	Turbulance Model	k-ε, Realizable
	Near Wall Treatment	Standard Wall Func.
Boundary Conditions	**Inlet**	Pressure Inlet
	Outlet	Pressure Outlet
	Operating Density(kg/m3)	1.225
	Gravity (m/s2)	-9.808
	Turbulent Intensity(%)	1
	Turbulent Viscosity Ratio	1
Solution Methods	**Pressure-Velocity Coupling**	SIMPLE
	Gradient	Least Squares Cell Based
	Pressure	Body Force Weighted
	Momentum	Second Order Upwind
	Volume Fraction	QUICK
	Turbulent Kinetic Energy	Second Order Upwind
	Turbulent Dissipation Rate	Second Order Upwind
Solution Controls	**Under - Relaxation Factors**	Shown in Table 3.5
Solution Initialization	**Initialization Method**	Standard Initialization
	Open Channel Initialization Method	Flat
	Reference Frame	Relative to Cell Zone

4.2.2.3 Validation and Results for a Modern Displacement Tanker

Up to now, the proposed method has been validated for submerged and surface piercing benchmark problems. The robustness of the method has also been tested for a tanker (displacement hull) with a bulb, transom stern and double skeg. The experiments were carried out in Ata Nutku Ship Model Testing Laboratory located in Istanbul Technical University [34]. The main dimensions for the vessel are given in Table 4.16.

Table 4.16 : Hydrostatic properties of the tanker in model scale.

Lbp (m)	3.823
Lwl (m)	4.047
B (m)	0.571
T (m)	0.179
Service Speed	1.658m^2/s

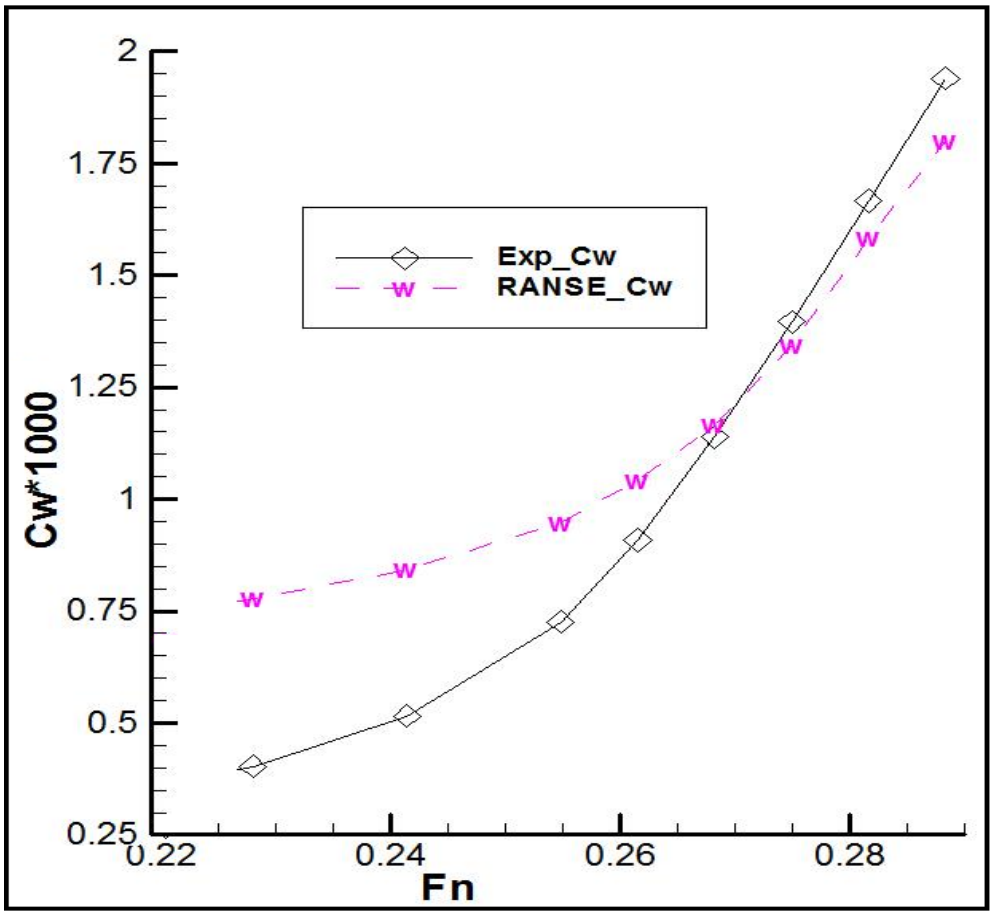

Figure 4.33 : Wave resistance coefficient, numerical and experimental.

Figure 4.33 shows the wave resistance coefficient values of the tanker. As the Froude number increases, the discrepancy between the numerical and experimental values decreases. This was not the case as in Wigley hull; however, the analyses for Wigley hull included Froude numbers up to 0.9 where wetted area is likely to change considerably. For displacement vessels; on the other hand, the service limit is about Fn=0.3 and although wetted area is changing (due to trim and sinkage), this is a negligible deviation. The discrepancy for the vessel is higher at lower Froude numbers and RANSE has a tendency to exaggerate the values obtained for wave resistance. It may be due to decreasing Reynolds number where the used turbulence model starts to fail.

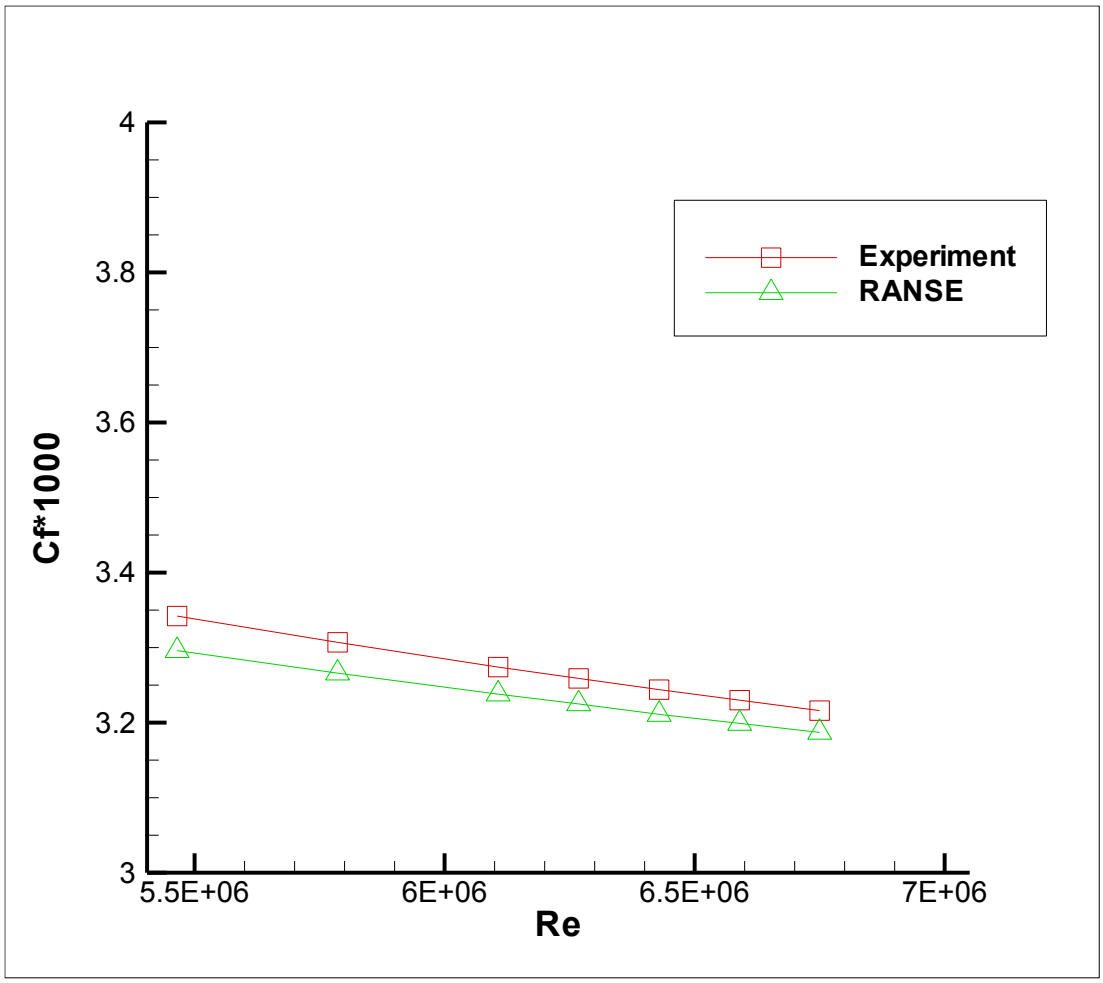

Figure 4.34 : Frictional resistance coefficient of the tanker.

.

RANSE is on the other hand very efficient in calculating the frictional resistance as it can be seen from Figure 4.34. The calculated total resistance characteristics of the vessel seem compatible with the experimental results. The form factor can be found via RANSE based CFD and k is calculated in this study as:

$$k = \frac{C_{vp}}{C_f}$$

Viscous pressure and frictional resistances are computed by single phase analyses. k changes with the Reynolds number and this change may be examined from Figure 4.35. The range of this study was between Froude numbers 0.2 and 0.3 (which is about $5 \cdot 10^6 < Re < 7 \cdot 10^6$) and if a quick linear calculation is made, it is found that k is about 0.14 which in turn gives a form factor of 1.14. Form factor calculated in experiments implementing the method of Prohaska was 1.12. The calculated form factor at the ship's service speed (20knots) is 1.167.

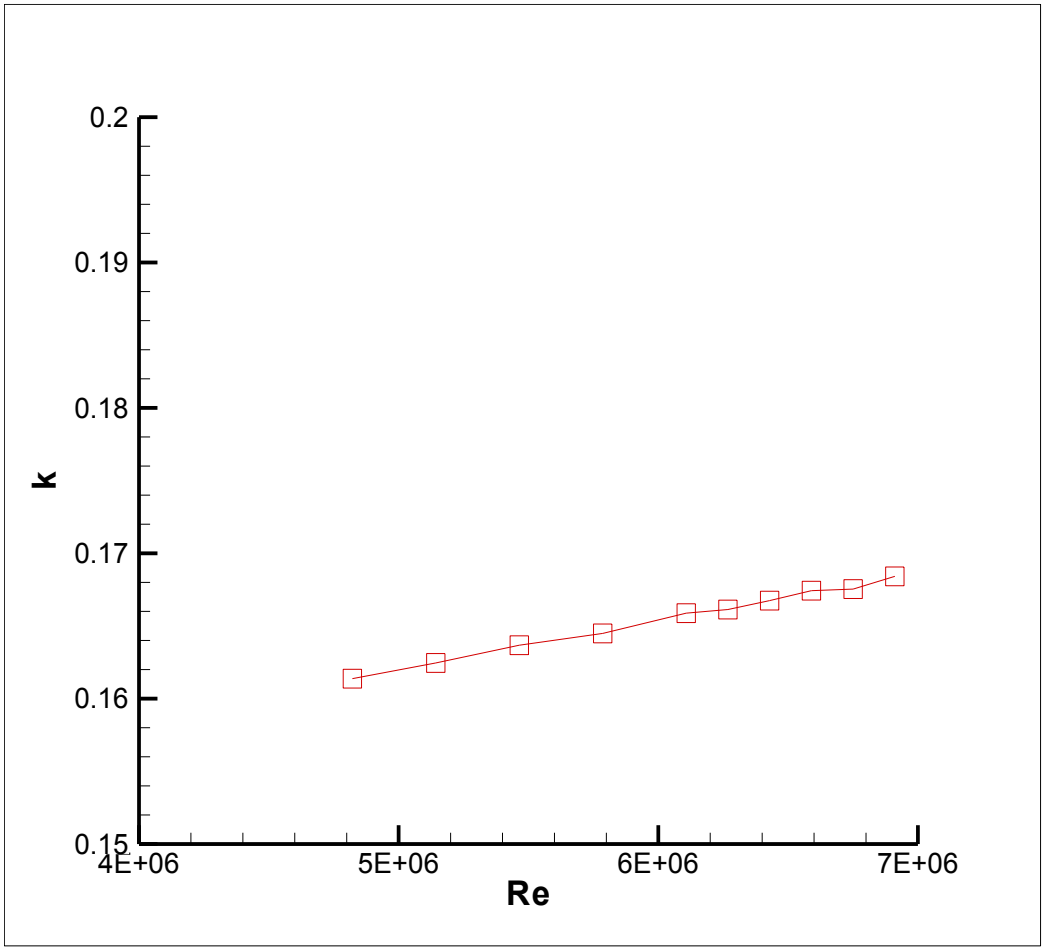

Figure 4.35 : A linear form factor analysis via single phase solutions by RANSE based CFD.

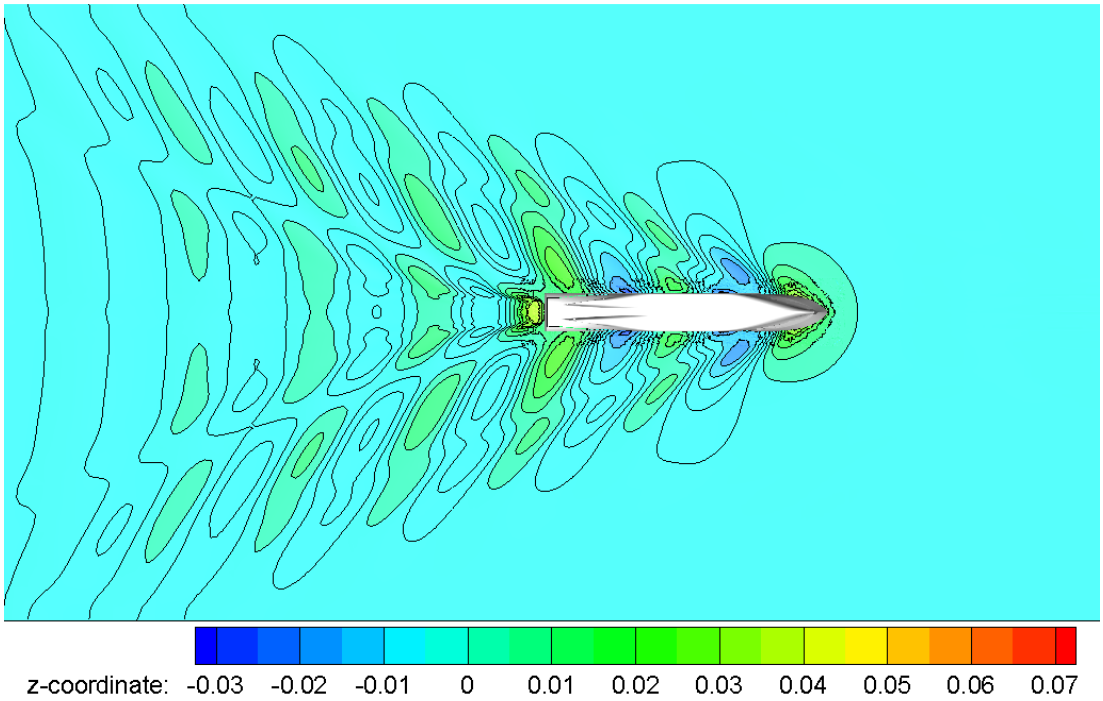

Figure 4.36 : Free surface contours of the tanker at Fn=0.27.

Kelvin wake pattern can be observed from Figure 4.36. The free surface has decreased the pressure in places of wave trough and increased it in places of wave crest. The effect of the free surface on the wetted area of the hull can be seen from Figure 4.37.

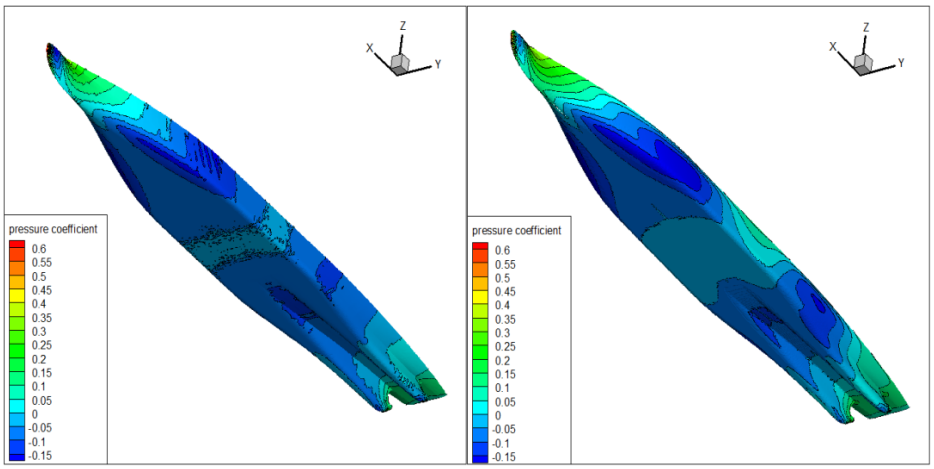

Figure 4.37 : Free surface effect on pressure coefficient distribution over the displacement tanker. The figure on the left is a single phase solution while the one on the right is multiphase.

Calculated and experimented bow wave formation on the hull can be examined from Figure 4.38. The calculated wave profile over the entire hull is given in Figure 4.39. The streamlines at the aft region of the ship can also be seen in Figure 4.40 as compared

with the results of tuft tests carried out at Ata Nutku Ship Model Testing Laboratory of Istanbul Technical University [34]. The satisfaction is good. The computed nominal wakes at the propeller disc are given in Figure 4.41 as compared with those of measured as well. The average nominal wake coefficient is found to be 0.78 with RANSE while the experimental method returns a value of 0.72. Again a satisfactory agreement is obtained.

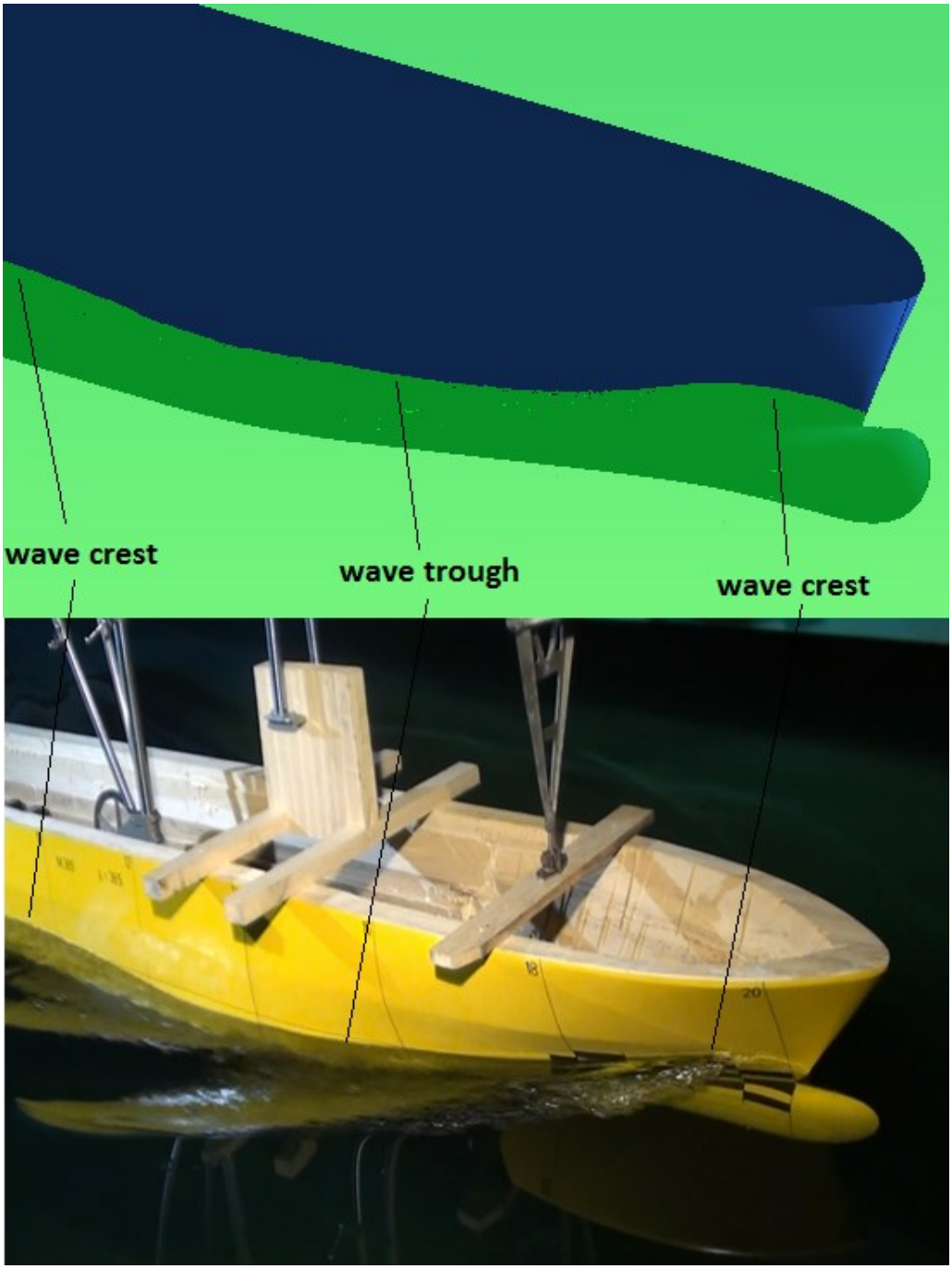

Figure 4.38 : A comparison of RANSE and experiment for generated waves at the bow of the tanker.

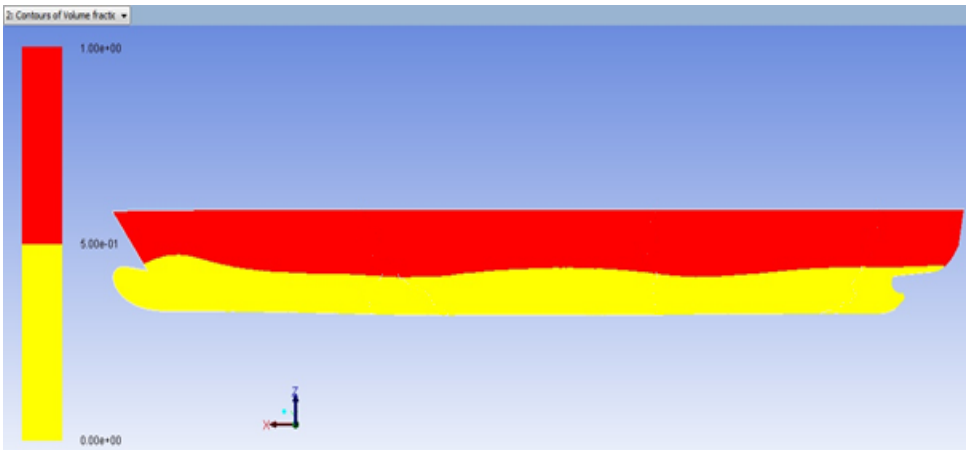

Figure 4.39 : Wave profile on the hull for Fn=0.27.

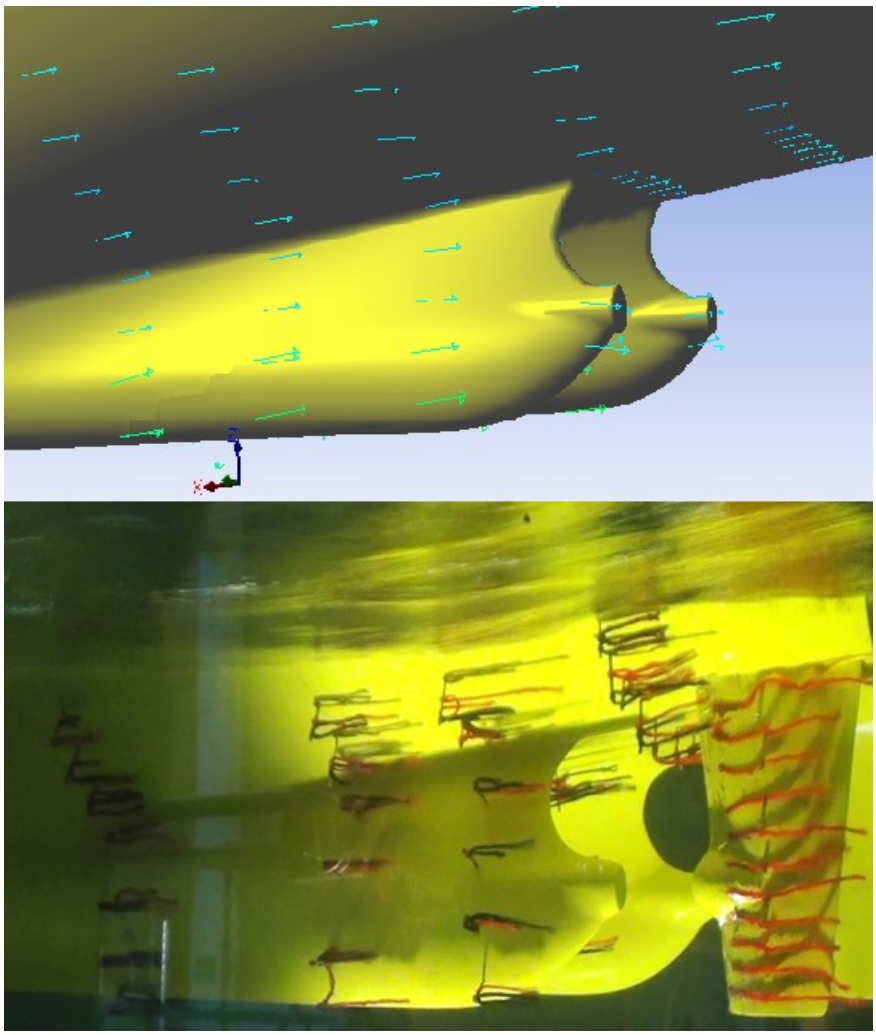

Figure 4.40 : Streamlines at the aft region of the model tanker (Up: RANSE solution, Bottom: Tuft test result.)

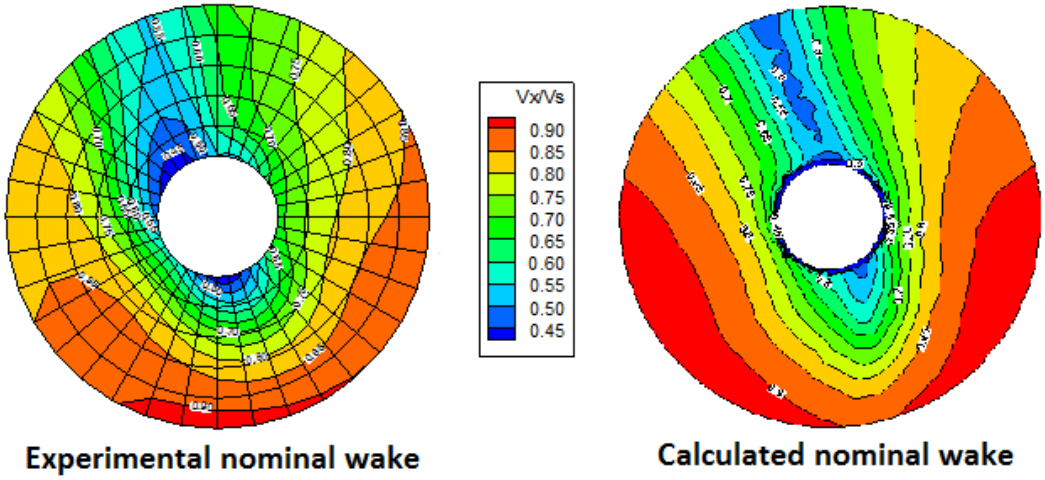

Figure 4.41 : Experimental and calculated nominal wakes at the propeller disc.

5. CONCLUSION AND DISCUSSION

The flexibility of RANSE based CFD allows users to choose the analysis to be made either in single phase (SP) or multiphase (MP). There are many parameters that may be observed by single phase analysis. One of them is the viscous pressure resistance which helps to determine the wave resistance of a ship. RANSE based CFD software do not specifically return wave resistance values of ships and in this thesis, a methodology to calculate wave resistance using RANSE has been proposed. Wave resistances of benchmark geometries with the proposed method are computed and compared with the values found in the literature. Our method has produced compatible results and the efficiency of the method was proved. The method could be used to optimize high speed marine vehicles' hull forms where a substantial part of the total resistance is of wave resistance. Also a towing tank test is performed for an ellipsoid with the help of a strut, however the incompatibility was observed at low Froude numbers that may caused by the interaction between the ellipsoid and strut. The vibration problem was not totally isolated and is caused by possibly due to welding locations of the rails and motion of the carriage. Isolation of vibration and experimental uncertainity analyses is recommended for future studies.

The proposed CFD methodology is an alternative to the classical method where the form factor is found with Prohaska method by subtracting the viscous resistance from total resistance to calculate wave resistance. The classical method omits the deviations in Reynolds number for the form factor; however, in this methodology form factor does not need to be calculated. Single phase analysis automatically resolves the issue of "zero wave resistance inclusion" inside the total resistance during the form factor calculation. In single phase analysis, the ratio of viscous pressure resistance to frictional resistance directly gives the form factor (1+k) value of the ship that is to be solved and it depends on the Reynolds number. Despite the traditional method that drives from the experiments that there is only one result for the form factor, this

method includes the deviations that may happen in the form factor with increasing Reynolds number.

The methodology returns good results for both submerged and surface piercing benchmark problems. It is also tested on a displacement tanker and the results once again encouraging. RANSE tends to return higher values for wave resistance in lower Froude numbers and this is considered to be due to Reynolds number getting digressed from the range that the used turbulence model supports. The turbulence models return good results in fully turbulent flows and if the flow is in transition, the model may not work properly. As the Froude number is lowered, the Reynolds number is as well lowered and the flow around the ship model may not be fully turbulent. Exaggerated values of wave resistance at relatively low Froude numbers for the displacement vessel may be resolved in time as new turbulence models or modifications to existing models show up. The discrepancy in lower Froude numbers will hopefully be investigated in a future work that involves the uncertainty analyses.

REFERENCES

[1] **ITTC 7.5-02-03-01.4,** (2011). Recommended Procedures and Guidelines, 1978 ITTC Performance Prediction Method, Revision 02.

[2] **Molland, A., F., Turnock, S. R., Hudson, D., A.,** (2011). *Ship Resistance and Propulsion*, Cambridge University Press.

[3] **Pranzitelli, A., Nicola, C., Miranda, S.,** (2011). Steady-state calculations of free surface flow around ship hulls and resistance predictions. *IX HSMV Naples 25-27 May 2011.*

[4] **Gomez, A., G.,** (2000). On the Form Factor Scale Effect. *Ocean Engineering*, 27(1), p. 97-109.

[5] **Havelock, T., H.,** (1934). The Calculation of Wave Resistance. *Proceeding of the Royal Society of London*, p. 144.

[6] **Gotman, A., S.,** (2007). A History of Ship Resistance Evaluation. *Journal of Ocean Technology*, Vol. 2, No. 1.

[7] **Farrell C.,** (1972). On the wave resistance of a submerged spheroid. *Journal of Ship Research*, Vol.17, p. 1-11.

[8] **Rigby, S., G., Nicolaou, D., Sproston, J., L., and Millward, A.,** (2001). Numerical Modeling of the Water Flow around Ship Hulls. *Journal of Ship Research*, 45(2), p. 85–94.

[9] **Uslu Y., Bal S.,** (2008). Numerical Prediction of Wave Drag of 2-D and 3-D Bodies under or on a Free Surface. *Turkish Journal of Engineering and Environmental Sci*ences, 32, p. 177-188.

[10] **Bal, S.,** (2008). Prediction of wave pattern and wave resistance of surface piercing bodies by a boundary element method. *International Journal for Numerical Methods in Fluids*, 56, p. 305-329.

[11] **Tarafder, S., Suzuki, K.,** (2008). Numerical calculation of free-surface potential flow around a ship using the modified Rankine source panel method. *Ocean Engineering*, 35, p. 536-544.

[12] **El Moctar, O., Shigunov, V., Zorn, T.,** (2012). Duisburg Test Case: Post-Panamax Container Ship for Benchmarking, *Ship Technology Research*, 59(3), p. 50-65.

[13] **Belibassakis, K., A., Gerostathis, Th.P., Kostas, K.V., Politis, C.G.,Kaklis, P.D., Ginnis, A.I., Feurer, C.,** (2013). A BEM-isogeometric method for the ship wave-resistance problem. *Ocean Engineering*, 60, p. 53-67.

[14] **Wehausen, J., V.,** (1973). The wave resistance of ships. *Advances in Applied Mechanics*, 13, p. 93-245.

[15] **Newman, J., N.,** (1977). *Marine Hydrodynamics*. MIT Press: Cambridge, MA, USA.

[16] **Tulin, M., P.,** (2005). Reminiscences and Reflections: Ship Waves, 1950-2000. *Journal of Ship Research*, 49(4), p. 238-246.

[17] **Repetto, R., A.,** (2001). Computation of Turbulent Free Surface Flows around Ships and Floating Bodies. PhD Thesis, Hamburg Techinal University.

[18] **Larsson, L., Stern, F., Bertram, V.,** (2003). Benchmarking of Computational Fluid Dynamics for Ship Flows: The Gothenburg 2000 Workshop. *Journal of Ship Research*, Vol. 47, No. 1 , p. 63–81.

[19] **Bartesaghi, S., Viola, I., M.,** (2008). Hull Resistance and Wave Pattern Computation with RANS Technique on a Simplified Experimental Benchmark.

[20] **Maki, K., J., Broglia, R., Doctors, L., J., Mascio, A., D.,** (2013). Numerical investigation of the components of calm-water resistance of a surface-effect ship. *Ocean Engineering*, 72, p. 375-385.

[21] **Launder, B., E., Sharma, B., I.,** (1974). Application of the Energy Dissipation Model of Turbulence to the Calculation of Flow Near a Spinning Disc. *Letters in Heat and Mass Transfer*, 1(2), p. 131-138.

[22] **Bardina, J., E., Huang, P., G., Coakley, T., J.,** (1997). Turbulence Modeling Validation, Testing, and Development. *NASA Technical Memorandum* 110446.

[23] **Shih, T., H., Liou, W., W., Shabbir, A., Yang, Z., Zhu, J.,** (1995). A new k-ϵ eddy viscosity model for high Reynolds number turbulent flows. *Computers and Fluids*, 24(3), p. 227-238.

[24] **ANSYS, Inc.,** (2011). ANSYS Fluent User's Guide, Release 14.0.

[25] **Marnet-CFD,** (d.s.). *Best Practice Guidelines For Marine Applications of Computational Fluid Dynamics.*

[26] **Coleman, H., W., Steele W., G.,** (2009). *Experimentation, Validation and Uncertainity Analysis for Engineers.* Third Edition. A John Wiley & Sons, Inc.

[27] **Seo, J., H., Seol, D., M., Lee, J., H., Rhee, S., H.,** (2010). Flexible CFD meshing strategy for prediction of ship resistance and propulsion performance. *International Journal of Naval Architecture and Ocean Engineering*, 2, p.139-145.

[28] **He, G.,** (2013). An iterative Rankine BEM for wave-making analysis of submerged and surface piercing bodies in finite water depth. *Journal of Hydrodynamics*, 25(6), p. 839-847.

[29] **Moraes, H., B., Vasconcellos, J., M., Latorre, R., G.,** (2004). Wave resistance for high-speed catamarans. *Ocean Engineering*, 31, p. 253-282.

[30] **Millward, A., Bevan, M., G.,** (1986). Effect of shallow water on a mathematical hull at high subcritical and supercritical speeds. *Journal of Ship Research*, 30, 2, p. 85–93.

[31] **Lee, J., H., Park, B., J., Seol, D., M., Rhee, S., H., Jun, D., S., Chi, H., R., Ryu, M., C.**, (2009). Hybrid Meshing Approach for Resistance Performance Prediction of a POD Propulsion Cruise Ship. 2nd Asian Symposium on Computational Heat Transfer and Fluid Flow, Jeju, Korea.

[32] **Rhee, S., H., Makarov, B., P., Krishinan, H., Ivanov, V.,** (2005). Assessment of the volume of fluid method for free-surface wave flow. *Journal of Marine Science and Technology*, 10(4), p. 173-180.

[33] **Jones, D., A., Clarke, D., B.,** (2010). Fluent Code Simulation of Flow around a Naval Hull: the DTMB 5415. Maritime Platforms Division, Defence Science and Technology Organisation. DSTO-TR-2465.

[34] **Versteeg, H., K., Malalasekera, W.,** (2007). *An Introduction to Computational Fluid Dynamics – The Finite Volume Method*, Pearson Education Limited.

[35] **Bal, S. (PI),** (2013). Model tests and analysis of a tanker. Project No: 2013-P08, *Ata Nutku Lab Report*, ITU.

[36] **Choi, J., E., Min, K., S., Kim, J., H., Lee, S., B., Seo, H., W.,** 2010. Resistance and propulsion characteristics of various commercial ships based on CFD results. Ocean Engineering, 37, p. 549-566.

[37] **Kinaci, O., K., Kukner, A., Bal, S.,** (2013). On propeller characteristics of DTC Post-Panamax Container Ship, *International Journal of Ocean System Engineering*, 3(2), p. 77-89.

[38] **Adamski, S., J.,** (2013). Numerical Modelling of the Effects of a Free Surface on the Operating Characteristics of Marine Hydrokinetic Turbines. Master of Science Thesis in Mechanical Engineering, University of Washington.

[39] **Johansson, S., H., Davidson, L., Olsson, E.,** (1993). Numerical simulation of vortex shedding past triangular cylinders at high Reynolds number using a k–ϵ turbulence model. *International Journal for Numerical Methods in Fluids*, 16, p. 859.

[40] **Nakos, D., E., Sclavounos, P., D.,** (1990). On steady and unsteady ship wave patterns. *Journal of Fluid Mechanics*, 215, p. 263-288.

[41] **Nakos, D., E., Sclavounos, P., D.,** (1994). Kelvin wakes and wave resistance of cruiser-stern and transom-stern ships. *Journal of Ship Research*, 38(1), p. 9-29.

[42] **Nestegard, A., Sclavounos, P., D.,** (1984). A numerical solution of two-dimensional deep-water wave-body problems. *Journal of Ship Research*, 28(1), p. 48-54.

[43] **Neulist, D.,** (2011). Experimental Investigation into the Hydrodynamic Characteristic of a Submarine Operating Near the Free Surface. Bachelor of Engineering Thesis, Australian Maritime College.

[44] **ITTC 7.5-01-01-01,** (2002). Recommended Procedures and Guidelines, Model Manufacture Ship Models, Revision 01.

[45] **Bettle, M., Toxopeus, S., L., Gerber, A.,** (2010). Calculation of bottom clearance effects on Walrus submarine hydrodynamics. *International Shipbuilding Progress 57*, p. 101-125.

[46] **Sclavounos, P., D.,** (1984). The diffraction of free-surface waves by a slender ship. *Journal of Ship Research*, 28(1), p. 29-47.

[47] **Larsson, L., Raven, H., C.,** (2010). Ship Resistance and Flow, Principles of Naval Architecture Series, SNAME, USA.

[48] **Chen, Z., M.,** (2013). A dissipative free-surface approach for an underwater body in a uniform stream. *Journal of Marine Science and Technology*, 18, p. 182-191.

[49] **Faltinsen, O.M.,** (2010). *High Speed Marine Vehicles.* MIT Press: Cambridge, MA, USA.

[50] **Chen, Z., M.,** (2012). A vortex based panel method for potential flow simulation around a hydrofoil. *Journal of Fluids and Structures*, 28, p. 378-391.

[51] **Michell, J., H.,** (1898). The wave resistance of a ship, *Philosophical Magazine Series* (5), 45, p. 106-123.

[52] **Wilson-Haffenden, J., S.,** (2009). An Investigation into the Wave Making Resistance of a Submarine travelling Below the Free Surface. Bachelor of Engineering Thesis, Australian Maritime College.

[53] **Fitzgerald, B., J.,** (2009). Prediction of Hydrodynamic and Manoeuvring Characteristic of the AUV Muallaya through CFD and Experimental Work. Bachelor of Engineering Thesis, Australian Maritime College.

CURRICULUM VITAE

Name Surname: Ömer Faruk SUKAS

Place and Date of Birth: İstanbul / 01.02.1990

Address: Barbaros Bulvarı / Beşiktaş – Yıldız Teknik Üniversitesi

E-Mail: ofsukas@yildiz.edu.tr

B.Sc.: Naval Architecture and Marine Engineering – Y.T.U (Graduation 2012)

Professional Experience and Rewards:

- **Yildiz Technical University , Research Assistant, November 2012**